The Impact of Strongly Interacting Relics on Big Bang Nucleosynthesis

by

Jonathan William Sharman
B.Sc., McGill University, 2007

A Thesis Submitted in Partial Fullfillment of the
Requirements for the Degree of

MASTER OF SCIENCE

in the Department of Physics and Astronomy

The Impact of Strongly Interacting Relics on Big Bang Nucleosynthesis

by

Jonathan William Sharman
B.Sc., McGill University, 2007

Supervisory Committee

Dr. Maxim Pospelov, Supervisor
University of Victoria Department of Physics and Astronomy
and Perimeter Institute for Theoretical Physics

Dr. Adam Ritz, Member
University of Victoria Department of Physics and Astronomy

Dr. Don A. Vandenberg, Member
University of Victoria Department of Physics and Astronomy

Supervisory Committee

Dr. Maxim Pospelov, Supervisor
University of Victoria Department of Physics and Astronomy
and Perimeter Institute for Theoretical Physics

Dr. Adam Ritz, Member
University of Victoria Department of Physics and Astronomy

Dr. Don A. Vandenberg, Member
University of Victoria Department of Physics and Astronomy

ABSTRACT

We study the impact of long lived strongly interacting particles on primordial nuclear abundances. Particularly we look at the case of anti-squark quark bound states called mesinos. These mesinos are similar to massive nucleons in that they have the same spin and isospin. Like nucleons, the mesinos take part in nucleosynthesis and are bound into nuclei. We incorporate the mesinos into the various stages of BBN, from the QCD phase transition, to their capture of nucleons, to their eventual decay. We identify the mechanisms by which the mesinos could impact primordial abundances and show which actually do so. We find that for the predicted mesino abundance, only one mechanism exists that has the potential of generating an observable signature.

Table of Contents

List of Tables

List of Figures

Acknowledgments

I would like to thank my supervisor Maxim Pospelov for his guidance on this project as well as Adam Ritz for useful discussions. I would also thank NSERC, and the Perimeter Institute for the funding that helped make this research possible.

Chapter 1

Introduction

We examine the impact of long-lived scalar quarks (squarks) on the formation of light elements in the early universe. There are many different models proposed to describe the physics beyond the Standard Model. However until experiments like the LHC are able to determine the validity of these models directly, we have to rely on other methods if we wish to constrain them. One such method is through the study of primordial element abundances. By calculating the impact various relics have on Big Bang Nucleosynthesis (BBN), we are able to place constraints on physics beyond the Standard Model.

We will quickly review the cosmology and physics behind BBN. This includes introducing the assumptions that underlay modern cosmology, outlining standard BBN, and introducing the Boltzmann equation as a tool for calculating nuclear abundances.

Of the many possible models of physics beyond the Standard Model, we focus on those that produce a long lived squark with mass on the order of $1TeV$. This can arise naturally from supersymmetry. We will discuss how we expect these particles to hadronise and present the estimate calculated in [1] for their freeze out abundance.

The hadronised squarks will form bound states with standard nucleons, we call these states mule nuclei. The large mass of the squarks causes the mule nuclear binding energies to be larger than their purely nuclear counterparts. The result is that mule nuclear synthesis begins earlier than standard BBN. We calculate the binding energy and synthesis temperature of the mule nuclear equivalent of the deuteron. This gives us the temperature at which the hadronised squarks start a nucleosynthetic chain.

Unfortunately we were unable to calculate the binding energies and formation rates of more complicated mule nuclei. The uncertainties simply become too large to get a meaningful estimate on their properties. There are however certain general mechanisms of mule nucleosynthesis that could generate an impact on primordial abundances. An example is the early production of α particles. We will go through these mechanisms in Chapter 7. We find that with a single exception, these mechanisms do not generate an observable signature. This is mostly due to the very small abundance of strongly interacting relics.

The one exception arises from the nuclear remnant of the mule nucleon, ejected

when the squark decays. If enough of the ejected nuclear matter settles into the ground states of Li, Be, or B then their abundance could be observable today. This is because these elements can be observed down to very small abundances. Unfortunately calculating this nuclear remnant appears to be beyond the current scope of nuclear theory.

Chapter 2

Background Physics

In this section we review the physics required to study BBN and possible extensions of the Standard Model. This includes an introduction to the cosmology relevant to BBN, followed by a summary of the actual results of classical BBN. Here we will introduce the reactions that contribute to BBN and describe the current discrepancy between the predicted and observed abundances of lithium isotopes. Finally we will review the Boltzmann equation and show how it allows us to calculate the abundances of the light elements during BBN.

2.1 The Cosmology Behind BBN

There are several features of the universe that are observed at its largest scales. These observations describe how it evolves both at early times and today. The most basic

observation is that the universe is homogeneous and isotropic on large scales. The second is that the overall curvature of the universe is consistent with zero. The measured curvature is, $\Omega_{tot} = 1.011 \pm 0.012$ [2], where $\Omega_{tot} = 1$ is consistent with a flat universe. This curvature will not be a dominant effect in the early universe where radiation is seen dominating the energy density.

Homogeneity, isotropy and zero curvature allows us to use the Freedman Roberson Walker (FRW) metric to describe the universe at its largest scales:

$$ds^2 = -dt^2 + a(t)^2 \left(dx^2 + dy^2 + dz^2\right), \tag{2.1}$$

where $a(t)$ is the scale factor.

Calculating Einstein's equations for this metric give the equations of motion:

$$\left(\frac{\dot{a}}{a}\right)^2 = \frac{8\pi G}{3}\rho, \tag{2.2}$$

where ρ is the total energy density from matter, radiation, and dark energy. Note that the definition of the Hubble rate is:

$$H = \dot{a}/a = \sqrt{\frac{8\pi G\rho}{3}}. \tag{2.3}$$

When the universe is radiation dominated, $a \propto \sqrt{t}$, meaning $H = \frac{1}{2t}$.

This rate is extremely important in BBN, as it determines which reactions contribute to nucleosynthesis and when. If a given reaction rate is greater than the Hubble rate then the reaction is said to be in chemical equilibrium. If a reaction rate is much smaller than the $H(T)$ it means the reaction would not have have had a chance to occur during the lifetime of the universe.

During the radiation dominated period, the energy density in Eq. (2.2) is:

$$\rho = \frac{\pi^2}{30} T^4 \left[\sum_i g_i + \frac{7}{8} \sum_j g_j \right] \tag{2.4}$$

$$= \frac{\pi^2}{30} T^4 g_*, \tag{2.5}$$

Here i is over relativistic bosons, and j is over relativistic fermions. g_i are the degrees of freedom of the particles and g_* is the effective number of relativistic d.o.f. Equations Eq. (2.4) and Eq. (2.5) assume all relativistic species are in thermal equilibrium. After neutrinos fall out of thermal equilibrium their contribution to ρ is proportional to T_ν^4. The more relativistic species present at this temperature the greater the Hubble rate is during the radiation dominated epoch. More details on early universe cosmology can be found in [3].

The last cosmological input required by BBN is η. This is the fraction of the number density of baryons to the number density of photons. Knowledge of this parameter is required if one wishes to calculate the reaction rates of any compound

nuclei. Originally BBN codes along with measurements of light element abundances were used as a way of determining the baryon number to photon ratio. However with the advent of precision measurements of the power spectrum of CMB anisotropies, η can be calculated independently and to higher precision by fitting the CMB data. η can be derived from the measured quantity,

$$\Omega_B h^2 = 0.02265 \pm 0.00059, \tag{2.6}$$

where Ω_B is the baryon density and h is the Hubble parameter [4]. Using the calculation in [3], one finds that after e^+ e^- annihilation [5]:

$$\eta = 6.23 \pm 0.17 \times 10^{-10}. \tag{2.7}$$

2.2 BBN

In the previous section we dealt with the cosmological parameters and inputs required for BBN. Here we will deal with the nuclear and particle physics reactions required as inputs in the theory. The major difference between these inputs and the cosmological ones is that it is possible to measure most of these rates and binding energies in laboratory experiments, although often away from the energy intervals of interest.

Even though the formation of compound nuclei only begins at $T \approx 0.1MeV$, it

is important to work out the physics at significantly higher temperatures in order to correctly generate the light element abundances. The first stage of BBN is the freeze out of the ratio of neutrons to protons. At high temperatures, $T > 1MeV$, the neutrons and protons are in chemical equilibrium through the weak interaction [6]. At these temperatures the reactions,

$$p + e^- \leftrightarrow n + \nu \tag{2.8}$$

$$p + \bar{\nu} \leftrightarrow n + e^+, \tag{2.9}$$

are faster than the Hubble rate. The decay rate of the neutron does not become important until the after ^4He synthesis. This means the fraction of neutrons to the total number of baryons is given by the distribution:

$$X_n \equiv \frac{n_n}{n_B} = \frac{1}{1 + e^{Q/T}} \tag{2.10}$$

$$Q = m_n - m_p = 1.293MeV. \tag{2.11}$$

Here n_i is the number density of the species i [7]. At temperatures greater than the proton-neutron mass difference, $X_n \approx \frac{1}{2}$. However when T drops below Q, X_n begins to fall exponentially. If the baryons were to remain thermally coupled to the neutrinos then by the time the universe was cool enough for deuterium to form, there would be

almost no neutrons left:

$$X_n(T = 0.1MeV) \approx e^{-12.93} = 2.4 \times 10^{-6} \tag{2.12}$$

Fortunately for BBN, the neutrinos and baryons are only weakly coupled meaning they fall out of thermal equilibrium considerably earlier than the reactions mediated by the strong force. At $T \approx 1MeV$ the Hubble rate overtakes the reactions slowing the exponential depletion of neutrons. This temperature coincides with an age of the universe on the order $t \approx 1sec$, far smaller than the neutron lifetime of approximately $1000sec$. Soon the neutrino-mediated reactions are completely frozen out leaving β-decay as the only available channel for X_n to change. The neutron decay time is still an order of magnitude longer than the age of the universe at helium synthesis $t(T = 0.1MeV) = 132sec$ [3]. The freeze out of the weak rates explains the large value of $X_n \approx 0.15$ at deuterium synthesis [6]

As the universe continues to cool, it is possible for the proton and neutron to bind long enough for BBN to begin in earnest. In standard BBN the deuteron binding energy places an extremely important constraint on the light element abundances. The weak binding energy of deuterium allows thermal photons to break it apart until the universe has cooled to a temperature of order $0.1MeV$. No other nuclear reactions can start until the two nucleon state is stable. This is called the deuterium bottleneck.

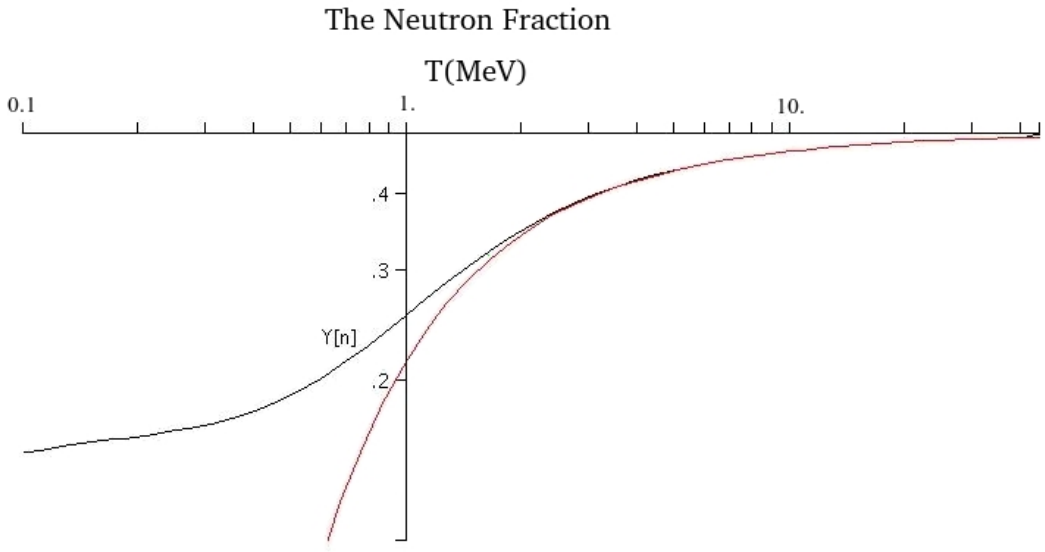

Figure 2.1: The red curve would be the abundance of neutrons in the early universe if they stayed in equilibrium. The black curve is the actual abundance.

Once the bottleneck has been overcome the free neutrons are very quickly processed into ^4He through the reactions:

$$\begin{array}{rcl} p+n & \rightarrow & d+\gamma \\ d+\gamma & \rightarrow & p+n \\ d+d & \rightarrow & {}^3He+n \\ d+d & \rightarrow & T+p \\ d+p & \rightarrow & {}^3He \\ d+n & \rightarrow & T \\ {}^3He+d & \rightarrow & {}^4He+p \\ {}^3He+n & \rightarrow & T+p \\ T+d & \rightarrow & {}^4He+n. \end{array}$$

While it is still energetically favourable for higher Z nuclei to form there are three issues that prevent nucleosynthesis from generating large abundances of nuclei with $Z > 2$. The first is that the coulomb barrier becomes all but insurmountable at high

Z and low temperature. A way around this could be through the capture of free neutrons that soon β decay into protons once bound. This avenue is blocked by the lack of a stable nuclei with 5 nucleons, as well as the fact that all the free neutrons are bound into other nuclei by this temperature, predominantly into ^4He.

The final abundances of ^7Li and ^7Be are established by the reaction channels:

$$^3He +^4 He \rightarrow {}^7Be \tag{2.13}$$

$$T +^4 He \rightarrow {}^7Li \tag{2.14}$$

$$^7Be + n \rightarrow {}^7Li + p \tag{2.15}$$

$$^7Li + p \rightarrow {}^4He +^4 He \tag{2.16}$$

The actual abundances are calculated numerically using a network of Boltzmann equations. This equation is discussed at length in Appendix A. For a nuclear species of number density n_i, and number fraction $Y_i \equiv \frac{n_i}{n_B}$, there are three cases that will be used in the nuclear reaction rates of interest. The first case is of two nuclei in the initial state and two in the final state.

$$\frac{dY_1}{dT} = -\frac{n_1^{(0)} n_2^{(0)} \langle \sigma v \rangle}{H(T)T} \left(\frac{Y_3 Y_4}{n_3^{(0)} n_4^{(0)}} - \frac{Y_1 Y_2}{n_1^{(0)} n_2^{(0)}} \right) n_B. \tag{2.17}$$

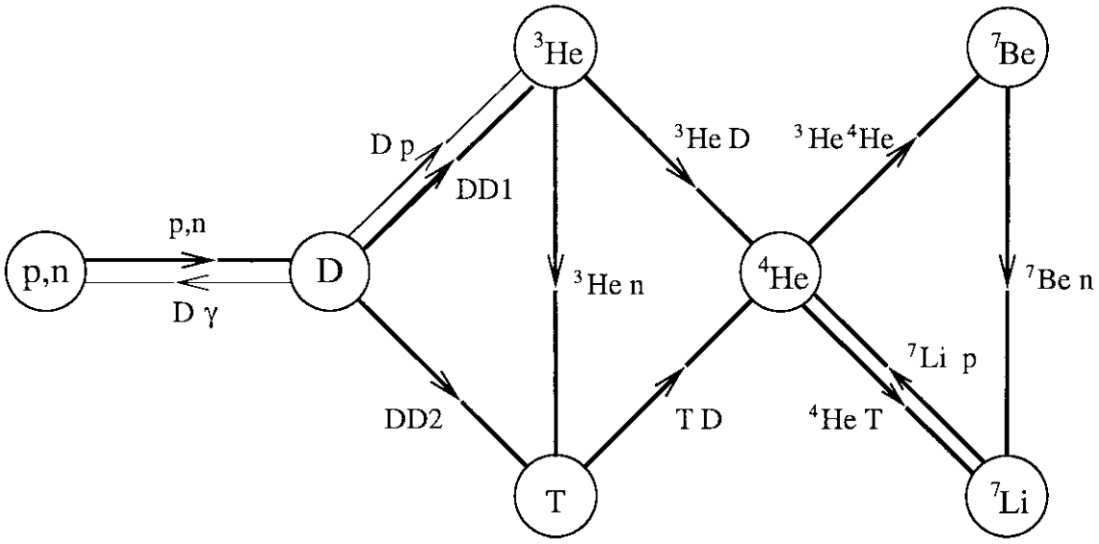

Figure 2.2: The network of reactions that contribute to BBN abundances. The figure is taken from [8].

The second is a single nuclei being broken into two smaller nuclei by a photon:

$$\frac{dY_1}{dT} = -\frac{n_1^{(0)} n_2^{(0)} \langle \sigma v \rangle}{H(T)T} \left(\frac{Y_3 Y_4}{n_3^{(0)} n_4^{(0)}} n_B - \frac{Y_1}{n_1^{(0)}} \right). \tag{2.18}$$

The third is the Boltzmann equation for a relativistic particle scattering off a single nuclei:

$$\frac{dY_1}{dT} = -\frac{n_1^{(0)} n_2^{(0)} \langle \sigma v \rangle}{H(T)T} \left(\frac{Y_3}{n_3^{(0)}} - \frac{Y_1}{n_1^{(0)}} \right). \tag{2.19}$$

Using the Boltzmann equations and reaction cross sections it is possible to compute the abundances of the light elements in the early universe. A plot of their

temperature dependence is given in Fig(2.3). Using WMAP's constraints on η [4] shows how BBN predictions compare with experimental measurements. Their results are summarised in Fig(2.4).

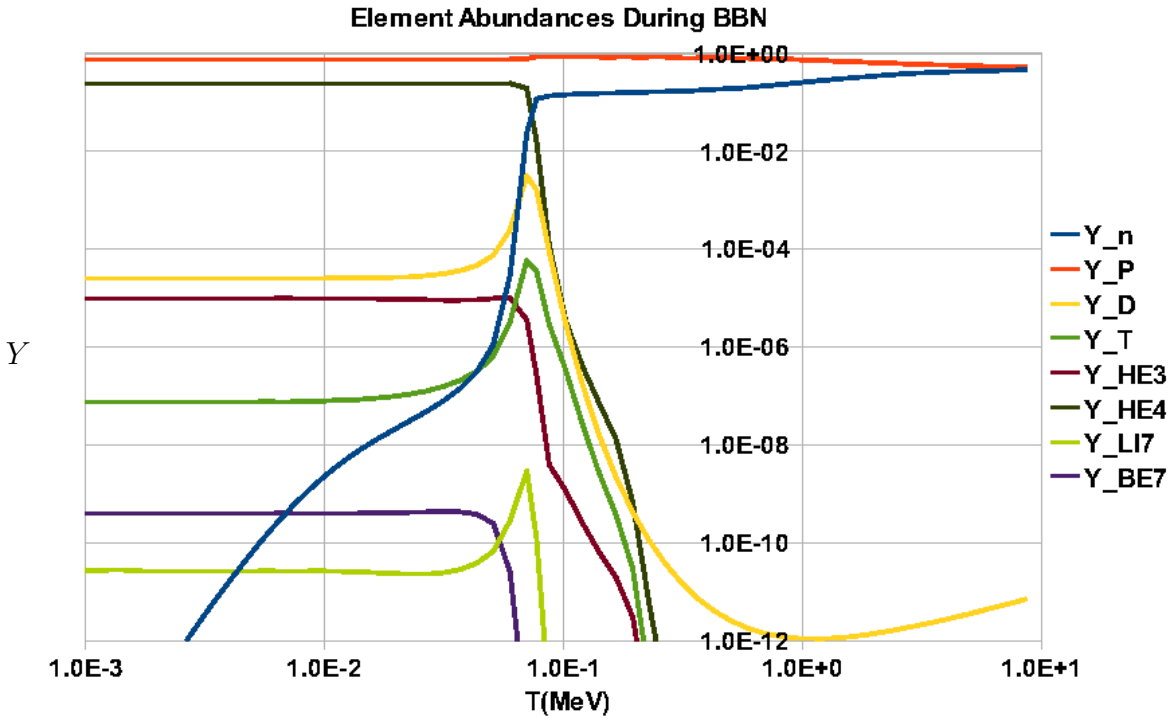

Figure 2.3: The number densities of the light elements generated by the BBN code from [9] with η calculated from the CMB measurements [5].

The abundances predicted agree with experiment up to ^7Li which is overproduced in standard BBN. In addition to this problem, recent observations of metal poor population II stars [10] show hints of an abundance of ^6Li on the order of one twentieth of the ^7Li abundance. This is three orders of magnitude larger than what is predicted by standard BBN and implies some pre-galactic origin for ^6Li. These claims are

however disputed [11], and the observational status of ^6Li is still unclear.

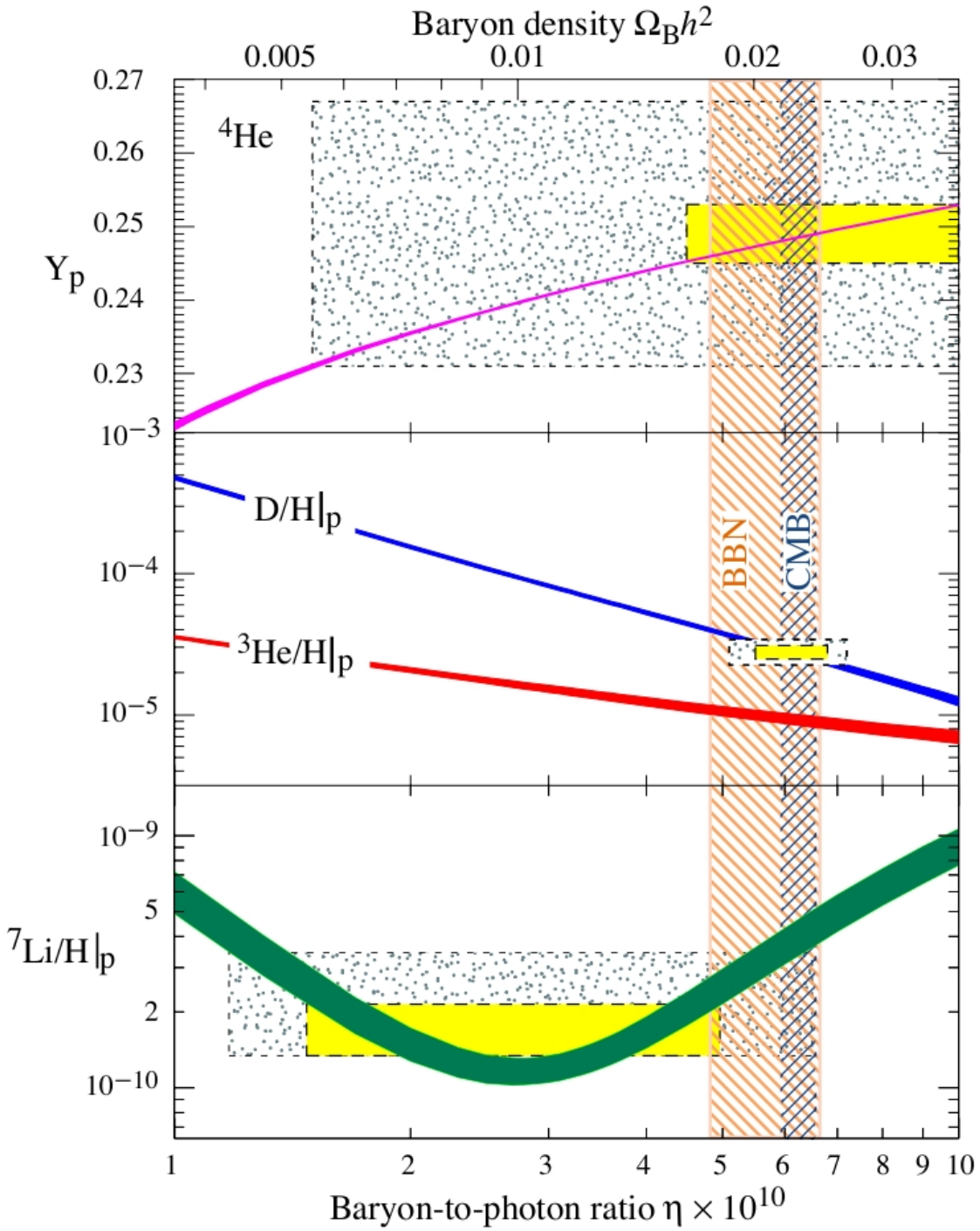

Figure 2.4: The bands are the 95% confidence level of the abundances of ^4He, D, ^3He, ^7Li. The small boxes indicate the 2σ statistical bounds, while the larger boxes are the 2σ statistical and systematic errors. The narrow vertical band is the CMB measure of η. The wider band is the range of η allowed by BBN. This plot was taken from [2].

Chapter 3

Strongly Interacting Relics: Motivation, Hadronisation, and Abundance

One speculative approach particle physicists have used in an attempt to fix the Lithium problems is Catalysed BBN or CBBN. This approach consists of introducing a metastable relic in the early universe and seeing if it has an observable impact on the reaction rates of BBN.

Relic particles can impact light element abundances by opening reaction channels that were previously closed. One definition of a catalyst is that it is used, but not consumed by a reaction. This means that in reactions where the relic functions as

a catalyst it can impact the abundances of elements far more numerous than itself. Finding and studying these mechanisms is the concept behind CBBN.

It has already been shown that an electrically charged relic can catalyse nuclear reactions in the early universe by forming coulomb bound states which open new reaction channels [12], [13]. These states form at temperatures of the order $10-40keV$.

While there has been a significant amount of work done with electrically charged relics, very little has been done to tackle the problem of strongly interacting relics. The main reason being that the interactions of these particles with regular matter are inherently complicated. Still we have managed to make considerable headway with the problem.

There are three major topics we address in this chapter. We introduce a supersymmetry model that allows for the existence of long-lived strongly interacting relics. We discuss how we expect these relics to hadronise as the universe cools. Lastly, we discuss the expected abundances of these strongly interacting particles.

3.1 SUSY Review

The standard model is a remarkable theory that has a place for every particle observed to date. The range of energies covered by the theory is staggering, ranging from the mass of the electron $0.511MeV$ to the top quark $170GeV$, spanning six orders of magnitude.

Of course as with any theory there are always loose ends to tie up. We have yet to observe the Higgs boson, which the theory requires in order to generate the masses of the particles in the standard model. Even with the Higgs boson, there is still a massive difference in the scales between its mass and the Planck scale $\approx 10^{19} GeV$.

This presents certain problems to the renormalisation of the masses in the standard model. The one loop renormalisation of the mass term diverges as the cut-off squared, Λ^2. It would be unnatural for the masses of the standard model particles to be as small as is observed if there is no new physics between the Higgs and Plank scale.

At the moment one of the more promising theoretical models for physics beyond the standard model is Supersymmetry (SUSY). The premise of SUSY is that every particle in the Standard Model has a superpartner. These SUSY particles have the same couplings as their partners, however their spin is shifted by $\frac{1}{2}$. This means every Standard Model boson has a fermionic superpartner and every Standard Model fermion has a bosonic super partner. The difference in sign between boson and fermion loops ensures that a Λ^2 divergences from the one loop corrections to the masses will be cancelled off. All that is left is a term logarithmic in Λ, which is nowhere near as problematic as a quadratic divergence.

One of reasons physicists favour SUSY is that on top of resolving the renormalisation issues of the Standard Model, it also provides a natural candidate for dark

matter. Imposing R-parity on the SUSY model forbids interactions with initial and final states having different signs under the R-parity operator.

The R-parity of a state is defined as:

$$R|\psi\rangle \quad = \quad (-1)^N|\psi\rangle, \tag{3.1}$$

where N is the number of SUSY particles in the state $|\psi\rangle$.

A consequence of conservation of R-parity is that the lightest super partner (LSP) is stable. The fact that we do not directly observe any of these relics in the universe today means that it can only interact weakly or gravitationally with Standard Model particles. This would be an ideal candidate for dark mater.

An interesting corollary to the stable and weakly interacting nature of the LSP is that the next-to-lightest superpartner (NLSP) can have a fairly long lifetime. This is because the NLSP's only decay channel is to the weakly or gravitationally coupled LSP. This occurs naturally if the LSP is the gravitino.

This means that it is possible to have some massive SUSY particles survive until the BBN era that are strongly or electromagnetically interacting. There has been a significant amount of research done on electrically charged relics. Here we will focus on the strongly interacting ones.

There are two different types of strongly interacting particles in the SUSY frame-

work. These are the squark (the scalar quark), and the gluino (the fermion partner of the gluon). In this thesis we will focus on the squark's impact on BBN since it is possible to make predictions about how these particles interact with Standard Model matter. We favour the squarks because the predictions we make have a higher degree of certainty than those that come from a gluino.

There are other strongly interacting relics could exist in the early universe such as a long lived higher generation of quarks. However these models do not have the same motivation as SUSY and in particular do not have the nice consequence of providing a dark matter candidate as its decay product. We will not be looking at them here.

3.2 The Mixed Hadron Spectrum

Before the QCD phase transition the squarks and quarks are not bound into colour neutral objects. As the universe cools, the squarks bind into exotic meson and baryon-like bound states.

While the complex nature of the strong force prevents us from knowing exactly how the squarks undergo hadronisation, it is fortunate that the details of the process are mostly unimportant in discussing the final bound states the squarks find themselves in.

In a naively simple model, all the squark-hadrons would decay to the lightest possible colourless combinations of quarks, squarks, and their antiparticles. These

would be meson like objects called mesinos. They can be made up of a squark and antiquark $Q\bar{q}$ or an antisquark and quark $\bar{Q}q$.

It turns out that this is an oversimplification of the physics and quite simply not true. This model of the mesinos ignores the presence of other baryons in the early universe. The $\bar{Q}q$ system will not be affected by these baryons. The $Q\bar{q}$ system however is a different matter. The ambient protons or neutrons will quickly destroy the anti-quark in this bound state, creating a mixed baryon of the form, Qqq.

In order to understand the qualitative behaviour of the single squark bound states we look to the mesons and hadrons that contain a single heavy quark. The reason we expect the behaviour of these two systems to be similar is because the terms in the Lagrangian that can cause a difference in their properties are those that couple the spins of the two particles. This spin spin coupling is suppressed by a parameter on the order of Λ_{QCD}/m, where m is the mass of the squark or heavy quark. In both cases this ratio is much less than one. This means one can use the spectrum of charm- and beauty-containing hadrons to infer the spectrum of the hadronised squark. The expected behaviour of each of these objects will be covered in the sections 3.2.1 and 3.2.2.

3.2.1 Mixed Hadrons

When we look at the three quark objects with a single charmed or strange quark and two light quarks, we find that the mass spectrums of the two are qualitatively similar.

That is, the lightest baryon is an isospin singlet *qud*. This is separated by $\Delta_m = 77MeV$ for the strange baryons and $\Delta_m = 166MeV$ for the charm baryons from an isospin triplet of the three baryons, *quu*, *qud*, *qdd*. The splitting in the triplet is below the order of $10MeV$.

This means that the Qqq bound state will quickly decay to the singlet, Qud, which, unlike the mesinos, cannot interact with nuclei through single pion exchange. This greatly reduces the possibility of contributing to nucleosynthesis through nuclear interactions.

Moreover, in the case of a bottom type squark, the electric charge of the hadron is zero and while it is +1 for the stop squark. This means that the relic squarks will not be able to catalyse nucleosynthesis through electromagnetic interactions. The same is not true of the anti-squarks.

3.2.2 Mesinos

There are two types of anti-squark that can bind into mesinos. Depending on the SUSY model, the NLSP could be a down or up type squark. I am focusing on the

sbottom and stop scalar quarks, meaning the mesino doublets are

$$M_0 = u\bar{\tilde{t}} \tag{3.2}$$

$$M_- = d\bar{\tilde{t}} \tag{3.3}$$

for the stop and

$$M_+ = u\bar{\tilde{b}} \tag{3.4}$$

$$M_0 = d\bar{\tilde{b}} \tag{3.5}$$

for the sbottom. Table(3.1) shows the mass splitting measured in heavy mesons [2].

	$\bar{c}$	$\bar{b}$
u	$1864.5MeV$	$5279.0MeV$
d	$1869.3MeV$	$5279.4MeV$
Δ_m	$4.78 \pm 0.1MeV$	$0.33 \pm 0.28MeV$
$\frac{\Lambda_{QCD}}{m}$	0.12	0.038

Table 3.1: The masses of c and b heavy mesons and the mass splitting of their isospin doublets. The last entry shows expected size of QCD spin-spin corrections to the mass splitting, $\frac{\Lambda}{m}$

The QCD scale we use is $\Lambda_{QCD} \approx 180MeV$. We estimate the difference in mass between the isospin states will be $\approx 0.3MeV$ for the sbottom mesinos, and $\approx 4.8MeV$ for the stop case. We will look at the binding energy of the nucleon-mesino system, or mule deuteron, as a function of this mass splitting.

3.2.3 Multi-Squark Bound States

Up until now we have looked solely at single mesino bound states. However there are certain cases where a multi-squark object can not only survive until BBN, but survive with a much larger number density than the single mesino baryons.

The formation of $Q\bar{Q}$ states is not particularly interesting since they quickly decay. However, depending on the SUSY model, the states QQq may be long lived. Most models will still allow them to decay very quickly via a reaction like that shown in figure 3.1.

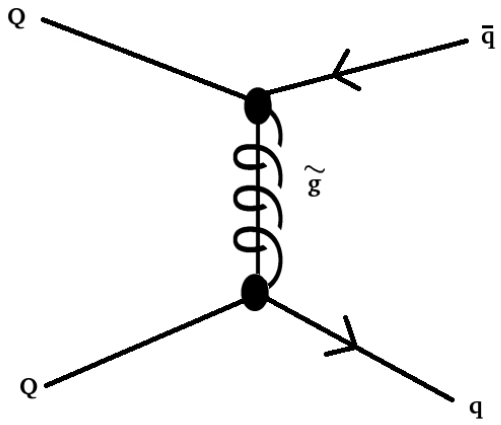

Figure 3.1: A possible annihilation channel for the QQ system.

The estimate of the lifetime of this bound state can be calculated in a manner similar to the decay time of positronium [14]. The quantity called the decay probability is defined as the inverse of the lifetime of the state. The decay probability of the QQ state is given by multiplying the annihilation cross section for the state by the

flux density of the particles, $v|\psi(0)|^2$. Here $\psi(0)$ is the wave function for the bound state at the origin.

Ignoring QCD colour factors, the squark squark potential is Coulomb-type at the energy scales of interest. This means that we can approximate the squark-squark bound state with the wave function:

$$\psi(r) \;=\; \frac{1}{\sqrt{\pi a^3}} e^{-r/a}, \quad a = \frac{2}{m_Q \alpha_{eff}}. \tag{3.6}$$

$\alpha_{eff} \equiv C\alpha_s$, where C is some colour factor that is order one. The actual value of C will have little impact on the approximation. In this problem, the squark momentum $\alpha_{eff} m_Q$ is much less than the mass of the squarks so that we are looking at the decay cross section in the limit of small velocity. In this limit we calculated the cross section times velocity to be approximately:

$$\sigma v \;\approx\; \frac{\alpha_s^2}{32\pi} \frac{\left(m_Q^2 - m_q^2\right)^{3/2}}{m_Q^3 m_{\tilde{g}}^2}, \tag{3.7}$$

m_q is the mass of the quarks the squarks decay into and $m_{\tilde{g}}^2$ is the mass of the virtual gluino from Fig(3.1). For our approximation of the cross section we ignored the colour factors and assume the gluino is much heavier than the squark mass. We will also ignore the mass of the quarks.

The decay probability is now given by:

$$\begin{aligned} w &= |\psi(0)|^2 (v\sigma)_{v\to 0} && (3.8)\\ &\approx \left(\frac{m_Q^3 \alpha_{eff}^3}{\pi}\right) \frac{\alpha_{eff}^2}{32\pi} \frac{1}{m_{\tilde{g}}^2} && (3.9)\\ &= \frac{\alpha_{eff}^5}{32\pi^2} \frac{m_Q^3}{m_{\tilde{g}}^2}. && (3.10) \end{aligned}$$

This corresponds to a lifetime of:

$$\tau \approx \frac{32\pi^2}{\alpha_{eff}^5} \frac{m_{\tilde{g}}^2}{m_Q^3}. \quad (3.11)$$

Estimating $m_Q \approx 1TeV$, and $m_{\tilde{g}} \approx nTeV$ gives a lifetime of:

$$\tau \approx \frac{32\pi^2}{\alpha_s^5} \frac{n^2}{TeV}. \quad (3.12)$$

Converting this to seconds we get:

$$\tau \approx n^2 \times 10^{-20} sec. \quad (3.13)$$

This is about 22 orders of magnitude shorter than the age of the universe at BBN. A consequence of this rapid decay channel is that introducing a difference in the squark-antisquark abundances will not help preserve the relics until BBN.

One could pick a very specific class of SUSY models where this decay channel and others like it are suppressed until after BBN. However most natural models would not allow these states to survive.

As a side note, this approximation has ignored the issue of the chirality of the squarks. It is possible for the left handed squark (Q_L) and right handed squark (Q_R) to have different masses and couplings. This means the coupling of their mass eigenstates to the gluino is somewhat model dependant. This could suppress the annihilation cross section, and therefore increase the lifetime of the particles. Unfortunately this increased lifetime would not bridge the 20 orders of magnitude needed for the bound state to survive until BBN.

The motivation for examining this bound state will become more evident after having reviewed the squark annihilation mechanism that takes place before the QCD phase transition. Therefore we will look at it after dealing with abundance calculations.

3.3 Squark Relic Abundances

There is a standard way of calculating the relic abundance of a cold or hot relic [6]. The basic approach is to calculate the annihilation cross section of the relic. This rate is then compared to the Hubble rate and, when the annihilation rate drops below the Hubble rate, the annihilation processes freezes out. The abundance of the relic

at the freeze-out temperature is then be preserved until some other mechanism that can affect the relic abundance, such as a decay channel, opens up.

3.3.1 Naive Perturbation Theory Calculation

For weakly and gravitationally interacting relics, perturbation theory is sufficient to calculate the annihilation cross section. However in the strongly interacting case that approach is no longer valid at the temperatures below the QCD phase transition. An estimate of the relic abundance that takes into account the effects of QCD is calculated in [1]. We will quote this result and contrast it to the naive perturbative calculation.

When calculating a relic abundance pertubatively it is useful to write the Boltzmann equation in the form [6]:

$$\frac{dY}{dx} = -\frac{x\langle\sigma|v|\rangle s}{H_m}\left(Y^2 - Y_{eq}^2\right). \tag{3.14}$$

Y is the fraction of the number density of relic particles to the entropy density of the universe, while Y_{eq} is the value this fraction would have if reaction were in chemical equilibrium. $x \equiv \frac{m}{T}$ is a useful variable to work with, and m is the mass of the relic particle. $H_m \equiv x^2 H(T)$ is the temperature independent expression of the Hubble rate. Finally, $\langle\sigma|v|\rangle$ is the total velocity averaged annihilation cross section.

The calculation of the squark to baryon number density freeze-out fraction is done in Appendix B. The final step required in this calculation is to evaluate the annihilation cross section for the squarks. This is done by considering the possible decay channels of the squarks scattering into two gluons, or into a pair of quarks. The end result of this calculation is:

$$\langle \sigma v \rangle = \frac{7}{27}\frac{2\pi}{m^2}\alpha_s^2, \tag{3.15}$$

The QCD coupling varies significantly over the energy range $1GeV$ to $1TeV$. In order to get a correct approximation of the freeze-out temperature, $T_f = \frac{m}{x_f}$, the coupling, α_s must correspond to roughly the energy of the annihilating relics. For a mass of $1TeV$, this gives $\alpha \approx 0.1$ [15]. For $g_* = 100$ and $T \approx 1TeV$, the result of the calculation in Appendix B is that $x_f \approx 30$. This results in the mass density for the relic,

$$\Omega_Q h^2 = \frac{1.07 \times 10^9 x_f GeV^{-1}}{m_{pl}\sigma_0}, \tag{3.16}$$

and a relic fraction of:

$$A \equiv \frac{n_Q}{n_B} = 7.3 \times 10^{-4}. \tag{3.17}$$

This abundance will exist until the universe cools to a temperature below the QCD phase transition, at which point the annihilation cross section becomes much larger, allowing the relic abundance to decay further. The reason behind this will be explained in the section 3.3.2.

3.3.2 The Actual Expected Abundance

A more accurate estimate of the abundance is calculated by [1]. Here the authors are able to get an estimate on the freeze out abundance and temperature by treating the strongly interacting relics as a massive coloured particle surrounded by a cloud of much less dense QCD 'muck'(light quarks and gluinos). This calculation is completely general in that it does not rely on the relic being a squark or gluino, only that it be strongly charged.

The cloud of muck that surrounds the relic enhances the annihilation cross section by allowing the formation of bound states with large angular momentum L. These states shed their angular momentum by the emission of photons or pions, until the relics annihilate.

The derivation of this abundance is fairly straightforward. The cross section for the formation of the large L bound state is geometric, and on the order of the hadron

radius. This means the cross section is given by:

$$\sigma = \pi R_{Had}^2. \tag{3.18}$$

The velocity of the particles when they form these bound states will be the thermal velocity at the temperature of formation. This gives a velocity-averaged cross section:

$$\langle \sigma |v| \rangle = \pi R_{Had}^2 \left(\sqrt{\frac{T_B}{m}} \right), \tag{3.19}$$

here m is the relic mass and T_B is the temperature where the bound state is formed. The freeze out abundance is reached when the annihilation rate drops below the Hubble rate:

$$n_Q \langle \sigma |v| \rangle \leq H \sim \sqrt{g_*} \frac{T_B^2}{M_P}, \tag{3.20}$$

where M_P is the reduced Plank mass.

$$\frac{n_Q}{s} \approx \frac{45}{2\pi^3 M_P} \frac{m^{\frac{1}{2}}}{T_B^{\frac{3}{2}} R_{Had}^2} \tag{3.21}$$

$$\approx 10^{-18} \left(\frac{R}{GeV^{-1}} \right)^{-2} \left(\frac{T_B}{180 MeV} \right)^{-3/2} \left(\frac{m}{TeV} \right)^{1/2}. \tag{3.22}$$

Here n_R is the number density of the relic and $s = 2\pi^2 g_* T^3/45$ is the entropy density

of the universe. $g_* \approx 10$, $R \approx 1GeV^{-1}$ is the radius of the QCD muck. To put this in terms of a baryon fraction:

$$A \equiv \frac{n_Q}{n_B} = \frac{n_Q}{s}\frac{s}{n_\gamma}\frac{n_\gamma}{n_B} \tag{3.23}$$

$$\approx \frac{n_Q}{s}\frac{10}{45}\eta^{-1} \tag{3.24}$$

$$\approx 4 \times 10^{-10}\left(\frac{R}{GeV^{-1}}\right)^{-2}\left(\frac{T_B}{180MeV}\right)^{-3/2}\left(\frac{m}{TeV}\right)^{1/2}. \tag{3.25}$$

This gives us an order of magnitude approximation for mesino abundance when BBN begins. This is six orders of magnitude lower than the naively expected abundance.

3.4 A Possible Relic Abundance Enhancement

An enhancement of the relic abundance would be possible if the squark-squark annihilation were highly suppressed. This could be achieved if the strongly interacting relic were significantly lighter than the gluino and photino. In that case the decay of a QQq state would be suppressed.

The reason this is an interesting object is because it now has a chance of gaining a third squark. If this happens then the QQQ object is going to be colour neutral and extremely tightly bound. The reaction cross section of the QQQ system with another QQQ, a $\bar{Q}q$, or a Qqq is now orders of magnitude smaller, on the order $\frac{1}{(\alpha_S m)^2}$ as opposed to $20GeV^{-2}$ [1]. Thus allowing it to survive in greater abundances than

the result in reference [1] predicts.

What is more, depending on the type of quark, one can get a relic with charge -1 for $\tilde{b}\tilde{b}\tilde{b}$ or -2 for $\overline{\tilde{t}\tilde{t}\tilde{t}}$. We expect these to be large catalysts. The singly charged one has already been shown to affect rates during BBN [12], while the impact of the doubly charged relic has yet to be examined.

While interesting, this case requires some additional mass hierarchies than a SUSY model. Perhaps a more realistic application of this anomalously large relic abundance is the possibility of a stable fourth generation of quarks at the TeV scale.

Chapter 4

Mesino-Nucleon Bound States

As mentioned previously, the mesinos should have similar isospin splitting to the nucleons. This facilitates the formation of composite nuclei, by allowing binding through pion exchange. The first step in this process is the formation of a deuteron-like objects that we call mule deuterons.

It was mentioned earlier that the deuteron binding energy regulates the start of BBN through the deuterium bottleneck. The binding energy of the mule deuteron is equally important to catalysed nucleosynthesis. It is also one of the few mesino-nuclei systems whose binding energy can be calculated with any degree of confidence.

If the mule deuteron is very deeply bound, it could throw off the BBN predictions by allowing the deuterium bottleneck to be bypassed entirely. If it is very weakly bound, then the mesinos will interact completely differently with baryons during

nucleosynthesis.

In this section we calculate the mule deuteron's binding energy. We start from the one pion exchange potential and calculate how the isospin and spin states interact. The similarities between mesinos and nucleons lead us to expect that the mule deuteron will share many features with the standard deuteron.

We introduce a cutoff to the pion exchange potential that helps deal with short distance physics. The form of this cutoff is fixed using the deuteron's binding energy to calibrate it. If the one pion exchange potential generates the correct deuteron binding energy then its prediction for the mule deuteron binding energy is more likely to be in the correct ballpark.

We discuss the numerical methods used to calculate this binding energy. Lastly, we see how this binding energy depends on the mass splitting between the isospin doublet and the axial vector coupling.

4.1 One Pion Exchange Potential

The one pion exchange potential arises from the fact that at long ranges, greater than a fermi, the nucleon-mesino and nucleon-nucleon interaction can be described by pion exchange.

The potential arises from the terms in the effective Lagrangian [16]:

$$L_{int} = -\frac{g_A}{\sqrt{2}f_\pi} N^\dagger \left[\tau^a \overrightarrow{\sigma} \cdot \overrightarrow{\nabla}\pi^a\right] N - \frac{\tilde{g}_A}{\sqrt{2}f_\pi} M^\dagger \left[\tau^a \overrightarrow{\sigma} \cdot \overrightarrow{\nabla}\pi^a\right] M. \quad (4.1)$$

Where τ and σ are the Pauli spin and isospin operators. The isospin matrices act on the isospin doublets N and M, while the spin matrices act on the spin doublets. The index a is summed over the pion triplet. Finally, g_A ($\tilde{g}_A$) is the axial vector coupling of the pion to the nucleus (mesino). g_A is determined experimentally, while the value of $\tilde{g}_A$ will be allowed to vary.

The fact that the mesino isospin doublets have the same spin and similar mass splitting as the nucleons means that we expect the large distance potential will be similar for the two types of particle.

The one pion exchange potential between two nucleons is given by the integral [17]:

$$V(r) = \left(\frac{g_A}{\sqrt{2}f_\pi}\right)^2 (\tau_1 \cdot \tau_2)(\sigma_1 \cdot \partial)(\sigma_2 \cdot \partial) \int \frac{d^3q}{(2\pi)^3} e^{iq\cdot r} \frac{1}{q^2 + m_\pi^2} F^2_{\pi NN}(q^2), \quad (4.2)$$

$F_{\pi NN}$ is the pion nucleon form factor. If the inter-nucleon potential were solely mediated by pion exchange and neither the nucleons nor the pions had internal sub-structure, then the form factor would be one. It is well known, however, that this is not the case for high energies (short distance scales). At high energies there are

contributions to the potential from multiple pion exchange, heavier meson exchanges, and the effects caused by the finite size of the nucleon.

Dealing with these contributions analytically is not feasible. Instead the complicated high energy behaviour of the potential is grouped into the form factor, $F_{\pi NN}$.

The potential can be rewritten in a more compact form as:

$$V(r) = m_\pi f_0^2 \frac{1}{3} (\tau_1 \cdot \tau_2) (S_{12} v_T(r) + \sigma_1 \cdot \sigma_2 v_C(r)) \tag{4.3}$$

$$v_T(r) = h_0(x)'' - h_0(x)'/x \tag{4.4}$$

$$v_C(r) = h_0(x)'' + 2h_0(x)'/x \tag{4.5}$$

$$h_0(r) = \frac{1}{2\pi^2 m_\pi} \int d^3q e^{iq\cdot r} \frac{1}{q^2 + m_\pi^2} F_{\pi NN}^2(q^2). \tag{4.6}$$

Where $x = m_\pi r$, and $f_0^2 = 0.079$. S_{12} is the tensor operator with its explicit form given by:

$$S_{12} = 3\frac{(\sigma_1 \cdot \vec{r})(\sigma_2 \cdot \vec{r})}{r^2} - \sigma_1 \cdot \sigma_2 \tag{4.7}$$

For convenience I will use the notation:

$$V_T(r) = m_\pi f_0^2 v_T(r) \tag{4.8}$$

$$V_C(r) = m_\pi f_0^2 v_C(r). \tag{4.9}$$

We refer to the operator $\frac{1}{3}\tau_1 \cdot \tau_2 S_{12} V_T(r)$ as the tensor component of the potential; while $\frac{1}{3}\tau_1 \cdot \tau_2 \sigma_1 \cdot \sigma_2 V_C(r)$ will be refered to as the vector component.

4.1.1 Evaluating the spin and isospin contributions

The isospin dependence of the potential enters through the vector dot product $\tau_a \cdot \tau_b$. To evaluate this contribution to the potential we must write the ground state as a sum of isospin eigenstates. The basis as derived in [18] is:

$$|s=1, m=1\rangle = |+,+\rangle \tag{4.10}$$

$$|s=1, m=0\rangle = \frac{1}{\sqrt{2}}\left(|+,-\rangle + |-,+\rangle\right) \tag{4.11}$$

$$|s=1, m=-1\rangle = |-,-\rangle \tag{4.12}$$

$$|s=0, m=0\rangle = \frac{1}{\sqrt{2}}\left(|+,-\rangle - |-,+\rangle\right). \tag{4.13}$$

$\tau_a \cdot \tau_b$ acts on the states differently. To evaluate the operator we use the identity:

$$\frac{\tau_a}{2} \cdot \frac{\tau_b}{2} = \frac{1}{2}\left[S(S+1) - \frac{3}{2}\right], \tag{4.14}$$

which gives the results

$$\tau_a \cdot \tau_b |s=0, m=0\rangle = -3|s=0, m=0\rangle \tag{4.15}$$

$$\tau_a \cdot \tau_b |s=1, m\rangle = |s=1, m\rangle. \tag{4.16}$$

In the deuteron bound state the spins and isospins are arranged in such a way that insures both the vector and tensor components of the potential are attractive. That is, $I = 0$ and $S = 1$.

Unfortunately this is not possible for the mule deuteron. Unlike the deuteron, the nucleon-mesino systems are not invariant under the exchange of a virtual charged pion. In fact the rest masses of the two isospin combinations are different. This means the mule deuteron's isospin state will not be purely $|\uparrow,\downarrow\rangle$ or $|\downarrow,\uparrow\rangle$ The state can instead be written as a combination of $|I = 1, m = 0\rangle$ and $|I = 0, m = 0\rangle$ from equations Eq. (4.13) and Eq. (4.11), where the kets describe isospin rather than spin. Since the spin arrangement of the mule deuteron remains $s = 0$, the $I = 1$ contribution will be repulsive. This means we expect that contribution to vanish in the limit $m_{M^+} + m_n = m_{M^0} + m_p$.

The potential can now be written in terms of a vector product of the spin and isospin state contributions. Only looking at the isospin structure of the potential,

and grouping everything else into the term $V(r)$ results in a potential:

$$V_{total} = V(r) \times \tau_a \cdot \tau_b \begin{pmatrix} \uparrow\downarrow \\ \\ \downarrow\uparrow \end{pmatrix}. \tag{4.17}$$

The explicit matrix for $\tau_a \cdot \tau_b$ in the isospin basis $\begin{pmatrix} \frac{\uparrow\downarrow - \downarrow\uparrow}{\sqrt{2}} \\ \\ \frac{\uparrow\downarrow + \downarrow\uparrow}{\sqrt{2}} \end{pmatrix}$ is:

$$\tau_a \cdot \tau_b = \begin{pmatrix} -3 & 0 \\ \\ 0 & 1 \end{pmatrix}, \tag{4.18}$$

while in the basis $\begin{pmatrix} \uparrow\downarrow \\ \\ \downarrow\uparrow \end{pmatrix}$, it is the matrix:

$$\tau_a \cdot \tau_b = \begin{pmatrix} -1 & 2 \\ \\ 2 & -1 \end{pmatrix}. \tag{4.19}$$

Depending on the situation, we pick one or the other basis to calculate the ground state and binding energy.

4.2 Schrödinger Equation and the Importance of Isospin Mixing

The binding energy and ground state of the mule deuteron is calculated by deriving the Schrödinger equation then solving it numerically. There are several subtleties that must be taken into account when dealing with this differential equation. These will be discussed here.

One complication that does not arise when dealing with the deuteron is how to treat the exchange of charged pions. In the standard deuteron, charged pions are exchanged, enhancing the binding potential. However, this exchange does not alter the composition of the deuteron, see figure 4.1. We mentioned in the previous section

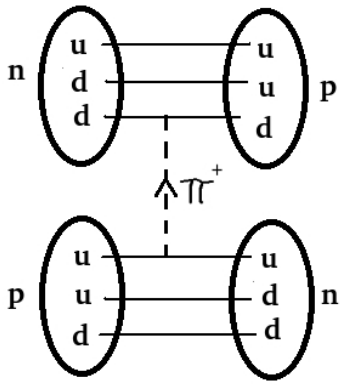

Figure 4.1: When a charged pion is exchanged the deuteron remains a deuteron.

that the mule deuteron is a mixture of two isospin configurations. If this mixing

were not allowed and the mule deuteron was made up purely of a neutron and down mesino, or a proton and an up mesino, then charged pion exchange would not be possible, see figure 4.2. A consequence of this is a potential too weak for the mule deuteron to bind.

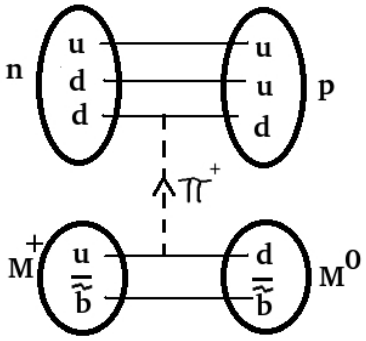

Figure 4.2: When a charged pion is exchanged in the mule deuteron, the system becomes a different state.

The mixing of isospin states is possible because the difference in mass between the two configurations is absorbed into the ground state. This is done by increasing the relative amplitude of one isospin configuration at the expense of the other. This section focuses on correctly setting up the Schrödinger equation to take these differences into account.

4.2.1 The Schrödinger Equation For The Deuteron

The Schrödinger equation for the deuteron is derived in Appendix C, including the form of the S and D components of the wave function. The deuteron wave function is given by Eq. (C.14):

$$\psi = \frac{1}{r}u(r)\Phi_{1,J_x,0} + \frac{1}{r}w(r)\Phi_{1,J_x,2}, \tag{4.20}$$

where $u(r)$ is the S wave component and $w(r)$ is the D wave component. The deuteron's Schrödinger equation is given by Eq. (C.15):

$$\begin{aligned} -\frac{1}{2m}\frac{d^2}{dr^2}u(r) - Eu(r) + V_c(r)u(r) + 2\sqrt{2}V_T(r)w(r) &= 0 \quad (4.21) \\ -\frac{1}{2m}\frac{d^2}{dr^2}w(r) - Ew(r) + (V_c(r) - 2V_T(t))\,w(r) + 2\sqrt{2}V_T(r)u(r) &= 0. \end{aligned}$$

This is the coupled ODE eigenvalue problem that must be solved to find the binding energy and ground state of the deuteron. The mule deuteron has added complications.

4.2.2 The Mass Shift Term

To correctly take the mass difference into account we look at the Schrödinger equation. In the centre of mass frame it is:

$$\begin{aligned} H &= \sqrt{p^2 + m_n^2} + \sqrt{p^2 + m_M^2} + V(r) && (4.22) \\ &= m_n + m_M + \frac{p^2}{2}\frac{m_n + m_M}{m_n m_M} + V(r). && (4.23) \end{aligned}$$

Normally the free mass of the system is unimportant and merely contributes to a shift in the vacuum energy of the system. However when the bound state is a mixture of two systems with different free rest masses the the relative mass difference becomes important.

Given some mixing potential V_{mix}, we can write the Schrödinger equation as:

$$\begin{aligned} \left(m_n + m_{M1} + \frac{p^2}{2}\frac{m_n + m_{M1}}{m_n m_{M1}} + V(r)\right)\psi_1(r) + V_{mix}(r)\psi_2(r) &= E\psi_1(r) && (4.24) \\ \left(m_p + m_{M2} + \frac{p^2}{2}\frac{m_p + m_{M2}}{m_p m_{M2}} + V(r)\right)\psi_2(r) + V_{mix}(r)\psi_1(r) &= E\psi_2(r). && (4.25) \end{aligned}$$

Shifting the ground state energy by picking a convenient normalisation puts the

Schrödinger equation in the form:

$$\left(\delta_m + \frac{p^2}{2\mu} + V(r)\right)\psi_1(r) + V_{mix}\psi_2(r) = E\psi_1(r) \quad (4.26)$$

$$\left(\frac{p^2}{2\mu} + V(r)\right)\psi_2(r) + V_{mix}\psi_1(r) = E\psi_2(r), \quad (4.27)$$

where $\delta_m \equiv (m_n + m_{M1}) - (m_p + m_{M2})$. The binding energy is now defined as the difference between the minimum eigenvalue of Eq. (4.27), E_{min}, and the energy of the least energetic free state. Under the normalisation of Eq. (4.27), the binding energy is $E_B = E_{min}$ when $\delta_m > 0$. However when $\delta_m < 0$ the binding energy is $E_B = E_{min} - \delta_m$ or $E_B = -|E_{min}| + |\delta_m|$.

4.2.3 Expressing The Coupled Schrödinger Equations As A Single Vector Operator

When solving a coupled system of differential equations like this, it is easiest to correctly match the boundary conditions if the Schrödinger equation is expressed a single operator acting on a vector that represents the wave functions.

In the case of the deuteron, the Hamiltonian can be built using the tensor product of the potentials and differential operators with the matrices $\begin{pmatrix} 1 & 0 \\ 0 & 0 \end{pmatrix}$, $\begin{pmatrix} 0 & 1 \\ 0 & 0 \end{pmatrix}$,

$$\begin{pmatrix} 0 & 0 \\ 1 & 0 \end{pmatrix}, \text{ or } \begin{pmatrix} 0 & 0 \\ 0 & 1 \end{pmatrix}.$$

This way the deuteron Schrödinger equation Eq. (C.15) can be converted from a coupled ODE to a single matrix equation:

$$\begin{aligned} H_{deuteron}U &= \left[\left(-\frac{1}{m_N}\frac{d^2}{dr^2}+V_C\right)\times\begin{pmatrix} 1 & 0 \\ 0 & 1 \end{pmatrix}+\left(\frac{6}{m_N r^2}-2V_T\right)\times\begin{pmatrix} 0 & 0 \\ 0 & 1 \end{pmatrix}\right. \\ &\quad \left.+2\sqrt{2}V_T\times\begin{pmatrix} 0 & 1 \\ 1 & 0 \end{pmatrix}\right]U \qquad (4.28) \\ &= EU. \qquad (4.29) \end{aligned}$$

Where $U=(u,w)$, and $m_N=2m$.

The Schrödinger equation for the mule deuteron is not much more complicated than that of the deuteron. The difference is that the wave function has to be split into the attractive $|s=0,m=0\rangle$ and repulsive $|s=1,m=0\rangle$ isospin components. The result is that there will be four wave functions in the general mule deuteron ground state; one for each possible isospin and angular momentum combination.

Like with the mixing between S and D states of the deuteron, the Schrödinger equation can be written as a tensor product of the overall potential calculated Eq.

(4.29). In the isospin $\begin{pmatrix} \uparrow\downarrow \\ \downarrow\uparrow \end{pmatrix}$ basis, the Schrödinger equation becomes:

$$\begin{aligned} H_{MD}U &= \left[D_2^2 \times \begin{pmatrix} 1 & 0 \\ 0 & 1 \end{pmatrix} + \frac{\tilde{g_A}}{3g_A} V \times \begin{pmatrix} -1 & 2 \\ 2 & -1 \end{pmatrix} + \delta_{Mx} \times \begin{pmatrix} 1 & 0 \\ 0 & 0 \end{pmatrix} \right] U \\ &= EU. \end{aligned} \tag{4.30}$$

In the $\begin{pmatrix} \frac{\uparrow\downarrow - \downarrow\uparrow}{\sqrt{2}} \\ \frac{\uparrow\downarrow + \downarrow\uparrow}{\sqrt{2}} \end{pmatrix}$ basis, the Schrödinger equation is:

$$\begin{aligned} H_{MD}U &= \left[D_2^2 \times \begin{pmatrix} 1 & 0 \\ 0 & 1 \end{pmatrix} + \frac{\tilde{g_A}}{3g_A} V \times \begin{pmatrix} -3 & 0 \\ 0 & 1 \end{pmatrix} + \frac{\delta_{Mx}}{2} \times \begin{pmatrix} 1 & 1 \\ 1 & 1 \end{pmatrix} \right] U \\ &= EU. \end{aligned} \tag{4.31}$$

Where:

$$D_2^2 = -\frac{1}{m_N} \frac{d^2}{dr^2} \times \begin{pmatrix} 1 & 0 \\ 0 & 1 \end{pmatrix} + \frac{6}{m_N r^2} \times \begin{pmatrix} 0 & 0 \\ 0 & 1 \end{pmatrix} \tag{4.32}$$

$$V = V_C \times \begin{pmatrix} 1 & 0 \\ 0 & 1 \end{pmatrix} - 2V_T \times \begin{pmatrix} 0 & 0 \\ 0 & 1 \end{pmatrix} + 2\sqrt{2}V_T \times \begin{pmatrix} 0 & 1 \\ 1 & 0 \end{pmatrix} \quad (4.33)$$

$$\delta_{Mx} \equiv \delta_M \times \begin{pmatrix} 1 & 0 \\ 0 & 1 \end{pmatrix}. \quad (4.34)$$

The factor in front of the potential term is the rescaling coefficient that comes from the fact that the axial vector coupling of the pion to the mesino is different from the coupling to nucleons.

U is now a 4-component vector with entries that consist of the components of the ground state wave function:

$$U \equiv \begin{pmatrix} u_1 \\ w_1 \\ u_2 \\ w_2 \end{pmatrix}, \quad (4.35)$$

where the subscripts 1 and 2 refer to the contributions from different isospin states.

The more physically intuitive basis is the second one. A good check of the numerics is to confirm that as the mass splitting goes to zero the u and w wave functions projected onto the $\frac{\uparrow\downarrow+\downarrow\uparrow}{\sqrt{2}}$ isospin state goes to zero. This means that in the limit $\tilde{g}_A = g_A$ and $m_N \to \frac{m_N}{2}$, the problem reduces to solving the deuteron Schrödinger

equation.

4.2.4 The electromagnetic contribution

The Schrödinger equation we just derived is valid for sbottom squark mesinos. In this case $M_+ = u\bar{\tilde{b}}$ and $M_0 = d\bar{\tilde{b}}$. The electric charge does not affect the binding energy and the overall charge of the mule deuteron is +1.

This is not the case with stop mesinos. The mule deuteron in this case will be a mixture of $M_0 n$ and $M_- p$. The overall charge of this mule deuteron is 0 and the Schrödinger equation describing the bound state must have a term that takes into account the Coulomb potential.

When $\delta_m \equiv m_{M^-} + m_p - m_{M^0} - m_n > 0$ the shift is equivalent to adding a term to the mass shift:

$$\delta_m \quad \rightarrow \quad -\frac{\alpha}{r} + \delta_m. \tag{4.36}$$

However if $\delta_m < 0$ then, as mentioned in section 4.2.2, the binding energy will be given by $B.E. = |E| - |\delta_m|$. The expected contribution to the binding energy will be on the order of $\frac{\alpha}{1fm} = \frac{197MeV}{137} = 1.44MeV$. This will turn out to be considerably smaller than the pion exchange contributions.

4.3 Cutoff-Dependent Form Factor

As mentioned earlier, the short distance nuclear potential is poorly described by the 1PE potential. In order to smooth over these unknowns we use a cutoff dependent form factor [17]:

$$F_{\pi NN} = \left[\frac{\Lambda^2 - m_\pi}{q^2 + \Lambda}\right]^n. \tag{4.37}$$

This was used to accurately model the deuteron and match the experimentally measured S-D mixing and binding energy of the ground state by varying the cutoff Λ. When $q \gg \Lambda$, the form factor becomes:

$$F_{\pi NN} = \left[\frac{\Lambda}{q}\right]^{2n}, \tag{4.38}$$

which goes to zero fairly quickly for $q > \Lambda$. Using the same form factor for the mesino-pion interaction as for the nucleon-pion interaction allows us to use the same Λ that was calculated for the deuteron. This will not be exact, but it should be a fairly good approximation since the mesinos have identical spin and isospin as the standard nucleon doublet.

Eq. (4.6) can now be defined recursively by:

$$h_0^{[m]} = \frac{e^{-x}}{x} - \beta e^{-\beta x} \sum_{j=0}^{m-1} \frac{\xi}{j!} (\delta_j - 2j\delta_{j-1}) \tag{4.39}$$

$$\delta_{n+1}(x) = (2n-1)\delta_n(x) + x^2\delta_{n-1}(x) \tag{4.40}$$

$$\delta_0(x) = 1/x \tag{4.41}$$

$$\delta_1(x) = 1 \tag{4.42}$$

$$\beta \equiv \frac{\Lambda}{m_\pi}. \tag{4.43}$$

where $m = 2n$ and $\xi \equiv (\beta^2 - 1)/(2\beta^2)$.

The potentials generated by this form factor are plotted in figure (4.3). Note that these potentials have been scaled by multiplying them by the radius. This is merely for presentation convenience, making it possible to see their short distance behaviour.

4.4 Numerics

As with virtually all problems in nuclear physics, the bound state has to be calculated numerically. While the variational method could be used to find a good approximation of the ground state, the fact that there are four components to the wave function means the number of parameters needed in a trial wave function would be large.

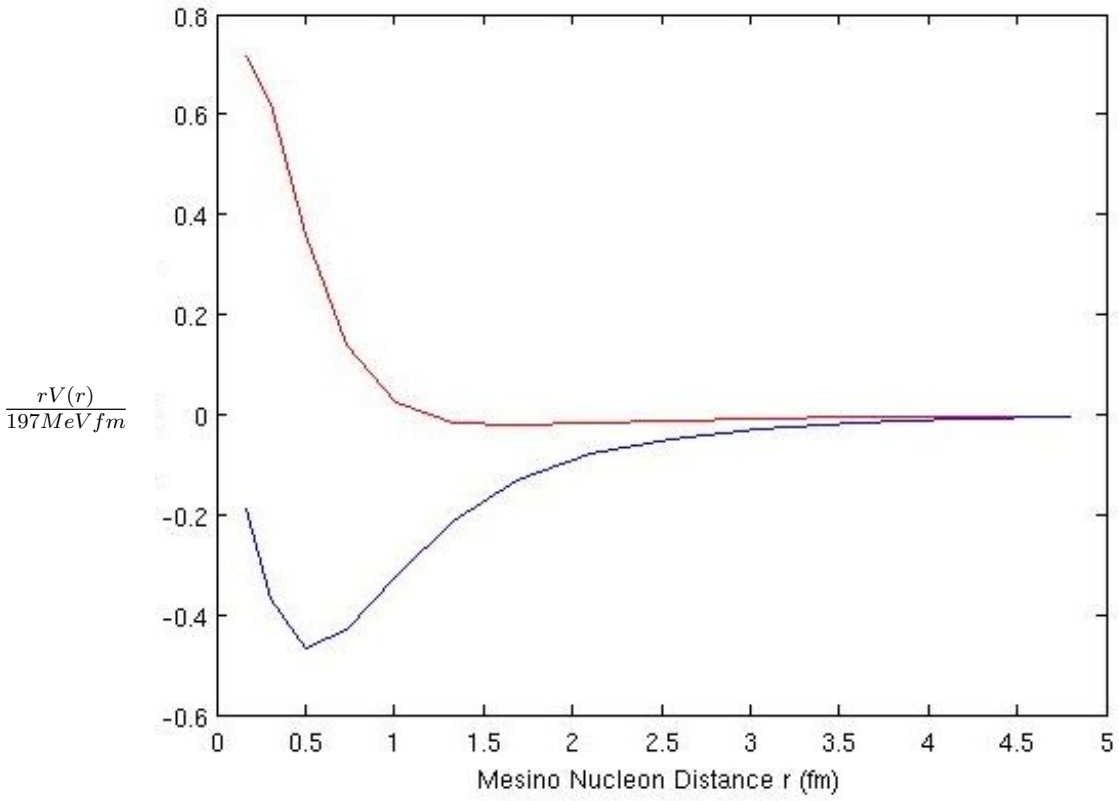

Figure 4.3: The red curve is the vector potential multiplied by the nucleon spacing r, while the blue curve is the tensor potential multiplied by r.

The multiple component ground state also rules out the shooting method approach. Instead we will use a Matlab tool box that was designed for this type of problem.

We know that the long distance distribution of the ground state wave function decays exponentially. This means that we only have to calculate the numerical solution for the range $[0, r_f]$ where r_f is some radius much larger than the expected proton meson spacing. This interval can then be broken into N pieces. An N vector

can now be used to describe each of the four components of the ground state wave function.

If the ground state has M components then the Hamiltonian can be written as an NM by NM matrix that acts on a vector of length NM.

The Matlab ODE toolbox that we use numerically calculates the derivative matrices and ideal divisions of the interval over which to solve the Schrödinger equation [19].

We know the wave function of a bound $\psi_B(r)$ state will behave as follows:

$$\psi_B(0) = 0 \tag{4.44}$$

$$\psi_B(r \gg m_\pi^{-1}) \propto \frac{e^{-\alpha r}}{r}, \tag{4.45}$$

where $\alpha = \sqrt{2m_n|E_B|}$. This means the long distance behaviour of the scaled wave function is, $u(r \gg m_\pi^{-1}) \equiv r\psi_B(r) = e^{-\alpha r}$. Finding a solution composed of Laguerre polynomials is ideal for dealing with these boundary conditions since they are described as a polynomial multiplied by an exponentially decaying envelope of the form, e^{-br}.

For a given value of b the ODE toolbox divides the interval into the first N roots of the Laguerre polynomials. It then generates the matrices that represent the needed derivative operator. In the case of the Schrödinger equation, only the second order operator is required.

The numerical equation that needs to be solved is now of the form:

$$\left(-\frac{1}{2m_n}D^{(2)}+V\right)u = Eu, \tag{4.46}$$

where $D^{(2)}$ is the second derivative operator, and V represents the potential terms, the mass difference term, and the angular momentum terms of the D or $l = 2$ states. u is a vector of length $4N$ for the ground state of interest.

The minimum eigenvalue is now found with a single line of Matlab code:

$$E_{min} \;=\; min\left(eig\left(-\frac{1}{2m_n}D^{(2)}+V\right)\right). \tag{4.47}$$

Initially b is a free parameter. When the system is barely bound, $E_{min} \approx 0.1MeV$, this energy is heavily dependent on the size of b. This dependence becomes far weaker when the parameters of the theory are such that the binding energy is greater than $5MeV$.

Even though the binding energy in the range of parameters of interest is not heavily affected by our initial choice of b, it is a good idea to make certain the choice of b has the correct physical motivation.

Since the long distance behaviour of $u(r)$ is a decaying exponential, the natural choice will be $b = \sqrt{2m_nE_B}$. Picking an initial guess for the binding energy of $10MeV$ gives an initial ansatz for b. By running the code and iterating the value of

b a consistent value for the binding energy is found. It usually takes less than six iterations for the binding energy to settle down to better than 0.1%.

4.5 Mule Deuteron: Results

Once the Schrödinger equation is coded into Matlab, it is possible to calculate both the binding energy and ground state wave function.

There are four parameters that can affect the bound state. They are the mesino-pion axial vector coupling, $\tilde{g}_A$; the rest mass difference between the components of each isospin combination, δ_M; β, the scaled cutoff in the potential form factor, and $m = 2n$, where n is the power of the form factor in Eq. (4.37).

We see in figures 4.4, 4.5, and 4.6 that the binding energy of the ground state depends heavily on $\tilde{g}_A$, while the dependence on δ_M is surprisingly weak. This weak δ_M dependence will be addressed in section (4.5.4).

The β dependence, or more generally the form factor dependence, of the mule deuteron state is our largest source of error. While we did use the deuteron's binding energy to constrain the parameter, even relatively small changes in β can have a significant effect on the binding energy. This issue will be discussed in section 4.5.3.

The power of the form factor ends up being relatively unimportant to the overall binding energy of the system. A plot of how the binding energy behaves for various values of n is given in Fig(4.6). The one outlier in this case is $m = 1$, however that

case is slightly unphysical since the large momentum cutoff is of the form:

$$F_{\pi NN} = \frac{\Lambda}{q} \tag{4.48}$$

This allows the nucleon and mesino to get closer than is strictly realistic, or possible when the cutoff has a larger power of n.

4.5.1 Binding Energy

One of the main difficulties with calculating the binding energy precisely is that it arises from the subtraction of two large numbers, the kinetic and potential energy. This means that even a small percentage uncertainty in a parameter like $\tilde{g}_A$ can lead to a large variation in the binding energy of the system.

This is one of the reasons why the binding energy of the mule deuteron is so much larger than that of the deuteron. The deuteron's binding energy of $2.225 MeV$ is the result of the cancellation of a large negative potential and a large positive kinetic energy. The reduced mass of nucleon in the mule deuteron system is twice that of a nucleon in the deuteron. In the most naive approximation of the binding energy of the system we merely divide the kinetic energy by two. The potential should similarly

be scaled by a factor of $\frac{\tilde{g}_A}{g_A}$. This gives:

$$B.E._{naive} = \frac{K.E.}{2} + \frac{1}{1.27} P.E. \tag{4.49}$$

$$\approx \frac{32MeV}{2} + \frac{1}{1.27}(-34MeV) \tag{4.50}$$

$$= -10.8MeV. \tag{4.51}$$

This is the minimum binding energy we could expect if we take $\tilde{g}_A \approx 1$.

We see from figure (4.4) and (4.5) that the binding energy should be on the order $15MeV$, regardless of the type of squark being modelled. Due to uncertainties however we will examine the impact on BBN of a mule deuteron with binding energy that ranges from $10MeV$ to $30MeV$.

4.5.2 The Ground State Wave Function

As mentioned before there are four components to the ground state wave function. Figure (4.7) shows how the the $|I = 1, m = 0\rangle$ contribution to the ground state goes from 0 when $\delta_M = 0$ to non-zero when $\delta_M = 5MeV$.

The increased effective mass of the nucleon in mule deuterium causes the components of the mule deuteron to be bound more closely than the components of

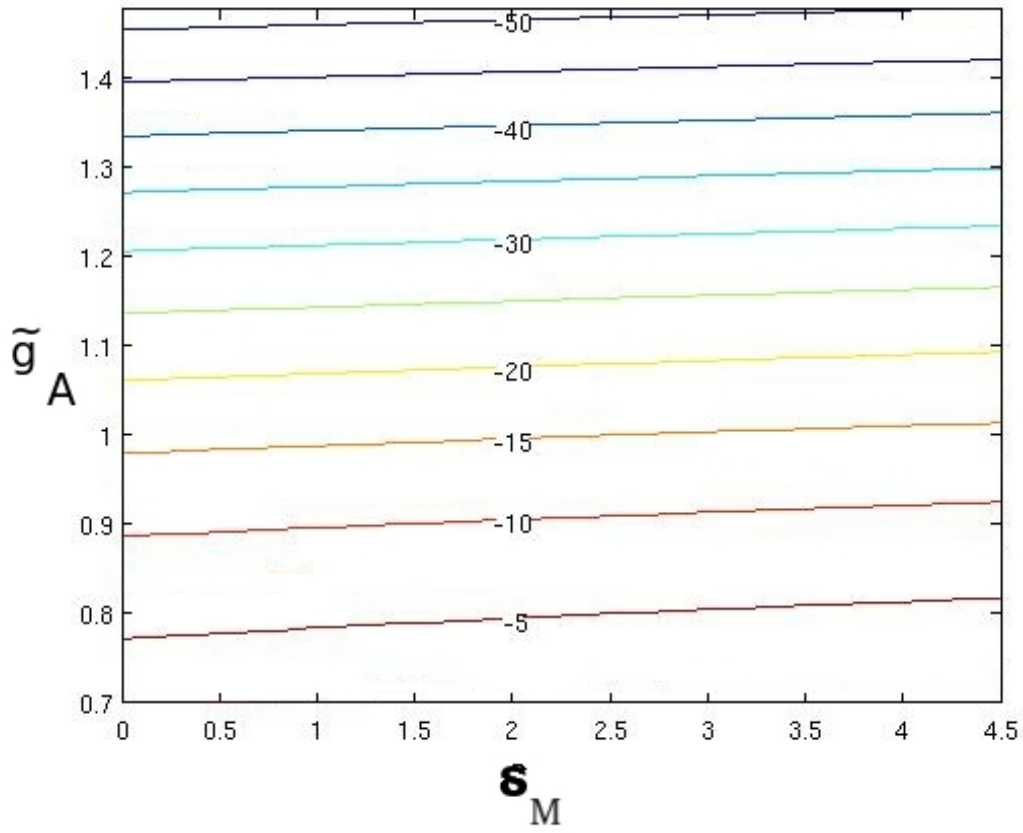

Figure 4.4: A contour plot of the binding energy as it depends on $\tilde{g}_A$ and δ_M.

deuterium.

$$\begin{aligned} \langle r^2 \rangle^{\frac{1}{2}} &= \frac{1}{2}\sqrt{\int dr r^2 \left(u_1(r)^2 + w_1(r)^2 + u_2(r)^2 + w_2(r)^2\right)} \\ &= 0.785 fm. \end{aligned} \tag{4.52}$$

The radius is calculated for $\tilde{g}_A = 1$, $\delta_M = 2$. This is about half the deuteron's root mean square radius which our model calculates to be $\langle r^2_{deu} \rangle^{\frac{1}{2}} = 1.923 fm$, which is

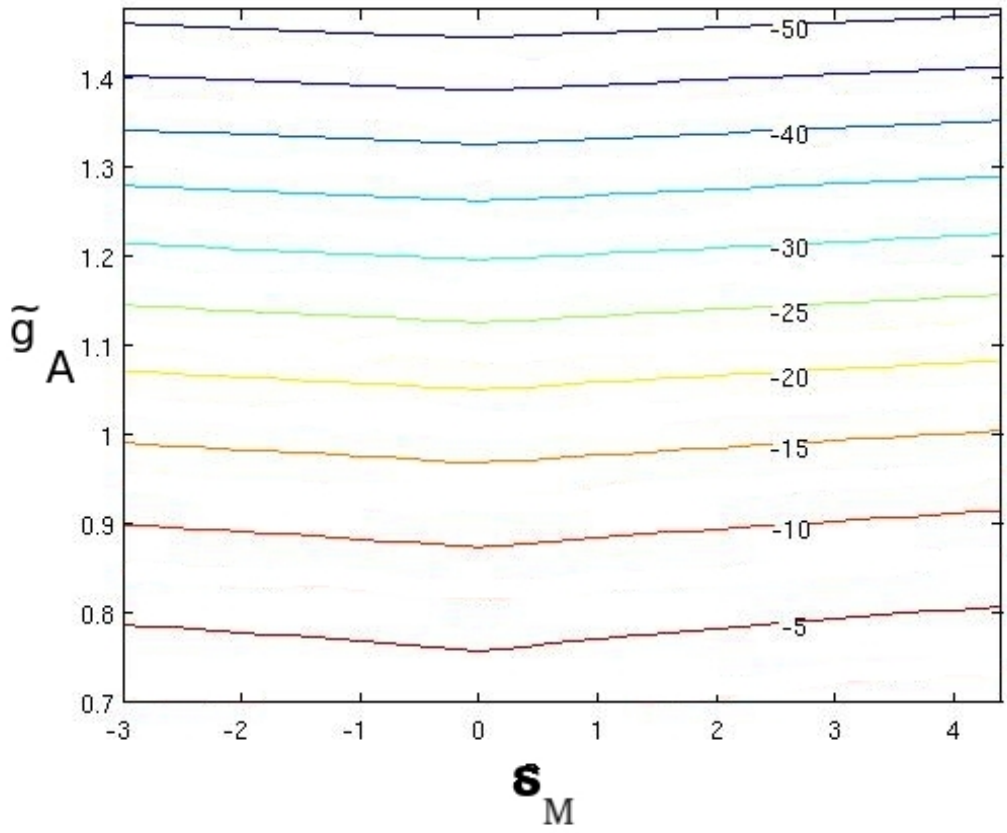

Figure 4.5: A contour plot of the binding energy as it depends on $\tilde{g}_A$ and δ_M when the isospin down mesino is negatively charged. In this case the binding energy gets an enhancement from the coulomb interaction between the down mesino and the proton.

very close to the experimental value of $\langle r^2_{exp} \rangle^{\frac{1}{2}} = 1.956 fm$ [17].

The small mesino-nucleon spacing is a cause for some concern over numerical accuracy. This is another reason to examine the impact on BBN by of a wide range of mule deuteron binding energies.

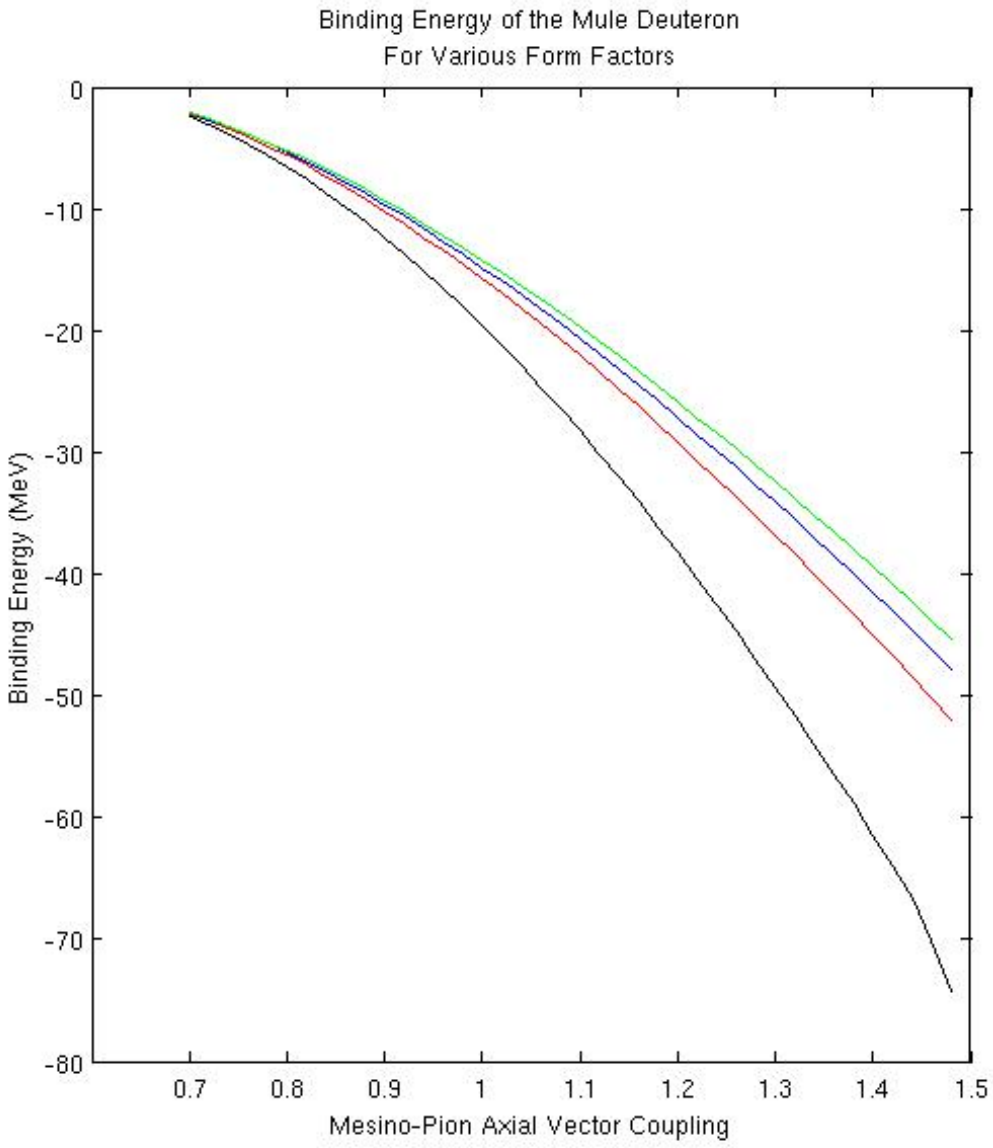

Figure 4.6: The black curve is the binding energy for $m = 1$, red if for $m = 2$, blue is for $m = 4$, and green is for $m = 50$.

4.5.3 Cutoff Dependence

We found that the binding energy of the mule deuteron is heavily dependent on the cutoff used. Varying β from $0.9\beta_{deu}$ to $1.1\beta_{deu}$ caused the binding to vary considerably,

see figure (4.8). This is why we consider β to be a major source of uncertainty in the binding energy calculation.

A related problem is the short distance behaviour of the wave function. If the binding energy depends heavily on the short distance physics at $r < 0.2fm$ then the likelihood of the binding energy being affected by some kind of numerics glitch or contact force is quite high. To investigate the importance of the short distance wave function, we added an impenetrable core to the mesino at $r = r_{min}$ and examined how this impacted the binding energy. The results are shown in figure (4.9) and (4.10). While the binding energies do vary slightly as r_{min} is increased, it is still within the range of binding energies that we will be investigating.

4.5.4 Understanding The δ_M Dependence

Despite the fact that the system requires isospin mixing to bind, the final binding energy has a remarkably weak dependence on the mass splitting. While not impossible, this behaviour was not expected.

The weak dependence is even more surprising when we look at the unphysical case where $\tilde{g}_A$ is large enough for the system to bind even when isospin mixing is forbidden. In this case we can compare the binding energy of the system for large values of δ_M to the binding energy of a system where isospin mixing is forbidden.

The expected result is that for large values of δ_M the binding energy converges to

the binding energy predicted when isospin mixing is forbidden. However, we found that even for extremely large mass splitting on the order of GeV, the two binding energies varied significantly as is shown in figure (4.11).

It seemed very suspicious that the binding energy could be affected by such a large mass splitting. That is, that there could be a enough isospin mixing to affect the binding energy, despite this mixing being suppressed by a mass two to three orders of magnitude larger than the binding energy.

In order to understand where this behaviour came from, and make sure it was not a coding error or numerical artefact, we looked at the much simpler case of an infinite square well potential with no S-D wave mixing. In this simple case the Schrödinger equation is:

$$\begin{aligned} 0 &= \left[\left(-\frac{1}{2m}\frac{\partial^2}{\partial r^2} - E\right)\begin{pmatrix} 1 & 0 \\ 0 & 1 \end{pmatrix} + \begin{pmatrix} -3V_1 & 0 \\ 0 & V_2 \end{pmatrix}\right. \\ &\quad \left. + \frac{\delta_M}{2}\begin{pmatrix} 1 & 1 \\ 1 & 1 \end{pmatrix}\right]\begin{pmatrix} \psi_1(r) \\ \psi_2(r) \end{pmatrix}, \end{aligned} \tag{4.53}$$

where the potential is given by:

$$\begin{aligned} V_1(r) &= V \quad , \quad r < R \\ &= -\infty \quad , \quad r > R \end{aligned} \tag{4.54}$$

$$\begin{aligned} V_2(r) &= V \quad , \quad r < R \\ &= \infty \quad , \quad r > R \end{aligned} . \tag{4.55}$$

Here V is some positive number and R is some radius on the order of femtometers.

The eigenvalues of the potential matrix are now $\frac{1}{2}\delta_M \pm \sqrt{\frac{1}{4}\delta_M^2 + 4V^2} - V$, and the ground state is:

$$\psi(r)_- = A\sin(\omega r) + B\cos(\omega r), \tag{4.56}$$

where $\omega = \sqrt{2m\left(\frac{1}{2}\delta_M \pm \sqrt{\frac{1}{4}\delta_M^2 + 4V^2} - V + |E_B|\right)}$. The boundary conditions set the wave function to vanish at $r = 0, R$. These conditions are met when $B = 0$ and $\omega R = \pi$. The end result is that the ground state has a binding energy:

$$E_B = \frac{\pi^2}{2mR^2} + \frac{1}{2}\delta_M - \sqrt{\frac{1}{4}\delta_M^2 + 4V^2} - V. \tag{4.57}$$

In the large δ_M limit, this becomes:

$$E_B \approx \frac{\pi^2}{2mR^2} - V - 4\frac{V^2}{\delta_M}. \tag{4.58}$$

As an approximation, take $V \approx 30MeV$ and $R \approx \frac{3}{197MeV}$. Even if $\delta_M \approx 1GeV$. The correction to E_B will be on the order of $\delta E \approx 3.6MeV$ which is sizable compared to

the uncorrected binding energy $7.3MeV$.

The purpose of this exercise was merely to demonstrate that the isospin mixing can allow for sizable corrections to the ground state binding energy despite being suppressed by a very large mass splitting.

The fact that a the nucleon-mesino forces can be affected by such a wide mass splitting may mean that we should rexamine the Qud objects. Depending on the signs of the pion exchange forces, it is conceivable that mixing with the higher mass triplet, $\{Quu, Qud, Qdd\}$, would allow for the formation of a bound state. This is unlikely, but should be checked in future work.

4.6 Summary of the mule deuteron bound state.

We calculated the binding energy of the mule deuteron to be on the order of $15MeV$ for $\tilde{g}_A \approx 1$. However due to uncertainties in the nucleon-mesino potential we will examine the impact on BBN of a mule deuteron that has a binding energy anywhere from $10MeV$ to $30MeV$.

We also calculated the ground state wave function and were able to find the mesino-nucleon spacing $\langle r^2 \rangle^{\frac{1}{2}} = 0.785fm$. One may note that this is actually slightly smaller than the charge radius of the proton $0.875fm$. This is a potentially large source of error and why we examine such a large range of possible binding energies in the nucleosynthesis code.

Finally we discussed the possible sources of error that could arise in the calculation. We have done our best to reduce these errors as much as possible. However there is only so much one can do with objects as complicated as nuclear systems with hypothetical particles when there is no experimental guidance available.

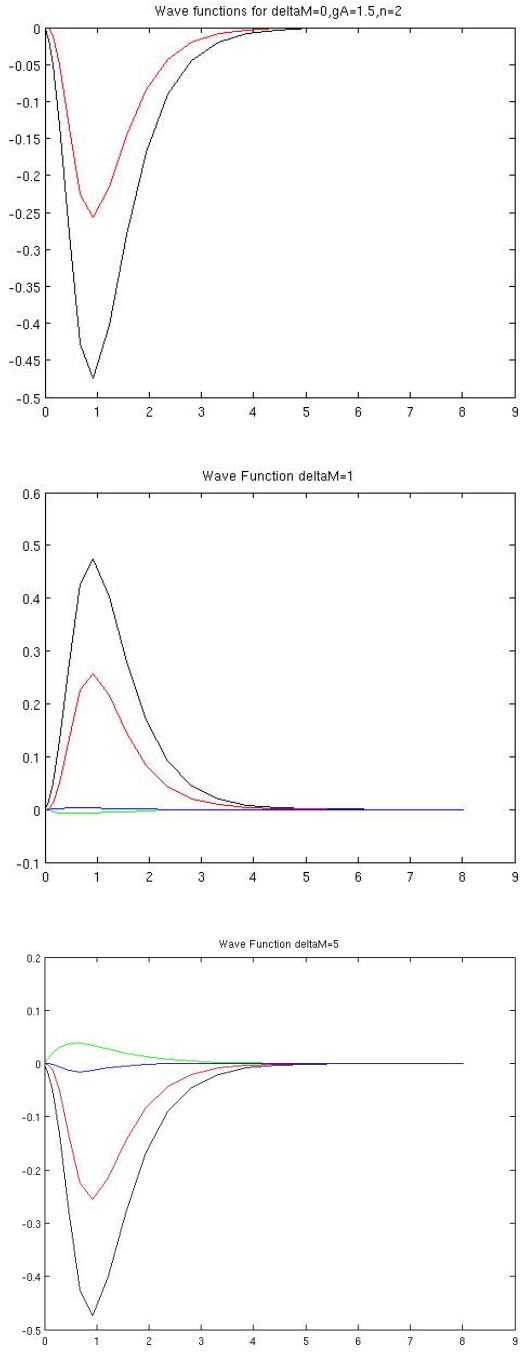

Figure 4.7: The ground state wave function of the mule deuteron. The black and red curves are the S and D components of the $|s = 0, m = 0\rangle$ component of the wave function. The green and blue curves are the S and D components of the $|s = 1, m = 0\rangle$ component. Note that as δ_M is increased the $|s = 1, m = 0\rangle$ component becomes more important.

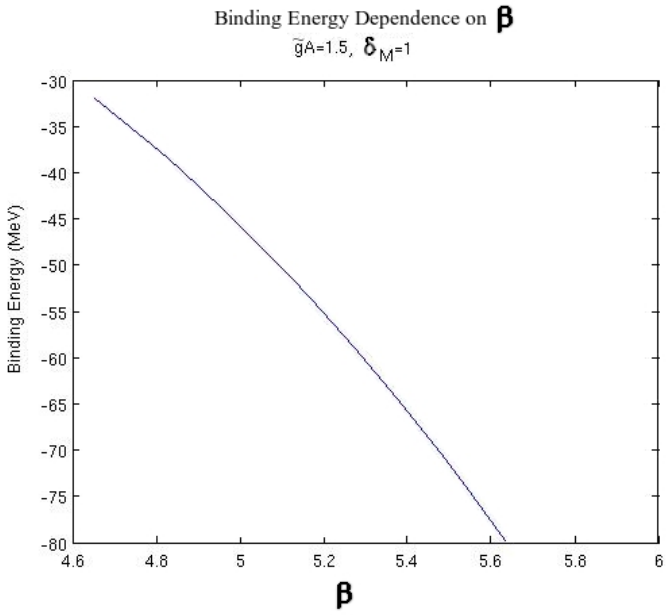

Figure 4.8: Varying β over the range $\beta \in [0.9\beta_d, 1.1\beta_d]$ causes a large shift in the mule deuteron binding energy. $\frac{\beta_d}{n} = 5.166$ is the value of β that reproduces the correct deuteron binding energy when $n = 2$.

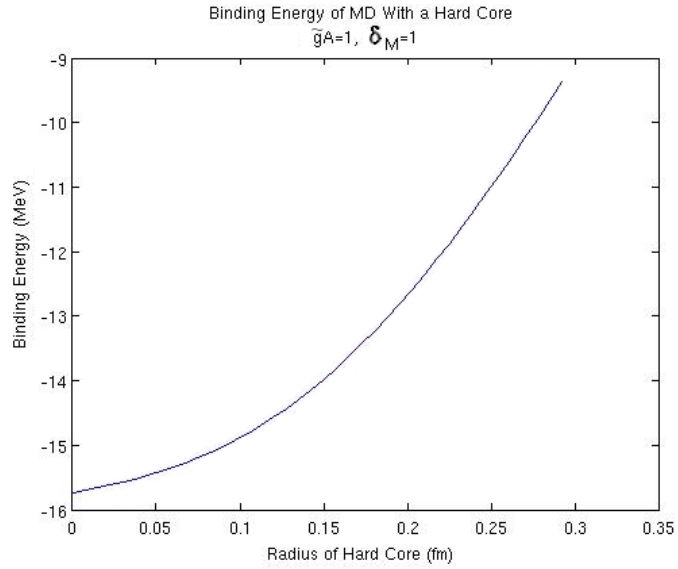

Figure 4.9: The effect of introducing a hard core in the the mule deuteron system on the binding energy for $\tilde{g}_A = 1$

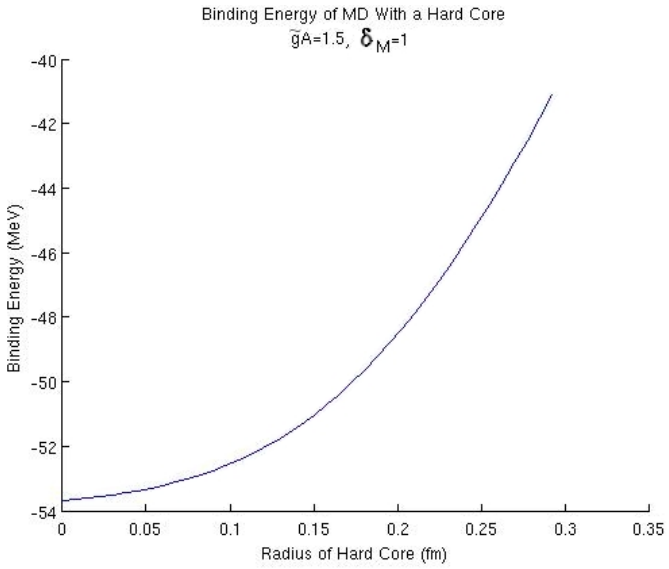

Figure 4.10: The effect of introducing a hard core in the the mule deuteron system on the binding energy for $\tilde{g}_A = 1.5$

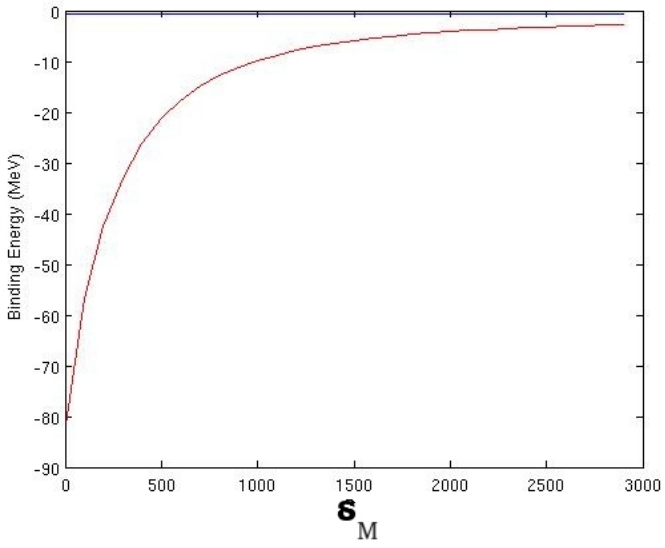

Figure 4.11: The red curve is the binding energy as a function of the mass splitting in MeV for $\tilde{g}_A = 1.8$. The blue line is the binding energy if no isospin state mixing is allowed.

Chapter 5

The Mesino Isospin Ratio And Mule Deuteron Synthesis Temperature

The goal of this chapter is to calculate the temperature at which the mule deuterons begin forming, T_{MDS}. To do so, we first verify that all the relevant rates are in chemical equilibrium. We then use the equations for a system in equilibrium to calculate the temperature where the abundance fraction of the mule deuteron, X_{MD}, becomes $O(1)$.

The two relevant rates are the isospin flipping rate and the nucleon capture rate. The temperatures at which these rates freeze-out will be called T_{flip} and T_{MDF}

respectively. T_{flip} and T_{MDF} must be below T_{MDS} for the assumption of chemical equilibrium to be valid. If the rates generating the mule deuteron were to freeze-out before T_{MDS}, then the abundances of mule deuterons and therefore all complex mule nuclei would be heavily suppressed. In this chapter we will show that T_{flip} and T_{MDF} are indeed below T_{MDS}.

Since calculating the cross section of these reactions analytically is very difficult, we will deliberately underestimate the rates that pertain to isospin flipping and nucleon capture. We will show that even when these rates are well below what is expected from simple parametric estimates, they are large enough to insure T_{MDS} can be calculated using the assumptions of chemical equilibrium.

5.1 Calculating T_{flip}

Just like the protons and neutrons, the transitions between isospin states of the mesinos occurs freely at large temperature, letting their abundances be described by the equations for dynamic equilibrium. As the temperature of the universe drops, the reaction rates that flip the mesino isospin will eventually freeze-out.

There are two interactions that can flip the isospin of the mesino. These two reactions are weak scattering off electrons and neutrinos and the scattering of nucleons off the mesinos. The nucleon scattering is a strongly mediated cross section however is suppressed by the small baryon density. The weak rate on the other hand has the

opposite properties, it is mediated by weak interactions, but there is a large density of thermal electrons and neutrinos in the universe.

The mass and electric charge of the proton lead us to believe that proton rather than neutron capture will be the dominant formation channel of the mule deuteron. The electric dipole transition is not the dominant formation channel of the standard deuteron due to a resonance at $E = 0.067MeV$. This resonance makes a magnetic dipole transition by the neutron the dominant contribution to the low energy cross section. However the source of this transition is a numerical coincidence, not guaranteed to be present in the mule deuteron. In order to have a firm lower bound on the mesino-nucleon capture cross section we will only calculate the contribution from the electric dipole transition.

The first step in calculating the mule deuteron synthesis temperature is to find the temperature dependent relation between the fraction of up mesinos $X_{M\uparrow} \equiv \frac{n_{M\uparrow}}{n_M}$ and the fraction of down mesinos $X_{M\downarrow} \equiv \frac{n_{M\downarrow}}{n_M}$, where again up and down refers to isospin components. The Boltzmann equation that describes up, or down, mesino fractions is:

$$\begin{aligned} \frac{dX_{M\downarrow}}{dT} &= -\frac{n_B\langle\sigma_{p+M\downarrow\rightarrow n+M\uparrow}v\rangle}{H(T)T}\left[X_nX_{M\uparrow}\left(\frac{n_p^{(0)}n_\downarrow^{(0)}}{n_n^{(0)}n_\uparrow^{(0)}}\right) - X_pX_{M\downarrow}\right] \qquad (5.1)\\ &\quad +\text{weak terms} + \text{MD terms}\\ &= -\frac{n_B\langle\sigma_{p+M\downarrow\rightarrow n+M\uparrow}v\rangle}{H(T)T}\left[X_nX_{M\uparrow}e^{\frac{-\delta_M}{T}} - X_pX_{M\downarrow}\right]. \qquad (5.2) \end{aligned}$$

Where

$$\delta_M \equiv (m_{M^0} - m_{M^+}) - (m_n - m_p)\,. \tag{5.3}$$

The MD terms refers to contributions to the Boltzman equation from the formation of mule deuterons. The Boltzmann equation for the mule deuteron fraction forces this term to zero and is independent of the fraction $X_\uparrow/X_\downarrow$. We will be discuss this further in section (5.2). The weak terms will be shown to be negligible in section (5.1.1).

The $n_i^{(0)}$ terms are simplified using Eq. (A.7). The equilibrium abundance of the up and down isospin mesinos are then related by:

$$X_n X_{M\uparrow} e^{\frac{-\delta_M}{T}} \quad = \quad X_p X_{M\downarrow}. \tag{5.4}$$

In normal nuclei the ratio of protons and neutrons is controlled by the rates in Eq. (2.8) to Eq. (2.9). Once these fall bellow the Hubble rate, the abundance freezes out. A numerical calculation of the neutron abundance follows the curve in Fig(2.1). In the case of the mesinos, the reaction in Eq. (5.2) dominate the isospin flipping reactions despite the small value of n_B. We can approximate this cross section as an area with radius on the order of the pion mass, similarly the velocity of the nucleon is approximately $\sqrt{\frac{T}{m_n}}$. In the case where $\delta_M > 0$ the velocity average cross section

of the reaction $p + M \downarrow \rightarrow n + M \uparrow$ is:

$$n_B \langle \sigma v \rangle \approx \eta \frac{2T^3}{\pi^2} \frac{\pi}{m_\pi^2} \sqrt{\frac{T}{2\pi m_n}}. \tag{5.5}$$

However when $\delta_M < 0$ the opposite reaction is energetically favourable. In this case we expect the rate of the reverse reaction to be given by Eq. (5.5).

Regardless of the sign of δ_M, these reactions freeze-out when the larger of the two rates drops bellow the Hubble rate, i.e., when $n_B \langle \sigma v \rangle / H \approx 1$. Taking the Hubble rate to be $H \approx 1.66\sqrt{g_*}\frac{T^2}{M_{pl}}$ results in a freeze-out temperature:

$$T_{flip} \approx 10^{-5} MeV. \tag{5.6}$$

Even if the cross section we used is off by a factor of 100, T_{flip} is still on the order $4 \times 10^{-4} MeV$.

We will see that the temperature at which mule deuterons form is never less than $0.25 MeV$ in the case of sbottom Mesinos $T_{flip} \ll T_{MDF}$ and $T_{flip} \ll T_{MDS}$. This means that the equilibrium is maintained and that the relative fraction of down to up mesinos will be given by Eq. (5.4) until long after the free mesinos are bound into mule deuterons.

5.1.1 The weak rate as it impacts isospin mixing.

Despite the fact that the cross sections involved in the weak interaction are far smaller than those of the strong interaction, the rates are not suppressed by the small baryon fraction η. If the weak isospin flipping rate were larger than the nucleon-mesino isospin fliping rate, then the ratio of up- to down-mesinos would be fixed by a relation similar to that of Eq. (2.11) rather than Eq. (5.4). This would change T_{MDS} and is why it is necessary to verify that the weak rates do not dominate the isospin mixing reactions.

The process of leptons scattering off nuclei is discussed in [7], while an analytic approximation is performed in [8]. The contribution to the isospin flipping of the mesino from lepton interactions arises from the following reactions:

$$M_\uparrow + e^- \leftrightarrow M_\downarrow + \nu \tag{5.7}$$

$$M_\uparrow + \bar{\nu} \leftrightarrow M_\downarrow + e^+ \tag{5.8}$$

$$M_\downarrow \leftrightarrow M_\uparrow + e^- + \bar{\nu}. \tag{5.9}$$

The last reaction is only present if $m_{M\downarrow} - m_{M\uparrow} > m_e$. To calculate the weak rate we follow the procedure in [7]. For $Q \equiv m_{M\downarrow} - m_{M\uparrow}$ there are four possible rates. In the

case $Q > 0$ the rates are:

$$\lambda_{M_\downarrow - M_\uparrow} = A \int dq (q+Q)^2 q^2 \sqrt{1 - \frac{m_e^2}{(Q+q)^2}} \left[1 + e^{q/T_\nu}\right]^{-1} \left[1 + e^{-(q+Q)/T}\right]^{-1} \quad (5.10)$$

$$\lambda_{M_\uparrow - M_\downarrow} = A \int dq (q+Q)^2 q^2 \sqrt{1 - \frac{m_e^2}{(Q+q)^2}} \left[1 + e^{-q/T_\nu}\right]^{-1} \left[1 + e^{(q+Q)/T}\right]^{-1}, \quad (5.11)$$

where:

$$\int = \int_{-\infty}^{-Q-m_e} + \int_{-Q+m_e}^{\infty}. \quad (5.12)$$

When $0 < Q < m_e$, the rates are:

$$\lambda_{M_\downarrow - M_\uparrow} = A \int dq (q+Q)^2 q^2 \sqrt{1 - \frac{m_e^2}{q^2}} \left[1 + e^{q/T}\right]^{-1} \left[1 + e^{-(q+Q)/T_\nu}\right]^{-1} \quad (5.13)$$

$$\lambda_{M_\uparrow - M_\downarrow} = A \int dq (q+Q)^2 q^2 \sqrt{1 - \frac{m_e^2}{q^2}} \left[1 + e^{-q/T}\right]^{-1} \left[1 + e^{(q+Q)/T_\nu}\right]^{-1}, \quad (5.14)$$

where:

$$\int = \int_{-\infty}^{-m_e} + \int_{m_e}^{\infty} \quad (5.15)$$

When $Q < 0$, the rates are:

$$\lambda_{M_\downarrow - M_\uparrow} = \lambda_{M_\uparrow - M_\downarrow}(|Q|) \tag{5.16}$$

$$\lambda_{M_\uparrow - M_\downarrow} = \lambda_{M_\downarrow - M_\uparrow}(|Q|). \tag{5.17}$$

The constant A is:

$$A \equiv \frac{1 + 3\tilde{g}_A^2}{2\pi^3} G_F^2. \tag{5.18}$$

$G_F = 1.17 \times 10^{-5} GeV^{-2}$, is the weak coupling. The neutrino temperature T_ν in Eq. (5.10) to Eq. (5.14) is the same as the photon temperature T until the electrons and positrons annihilate at $T \approx 0.5MeV$. The actual temperature of the neutrinos relative to the thermally coupled matter is shown in [7] to be:

$$T_\nu = \left(\frac{4}{11} L\left(\frac{m_e}{T}\right)\right)^{1/3} T \tag{5.19}$$

$$L(x) \equiv 1 + \frac{45}{2\pi^4} \int_0^\infty y^2 dy \left[\sqrt{x^2 + y^2} + \frac{y^2}{3\sqrt{x^2 + y^2}}\right] \left[\exp(\sqrt{x^2 + y^2}) + 1\right]^{-1} \tag{5.20}$$

We plot the ratio of the weak rates to the Hubble rate for several values of the mass splitting Q in figure 5.1. In the range of temperatures of interest the weak rates are never more than an order of magnitude larger than the Hubble rate. This means the weak rates are safely below the strong rates. Even increasing $\tilde{g}_A$ to 1.5 would not

allow the weak rate to become comparable to the strong mixing rate.

The weak could potentially impact the abundance of neutrons by allowing a cycle of neutron or proton conversion. However we will see in section 7.2 that this will not occur.

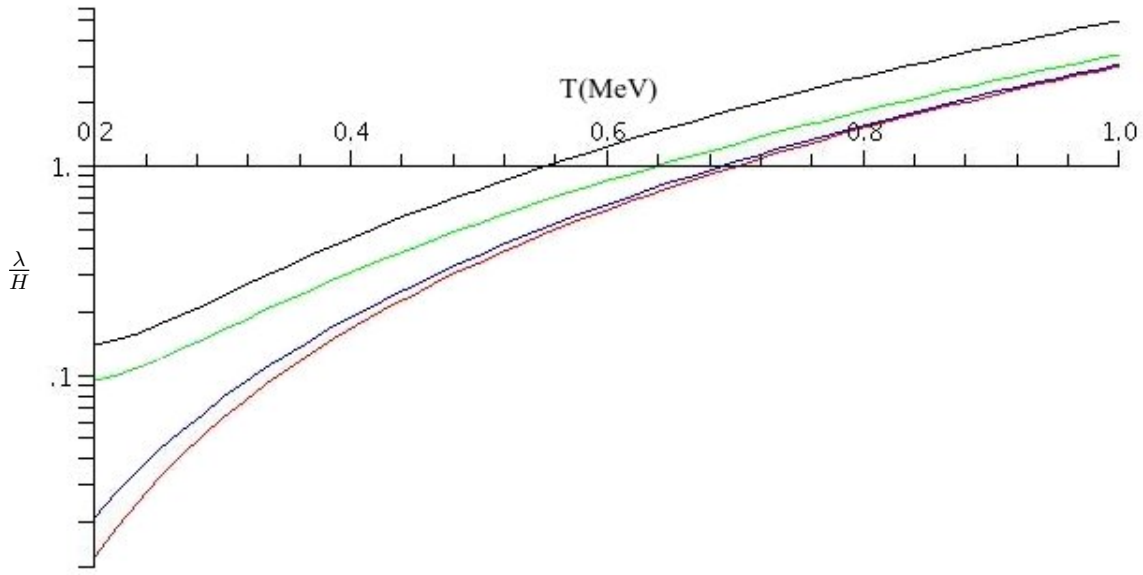

Figure 5.1: These curves are of the ratio $\frac{\lambda_{M\downarrow\to M\uparrow}+\lambda_{M\uparrow\to M\downarrow}}{H(T)}$, for various mass splittings Q, and with $\tilde{g}_A = 1$. Red for $Q = 0MeV$, blue for $Q = 0.511MeV$, and green for $Q = 1.29MeV$. The black curve is that of the ratio for protons and neutrons, not mesinos.

5.2 Calculating T_{MDS}

In order to correctly calculate T_{MDS}, we need to know when the rates of formation of mule deuterons falls out of chemical equilibrium, T_{MDF}. If this happens before

T_{MDS} then only a fraction of the mesinos will be bound into mule deuterons. If the freeze-out temperature is later than T_{MDS} the synthesis is described by the equations for a system in chemical equilibrium. If $T_{MDS} \approx T_{MDF}$ then it is necessary to solve the Boltzmann equations numerically. In practice we calculate T_{MDS} using the assumption that the system is in chemical equilibrium, then we confirm that $T_{MDS} > T_{MDF}$.

Since there are two ways of forming the mule deuteron, one through proton capture, the other through neutron capture, the Boltzmann equation is slightly more complicated than that of the standard deuteron.

$$\begin{aligned} \frac{dX_{MD}}{dT} &= -\frac{n_\gamma^{(0)}\langle\sigma_p v\rangle}{H(T)T}\left[\left(\frac{n_{MD}^{(0)}}{n_p^{(0)}n_{M\downarrow}^{(0)}}\right)X_p X_{M\downarrow} n_B - X_{MD}\right] \\ &\quad -\frac{n_\gamma^{(0)}\langle\sigma_n v\rangle}{H(T)T}\left[\left(\frac{n_{MD}^{(0)}}{n_n^{(0)}n_{M\uparrow}^{(0)}}\right)X_n X_{M\uparrow} n_B - X_{MD}\right]. \end{aligned} \tag{5.21}$$

The up and down arrows refer to the up and down isospin states for the mesinos and the subscripts on the cross section σ refers to photodisintigration of the neutron or the proton. To evaluate the quantity in the round brackets, we need the equilibrium

number density of the relevant species Eq. (A.7):

$$n_{MD}^{(0)} = 3\left(\frac{m_{MD}T}{2\pi^2}\right)^{3/2} e^{-m_{MD}/T} \tag{5.22}$$

$$n_{M}^{(0)} = 2\left(\frac{m_{M}T}{2\pi^2}\right)^{3/2} e^{-m_{M}/T} \tag{5.23}$$

$$n_{N}^{(0)} = 2\left(\frac{m_{N}T}{2\pi^2}\right)^{3/2} e^{-m_{N}/T}. \tag{5.24}$$

This means:

$$\left(\frac{n_{MD}^{(0)}}{n_{N}^{(0)}n_{M}^{(0)}}\right) n_B = \frac{3}{4}\left(\frac{2\pi}{Tm_N}\right)^{3/2} e^{\frac{-m_{MD}+m_M+m_N}{T}} n_B, \tag{5.25}$$

The exponential term for the lighter pair of nucleon mesino masses is:

$$-m_{MD} + m_M + m_N = B.E., \tag{5.26}$$

where BE is the absolute value of the binding energy of the mule deuteron. While the heavier isospin combination satisfies:

$$-m_{MD} + m_M + m_N = B.E. + |\delta_M|. \tag{5.27}$$

The source of this complication is the difference in energy required to disintegrate a mule deuteron into the two possible isospin configurations. A cartoon of this transition

is shown in figure (5.2).

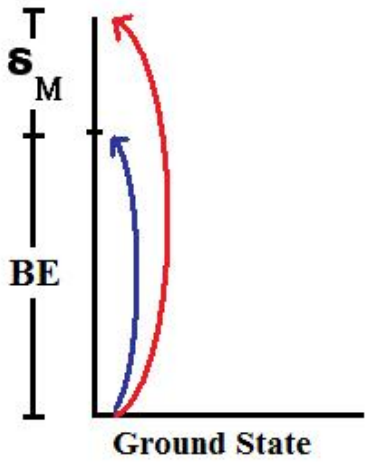

Figure 5.2: The energy required to break the mule deuteron into the lighter isospin combination is indicated by the blue arrow, while the transition to the heavier combination is indicated by the red arrow.

In the case of sbottom mesinos, where $\delta_M < 0$, the Boltzmann equation becomes:

$$\begin{aligned}\frac{dX_{MD}}{dT} &= -\frac{n_\gamma^{(0)}\langle\sigma_p v\rangle}{H(T)T}\left[\left(\frac{3}{4}\left(\frac{2\pi}{Tm_p}\right)^{3/2} e^{\frac{B.E.}{T}} n_B\right) X_p X_{M\downarrow} - X_{MD}\right] \\ &\quad -\frac{n_\gamma^{(0)}\langle\sigma_n v\rangle}{H(T)T}\left[\left(\frac{3}{4}\left(\frac{2\pi}{Tm_n}\right)^{3/2} e^{\frac{B.E.+|\delta_M|}{T}} n_B\right) X_n X_{M\uparrow} - X_{MD}\right].\end{aligned} \tag{5.28}$$

While in the stop case, where $\delta_M > 0$, the Boltzmann equation is:

$$\begin{aligned}\frac{dX_{MD}}{dT} &= -\frac{n_\gamma^{(0)}\langle\sigma_p v\rangle}{H(T)T}\left[\left(\frac{3}{4}\left(\frac{2\pi}{Tm_p}\right)^{3/2} e^{\frac{B.E.+|\delta_M|}{T}} n_B\right) X_p X_{M\downarrow} - X_{MD}\right] \\ &\quad -\frac{n_\gamma^{(0)}\langle\sigma_n v\rangle}{H(T)T}\left[\left(\frac{3}{4}\left(\frac{2\pi}{Tm_n}\right)^{3/2} e^{\frac{B.E.}{T}} n_B\right) X_n X_{M\uparrow} - X_{MD}\right].\end{aligned} \tag{5.29}$$

T_{MDS} is defined to be the temperature at which $X_{MD} \approx 1$. At first it seems as if we need to know the the relative strengths of the cross sections, σ_n and σ_p, however this is not the case. Since the nucleon and Mesino fractions are related by equation Eq. (5.4). This allows us to replace $X_n X_{M\uparrow}$ with $e^{-\frac{|\delta_M|}{T}} X_p X_{M\downarrow}$ when $\delta_M < 0$, or $X_p X_{M\downarrow}$ with $e^{-\frac{|\delta_M|}{T}} X_n X_{M\uparrow}$ when $\delta_M > 0$.

This causes Eq. (5.29) and Eq. (5.30) to become:

$$\begin{aligned}\frac{dX_{MD}}{dT} &= -\frac{n_\gamma^{(0)}\left(\langle\sigma_p v\rangle + \langle\sigma_n v\rangle\right)}{H(T)T} \\ &\quad \times\left[\left(\frac{3}{4}\left(\frac{2\pi}{Tm_n}\right)^{3/2} e^{\frac{B.E.}{T}} n_B\right) X_p X_{M\downarrow} - X_{MD}\right].\end{aligned} \tag{5.30}$$

When $\delta_M < 0$, and:

$$\begin{aligned}\frac{dX_{MD}}{dT} &= -\frac{n_\gamma^{(0)}\left(\langle\sigma_p v\rangle + \langle\sigma_n v\rangle\right)}{H(T)T} \\ &\quad \times\left[\left(\frac{3}{4}\left(\frac{2\pi}{Tm_n}\right)^{3/2} e^{\frac{B.E.}{T}} n_B\right) X_n X_{M\uparrow} - X_{MD}\right],\end{aligned} \tag{5.31}$$

when $\delta_M > 0$.

From here we can extract the equations for the abundance of mule deuterons in chemical equilibrium: When $\delta_M < 0$

$$\begin{aligned} X_{MD} &= \left(\tfrac{3}{4}\left(\tfrac{2\pi}{Tm_n}\right)^{3/2} e^{\frac{B.E.}{T}} n_B\right) X_p X_{M\downarrow} \quad , \quad \delta_M < 0 \\ &= \left(\tfrac{3}{4}\left(\tfrac{2\pi}{Tm_n}\right)^{3/2} e^{\frac{B.E.}{T}} n_B\right) X_n X_{M\uparrow} \quad , \quad \delta_M > 0. \end{aligned} \tag{5.32}$$

To solve for X_{MD} as a function of temperature we must remove the dependence of X_M from the previous two equations. This is done by using the definition of the mesino fractions:

$$1 \equiv X_{MD} + X_{M\downarrow} + X_{M\uparrow}. \tag{5.33}$$

Here we ignored the synthesis of more complex mule nuclei. Substituting in Eq. (5.4) results in:

$$\begin{aligned} 1 - X_{MD} &= X_{M\downarrow}\left(1 + \tfrac{X_p}{X_n} e^{\frac{\delta_M}{T}}\right) \quad , \quad \delta_M < 0 \\ &= X_{M\uparrow}\left(1 + \tfrac{X_n}{X_p} e^{-\frac{\delta_M}{T}}\right) \quad , \quad \delta_M > 0. \end{aligned} \tag{5.34}$$

Substituting Eq. (5.32) into the previous equations allow us to solve for X_{MD}:

$$X_{MD} = \frac{\xi}{1+\xi}, \tag{5.35}$$

where,

$$\begin{aligned} \xi &= \frac{\left(\frac{3}{4}\left(\frac{2\pi}{Tm_n}\right)^{3/2} e^{\frac{B.E.}{T}} n_B\right) X_p}{\left(1+\frac{X_p}{X_n} e^{\frac{\delta_M}{T}}\right)} \quad , \quad \delta_M < 0 \\ &= \frac{\left(\frac{3}{4}\left(\frac{2\pi}{Tm_n}\right)^{3/2} e^{\frac{B.E.}{T}} n_B\right) X_n}{\left(1+\frac{X_n}{X_p} e^{-\frac{\delta_M}{T}}\right)} \quad , \quad \delta_M > 0. \end{aligned} \tag{5.36}$$

It is interesting to note from this equation that, while the mass splitting δ_M is important when it comes to the freeze-out temperatures of the rates, it does not have a very large impact on the freeze-out temperature of the mule deuterons. In fact, because of the exponential dependence of the ratio on $\frac{B.E.}{T}$, the rate will not be affected much by proton or neutron faction either.

We plot T_{MDS} as a function of the mule deuteron's binding energy under the conditions, $X_{MD} = 0.1, 0.5, 0.9$. This translates to $\xi = \frac{1}{9}, 1, 9$. Figures 5.3 and 5.4 show the results for the two expected mass splittings. In the case of the sbottom mesino, we expect the isospin splitting to be on the order $m_{M^0} - m_{M^+} \in [0MeV, 0.6MeV]$ this means $\delta_M \in [-0.7MeV, -1.3MeV]$. In the case of the stop mesino we expect $\delta_M \in [3.4MeV, 3.6MeV]$.

5.3 Photodisintigration Freeze-Out Temperature

We were able to plot the mule deuteron synthesis temperature as a function of its binding energy under the assumption that the reactions involved were fast enough

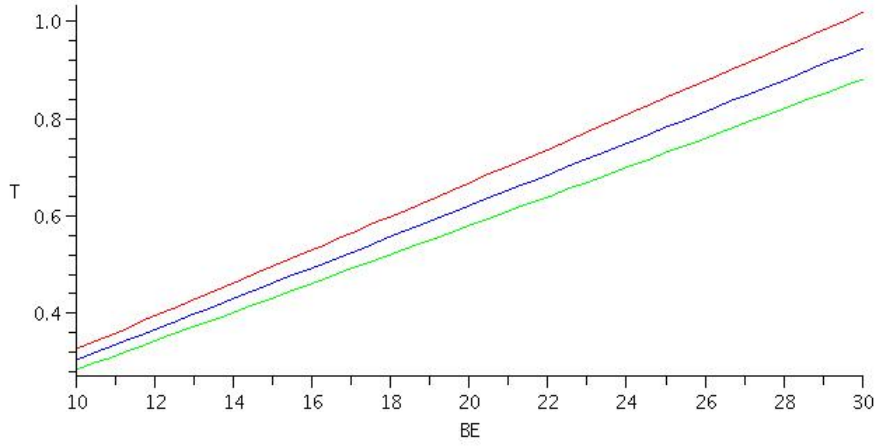

Figure 5.3: This plot shows T_{MDS} as a function of the mule deuteron binding energy for the case of $\delta_M = -1MeV$. The red curve corresponds to the temperature at which $X_{MD} = 0.1$, the blue curve to $X_{MD} = 0.5$, and the green curve to $X_{MD} = 0.9$.

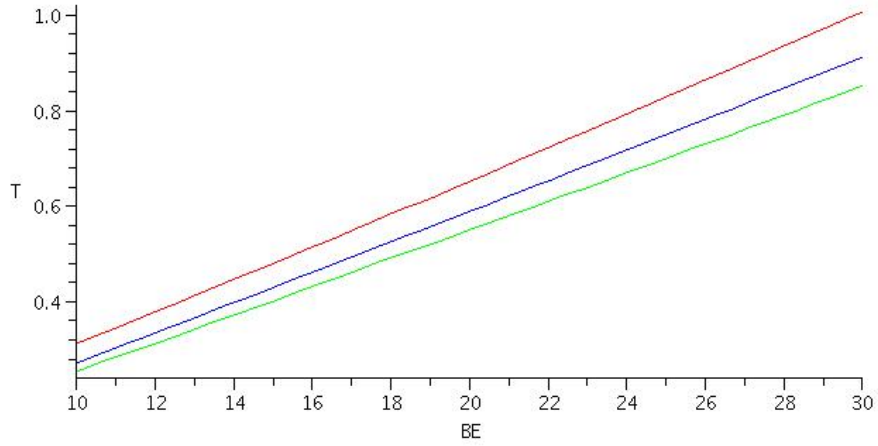

Figure 5.4: This plot shows T_{MDS} as a function of the mule deuteron binding energy for the case of $\delta_M = 3.6MeV$. The red curve corresponds to the temperature at which $X_{MD} = 0.1$, the blue curve to $X_{MD} = 0.5$, and the green curve to $X_{MD} = 0.9$.

to keep the mesinos and mule deuterons in chemical equilibrium. However it is now necessary to justify this assumption.

Here we will estimate the photodisintegration rate of the mule deuteron just before BBN. We will show that even if we are off by a factor of 100 the rate freeze-out will occur below T_{MDS}. That is, the mule deuterons will have formed before the synthesis rate freezes out.

We calculate an upper bound on the mule deuteron photodisintegration cross section in Appendix D. It is found to be:

$$\sigma > \frac{8\pi}{27}\alpha\frac{m\left(2m(\omega-BE)\right)^{\frac{3}{2}}\omega}{\kappa^7}\frac{2}{5}\left(5.4\right)^2. \tag{5.37}$$

ω is the energy of the incident photon, $\kappa=\sqrt{2mBE}$, and BE is the absolute value of the binding energy.

The minimum photodisintegration rate is:

$$\begin{aligned} n_\gamma\langle\sigma v\rangle &= \int \sigma dn_\gamma & (5.38)\\ &= \frac{1}{\pi^2}\int_x^\infty \sigma\omega^2 e^{-\omega/T}d\omega & (5.39)\\ &> \frac{0.273\alpha}{m}\frac{T^5\sqrt{T}}{BE^3\sqrt{BE}}\int_{x/T}^\infty\left(u-\frac{BE}{T}\right)^{\frac{3}{2}}u^3e^{-u}du & (5.40)\end{aligned}$$

The lower limit on the integral in Eq. (5.40) is the minimum energy required to eject

a proton from the mule deuteron. When $\delta_M < 0$, $x = BE$. However when $\delta_M > 0$ the photon must overcome the rest mass difference, this means $x = BE + \delta_M$. This will have a large impact on the cross section in the case of stop mesinos. When $\delta_M < 0$ the photodisintegration rate is:

$$\begin{aligned} n_\gamma \langle \sigma v \rangle &> \frac{0.0527}{m} \frac{T^5 \sqrt{T}}{BE^3 \sqrt{BE}} e^{-\frac{BE}{T}} \\ &\left(315 + 210 \frac{BE}{T} + 60 \left(\frac{BE}{T} \right)^2 + 8 \left(\frac{BE}{T} \right)^3 \right). \end{aligned} \tag{5.41}$$

When $\delta_M > 0$ we will leave the cross section in its integral form for concision:

$$n_\gamma \langle \sigma v \rangle = \frac{0.273\alpha}{m} \frac{T^5 \sqrt{T}}{BE^3 \sqrt{BE}} \int_{(BE+\delta_M)/T}^{\infty} \left(u - \frac{BE}{T} \right)^{\frac{3}{2}} u^3 e^{-u} du. \tag{5.42}$$

Eq. (5.41) and Eq. (5.42) give the rates at which mule deuterons are destroyed. Their rate of formation can be found using Eq. (5.30) and Eq. (5.31):

$$\begin{aligned} \lambda_{MD} &= n_\gamma^{(0)} \left(\langle \sigma_p v \rangle + \langle \sigma_n v \rangle \right) \left(\tfrac{3}{4} \left(\tfrac{2\pi}{T m_n} \right)^{3/2} e^{\frac{BE}{T}} n_B \right) X_p X_{M\downarrow} \qquad \delta_M < 0 \\ &= n_\gamma^{(0)} \left(\langle \sigma_p v \rangle + \langle \sigma_n v \rangle \right) \left(\tfrac{3}{4} \left(\tfrac{2\pi}{T m_n} \right)^{3/2} e^{\frac{BE}{T}} n_B \right) X_n X_{M\uparrow} \qquad \delta_M > 0. \end{aligned} \tag{5.43}$$

Note the inclusion of the terms $X_p X_{M\downarrow}$ and $X_n X_{M\uparrow}$ in these equations. The fractions $X_{M\downarrow}$ and $X_{M\uparrow}$ vary considerably depending on δ_M. We expressed the rates in Eq. (5.43) in such a way that, regardless of the sigh of δ_M, the mesino fraction in the

equation is of order of 0.5 as long as $X_{MD} \ll 1$.

The temperature at which the formation rate freezes out is found when λ_{MD} drops below $H(T)$. Using the lower bound for the rate, we replace $(\langle\sigma_p v\rangle + \langle\sigma_n v\rangle)$ with our approximation of $\langle\sigma_p v\rangle$. Solving the condition $\lambda_{MD}(T) = H(T)$ numerically generates the following bound on T_{MDF}. When $\delta_M = -1MeV$, the freeze-out temperature is less than $0.01MeV$, for any binding energy in the interval $[10MeV, 30MeV]$. Even if the cross section is reduced by a factor of 100 the freeze-out temperature is less than $0.08MeV$.

The case of $\delta_M = 3.6MeV$ is not quite so simple. The large positive value of δ_M generates a relative mesino fraction $X_{M\uparrow} \approx e^{\delta_M/T} X_{M\downarrow}$. Proton capture is heavily suppressed due to the vast majority of free mesinos being in the up isospin state. If proton capture were the sole mechanism of mule deuteron formation, then the rate would freeze-out at $T = 0.36MeV$. This temperature rises to $0.6MeV$ if the cross section is reduced by a factor of 100.

At this point it is important to take into account the possibility of neutron capture as it will become the dominant mechanism of mule deuteron formation. Unlike the proton capture rate, the neutron capture rate will not be suppressed by the exponential $\exp\left(\frac{\delta_M}{T}\right)$. This is because the fraction of up mesinos is not exponentially suppressed relative to the down mesinos.

Even if the neutron ejection cross section is a factor of α^2 smaller than the proton

capture cross section, T_{MDF} is well below T_{MDS} as seen in figure 5.5

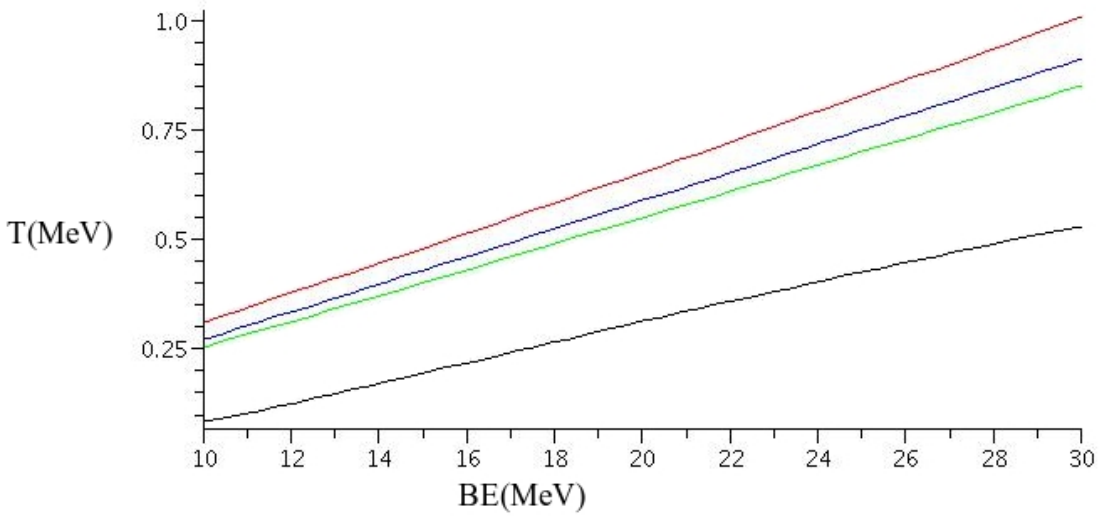

Figure 5.5: This plot shows T_{MDS} as a function of the mule deuteron binding energy for the case of $\delta_M = 3.6MeV$. The red curve corresponds to the temperature at which $X_{MD} = 0.1$, the blue curve to $X_{MD} = 0.5$, and the green curve to $X_{MD} = 0.9$.The solid black curve is the estimated T_{MDF} were neutron capture is the dominant formation channel of the mule deuteron.

5.4 Remarks on Mule Deuterium Synthesis

In this chapter we have shown how the mesino isospin ratio is coupled to the proton-neutron ratio. Using the mesino isospin ratio we were able to calculate the fraction of mesinos bound into mule nuclei as a function of temperature.

Strictly speaking CBBN does not have to wait until the mule deuterons are completely stable before further reaction rates can take place. It merely requires that the mule deuteron exist long enough for ambient nucleons to bind to it. This means

that T_{MDS} is actually a slight lower bound on the temperature where further mesino-nucleosynthesis will begin. Depending on the binding energy of the MN^2 system, mesino nucleosynthesis may take off before X_{MD} even reaches 0.1.

Chapter 6

Nucleosynthesis Scenarios With Mule Nuclei

Depending on the binding energies and reaction rates of mule nuclei, mule nucleosynthesis can take drastically different paths. In this chapter we introduce the three qualitatively different scenarios that are possible and discuss which is most likely to occur.

The first scenario is when the growth of the mule nuclei is stalled by the lack of an MN^A bound state for a specific value of A. If this gap exists then it will be impossible for a mesino to capture more than $A-1$ nucleons through reactions of the form (N, γ), where N is either a neutron or proton. This means the mule nuclei will have to wait until compound nuclei have formed in order to get past this bottleneck.

The second scenario is where the growth of mule nuclei is stalled by (N, α) reactions leading to the catalysed production of α particles. In this scenario the mule nuclei grow until the Q-value of an (N, α) reaction becomes positive. The ejected mule nuclei lose three nucleons and start the cycle of capturing them over. For a given nucleus it is possible for the (N, α) rate to be much larger than the (N, γ) rates. In this case the mule nucleus will be stuck in an α producing cycle until one of the rates involved drops bellow the Hubble rate, or the neutrons all become bound into ^4He at T_d. We discuss how the binding energy of a mule nucleus will determine whether or not a given mule nucleus is more likely to gain a nucleon or eject an α particle.

The last scenario is when the mule nuclei simply grow. This becomes possible if there are no gaps in the mule nuclear binding energy, and the (N, α) rates remain smaller than the nucleon capture rates. The Coulomb barrier is the controlling factor of this process. Eventually the charge of the mule nuclei will become so large that proton capture reactions (p, γ), and proton exchange reactions (p, n) freeze out. We will calculate at what charge this is likely to occur.

In the last part of this chapter we discuss how we expect mule nucleosynthesis to occur. We will explain the difficulties that arise when trying to calculate the spectrum of binding energies and which spectra are most likely to describe the mule nuclei.

6.1 The Effect Of Gaps In The Binding Energies

The concept of a bottleneck is not new in BBN, as the small deuterium binding energy prevents ^4He from forming despite the fact that it is stable at temperatures larger than T_d. The same effect can occur in the synthesis of mule nucleons.

If there is no nucleus of the form MN^A with binding energy larger than that of the deuteron then MN^{A-1} is the largest mule nuclei that can form pre-T_d. Since the reactions that generate MN^A are nucleon capture, the relation that describes the relative abundances of mule nuclei is:

$$X_A \approx \eta \left(\frac{T}{m_N}\right)^{3/2} \exp\left(\frac{Q}{T}\right) X_{A-1}. \tag{6.1}$$

This is the solution to the Boltzmann equation for a reaction in chemical equilibrium. If the binding energy is less than the deuteron's, the exponential in Eq. (6.1) will not be able to overcome the small value of η pre-T_d.

A break in the binding energy can make it difficult for the mule nucleus to capture α particles post T_d. Reactions of the form (α, N) and (α, d) are unlikely to be exothermic. The mule nuclei may be able to capture an α particles through an (α, γ) reaction, however at temperatures below T_d the coulomb repulsion may push this rate below the Hubble rate.

We mentioned earlier the lack of stable nuclei with $A = 5$, and $A = 8$. It is

natural to wonder if similar breaks occur in the spectrum of mule nuclear binding energies. The lack of a bound state for $A = 5$ nuclei is partially due to the fact that ^4He is so deeply bound. The protons and neutrons are spin $\frac{1}{2}$ fermions, meaning four is the largest number of nucleons that can occupy the ground state simultaneously. The constituents of the ^4He nucleus form a closed nuclear shell in a similar way that electrons can form closed shells in the noble gases.

The same effect could occur in the mule nucleus MN^4. If the five particles are deeply bound, it may not be energetically favourable for them to capture a fifth nucleon. In this case mule nucleosynthesis would be unable to catalyse α production, or become larger than MN^4 pre-T_d. We will see in the section 7.5 that the decay of the squark may produce high energy ^3He or T, allowing the formation of ^6Li

If the mesino is able to capture at least six nucleons, then it becomes possible for the squark's decay to result in the production of a ^6Li nucleus. A similar mechanism could generate observable amounts of pripordial ^9Be and B. We will discuss the experimental signature of these ejected remnants in section 7.6.

6.2 α production

In this section we study catalysed α production in mule nucleosynthesis. For certain standard elements, the (N, α) reaction is the dominant destructive channel. We will determine when this occurs in standard elements and generalise it to mesinos. We

then approximate the maximum number of α particles generated before T_d.

6.2.1 Relative Rate Size

Ignoring the weak interaction, the important reactions in the pre-T_d universe are (N,γ), (γ,N), (N,α), (n,p), (p,n). Note that the reverse of the (N,α) reaction does not occur at temperatures above T_d due to the small abundance of α particles. Three factors affect the relative sizes of these rates, the number density of incident particles on a nucleus, whether or not a reaction is exothermic, and whether or not the reaction requires the emission of a photon.

Assuming the nucleus has a large enough binding energy so that nucleons are not ejected through photodisintegration, the rates we are most interested in are the (N,γ), and (N,α) rates. The protons and neutrons have similar abundances pre-T_d and both the previous rates involve an incident nucleon. This means the number density of incident particles will not affect relative sizes of the rates. There are now two competing effects that must be taken into account. The (N,γ) rate requires the emission of a photon, implying a smaller cross section. However the (N,α) process is not always exothermic.

In this naive model of nuclear rates one expects the (N,α) rates to dominate the (N,γ) rates whenever (N,α) is exothermic. However this model ignored the impact of nuclear structure and Coulomb repulsion. In order to see how nuclear rates scale

in standard nuclei we plot the relative sizes of α producing rates relative to the other nucleon induced rates. There are six reactions we compare, they are (n,γ), (p,γ), (n,p), (p,n), (n,α) and (p,α). We are only interested in the relative sizes of the maximum α producing rates to the capture rates. To express this simply we define the quantity $R(x_n,x_p,T)_\alpha$ for an element with x_n neutrons and x_p protons:

$$R(x_n,x_p,T)_\alpha \equiv \frac{X_n\lambda_{x_n,x_p}(n,\alpha,T)+X_p\lambda_{x_n,x_p}(p,\alpha,T)}{X_n(\lambda_{x_n,x_p}(n,\gamma,T)+\lambda_{x_n,x_p}(n,p,T))+X_p(\lambda_{x_n,x_p}(p,\gamma,T)+\lambda_{x_n,x_p}(p,n,T))}, \tag{6.2}$$

$\lambda_{x_n,x_p}(i,j,T)$ is the rate at which a nucleus with x_n neutrons and x_p protons captures a particle i, and emits a particle j. The numerical values of these rates are conveniently summarised in [20].

If $R(x_n,x_p,T)_\alpha > 1$, then an element is more likely to eject an α particle than grow in size or have one of its nucleons change isospin. We plot the values of $R(x_n,x_p,T)_\alpha$ for every stable element between ^{16}O and ^{34}S in figure 6.1. This figure shows how certain elements are dominated by alpha emission while others are not.

In order to see the correlation between binding energy and $R(x_n,x_p,T)_\alpha$, we plot the Q-values of the (N,α) reactions that convert the most stable element of size A to the most stable element of size $A-3$ in figure 6.2. The elements where (N,α) reactions dominate are marked in blue.

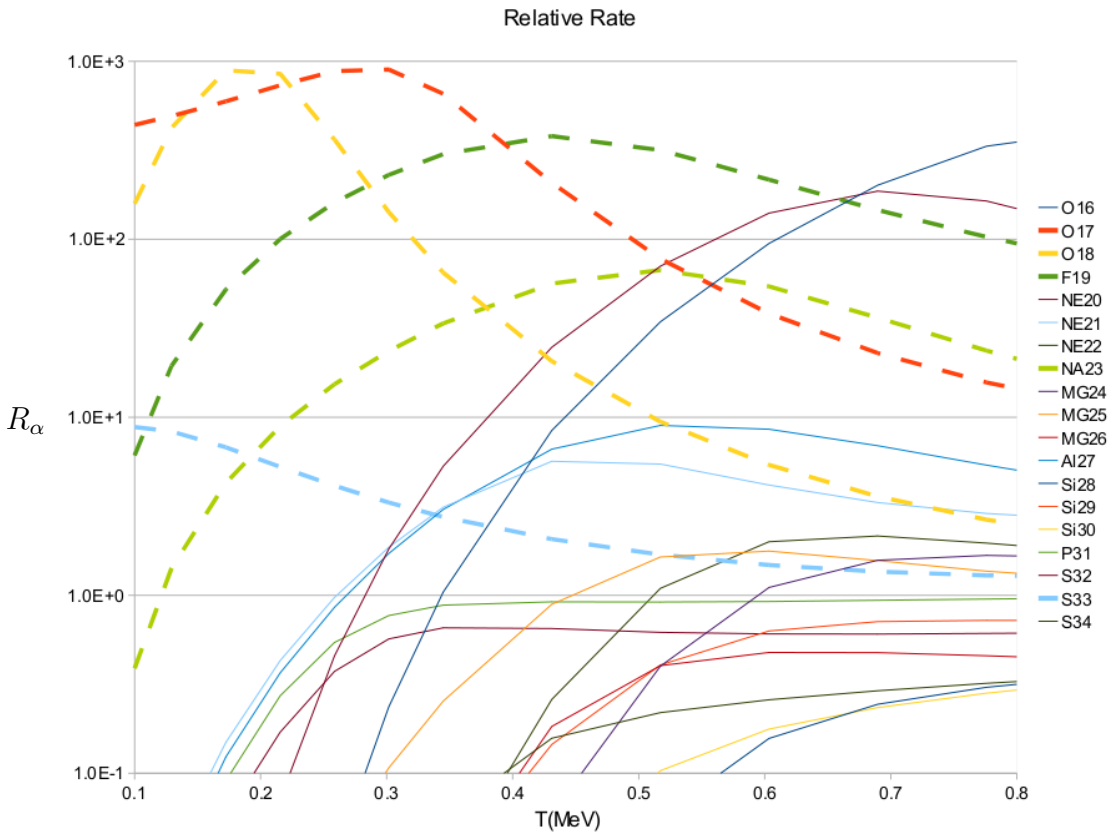

Figure 6.1: The relative rate of nucleon stimulated α emission compared to growth and isospin flipping reactions in standard nuclei.

Note that $R(x_n, x_p, T)_\alpha$ is not guaranteed to be larger than 1 whenever (N, α) is exothermic. This is most likely due to the fact that ejected α particles must tunnel through a Coulomb barrier before escaping the potential of the nucleus. When the Q-value of the reaction is small, the α particle will be heavily influenced by the Coulomb barrier. The cross section is expected to be suppressed by a factor:

$$\exp\left(-\pi\alpha Z_\alpha Z_1 \sqrt{\frac{2\mu}{E_\alpha}}\right), \tag{6.3}$$

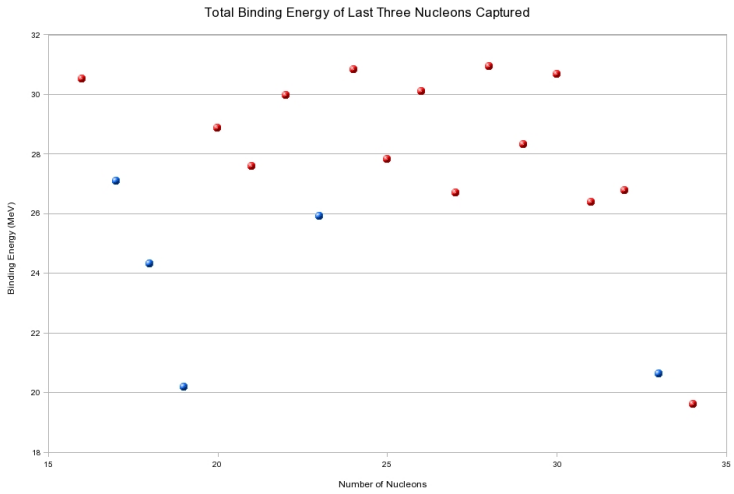

Figure 6.2: The binding energy gained by a nucleus from capturing three nucleons and forming the most deeply bound nucleus of size A from the most deeply bound nucleus of size $A-3$. (N,α) is exothermic for nuclei with points below $28.5MeV$. The blue points correspond to those nuclei where (N,α) dominates that nuclei's destruction channel.

$Z_\alpha = 2$, Z_1 is the charge of the remaining nucleus, and μ is the reduced mass of the α particle. When $Q \geq T$, the energy of the escaping α particle is $E_\alpha \approx Q$. The exponential suppression is approximately $\exp\left(-2Z_1\sqrt{\frac{MeV}{Q}}\right)$. If $Q = 1MeV$, and $Z_1 = 10$, this is becomes $\exp(-20)$. It is clear why a larger Z requires a larger Q for the (N,α) reaction in order to produce large amounts of helium.

We generalise these results to mule nuclei. For a weakly charged mule nucleus a positive Q-value for the (N,α) reaction is all that is required to begin emitting α particles. If the charge of the mule nuclei is large, on the order $Z > 10$, then the Q-value of the (N,α) reaction may need to be on the order of MeV to allow stimulated α emission to occur.

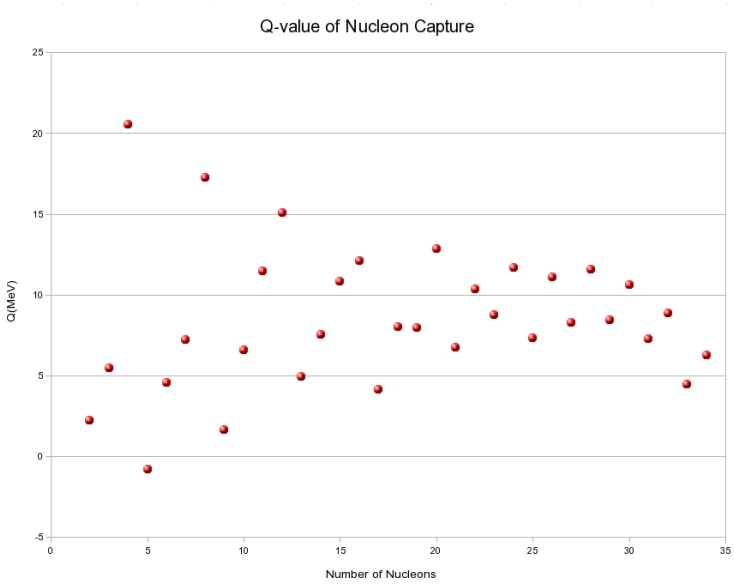

Figure 6.3: The binding energy gained by a nucleus from capturing a single nucleon and forming the most deeply bound nucleus of size A from the most deeply bound nucleus of size $A-1$. Note that after $N > 15$, the scatter in the binding energies decreases.

There is a complete list of the reactions (p,n), (N,γ), and (N,α) for the elements $8 \leq Z \leq 102$ compiled in [20]. For this reason we focus on the stable elements from ^{16}O to ^{34}S in our analysis. The lack of nuclei between ^{4}He and ^{15}N is not a major detractor to our study of nuclear rates due to the large fluctuations and gaps in the binding energy spectrum of these nuclei.

Figure 6.3 shows the binding energy gained through the capture of a single nucleon forming the most deeply bound nucleus of size A from the most deeply bound nucleus of size $A-1$. In the cases of ^{5}He and ^{8}Be where no bound state exists we used the resonance energy as a ground state of the nucleus. If there is a gap in the binding

energies then the (N, α) rates for ^7Li and ^7Be are dominant by default.

We expect the fluctuations in mule nuclear binding energies to be smaller than in standard nuclei. We have already discussed how nuclear binding energies in standard nuclei arise from a cancellation between a large kinetic and potential energy. When the reduced mass of a nucleon is doubled the kinetic energy term in the Shrödinger equation is halved. Due to the larger reduced mass, the binding energy in mule nuclei is the difference between a large number, the potential, and a significantly smaller number, the kinetic energy. This means we expect the mule nuclear binding energies to fluctuate less than those of standard nuclei for small A. We see in figure 6.3 that the binding energy of the captured nucleons stabilises considerably after $A = 13$ Therefore the nuclei between $A = 16$ to 34 are expected to be a better model of α emission for the mule nuclei than the nuclei in the range $A = 1$ to 12.

The α production process can constrain the possible distributions of mule nuclei. If there exists a mule nucleon number A such that the $MN^A(N, \alpha)MN^{A-3}$ rate is much larger than the nucleon capture rates of MN^A, then virtually all mule nuclei will be in the states MN^{A-1}, MN^{A-2}, and MN^{A-3}.

6.2.2 Maximum α Production

One of the reasons the (N, α) process is interesting is that the large capture rates make it possible for the mule nuclei to generate orders of magnitude more ^4He than the

relic abundance, pre-T_d. Here we will calculate an upper bound on this α production. In the next chapter we will estimate the maximum impact these α particles will have on primordial element abundances.

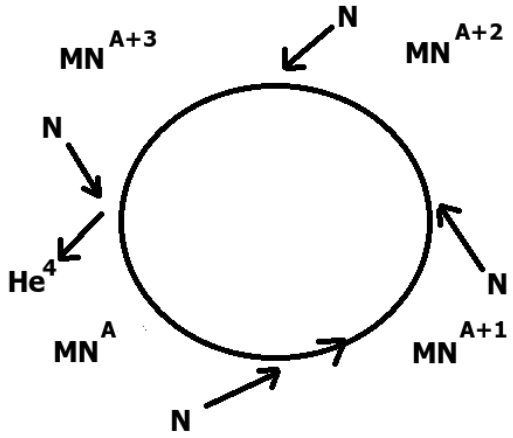

Figure 6.4: A cycle that can generate ^4He.

The cycle that generates the α particles is shown in Fig(6.4). The rate of α production in this cycle is controlled by the slowest step in the process. This means we can treat all but the slowest step in the cycle as infinite when calculating the amount of α particles produced. The α fraction is therefore:

$$\frac{dY_\alpha}{dT} \leq -\frac{n_M \langle \sigma v \rangle_{min}}{HT} X_N, \tag{6.4}$$

n_M is the mesino number density, and N is the nucleon captured in the slowest reaction. $n_M \langle \sigma v \rangle_{min}$ is the rate of the slowest reaction in the cycle in figure 6.4. In

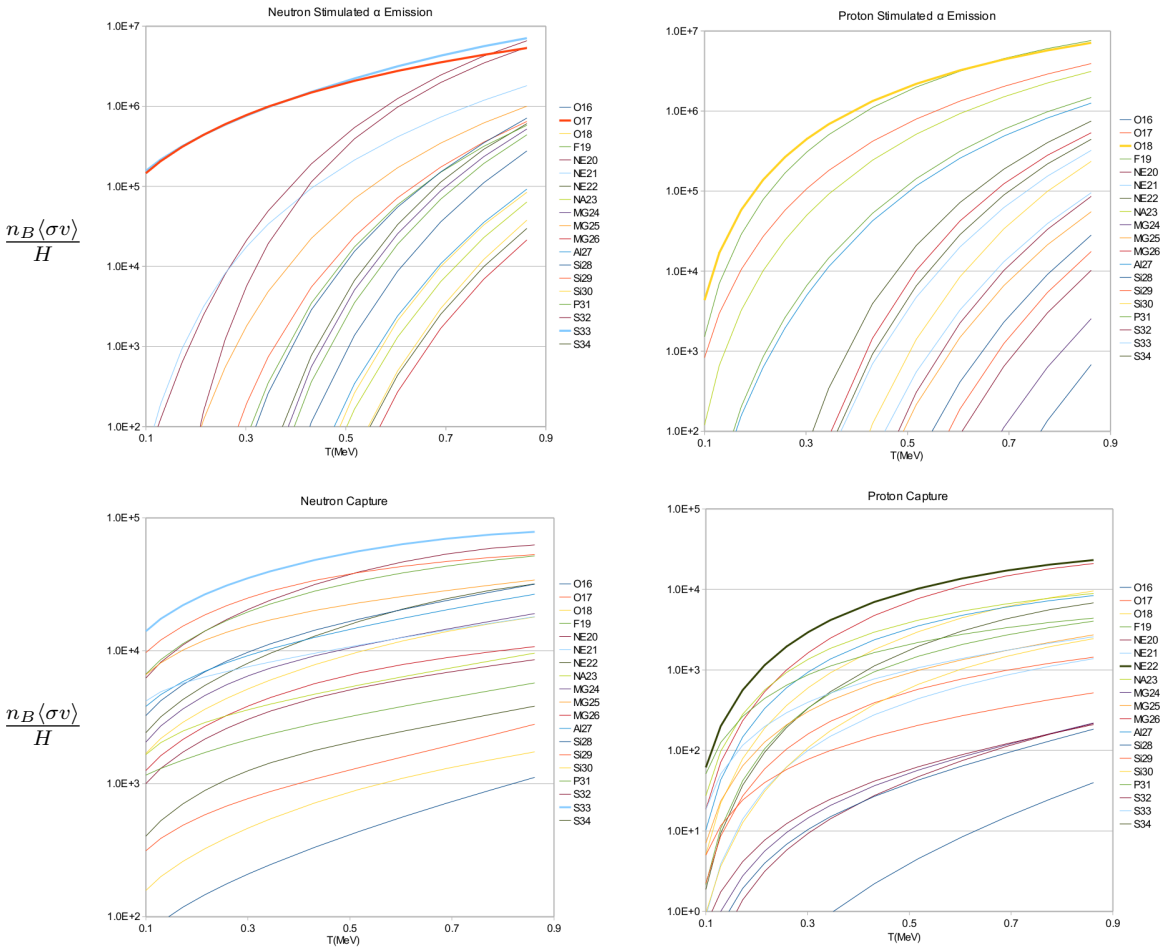

Figure 6.5: The relative sizes of the neutron and proton stimulated α emission rates (top) and the neutron and proton capture rates (bottom) divided by the Hubble rate. The maximum rates are plotted with thicker lines for visibility.

order to estimate an upper bound on α production we find the maximum rates for each step in the cycle and use the slowest of the four in our calculation of the ^4He abundance. The rates for (p,γ), (n,γ), (p,α), and (n,α) in the stable nuclei between $Z = 8$ and $Z = 34$ are plotted in figure (6.5).

The largest of each of these rates are summarised in Fig(6.6). The bottleneck

of this cycle is in the (p, γ) reaction. A possible enhancement to the formation of α particles is the capture of a neutron followed by the conversion of the neutron to a proton through a (p, n) reaction. This avoids the need for a $(p.\gamma)$ reaction in the cycle.

The (p, n) rates are plotted in Fig(6.7). At temperatures greater than approximately $0.3MeV$ this mechanism is more efficient than the (p, γ) channel. If the ^4He formed at temperatures larger than this, we would need to use the (p, n) mechanism. However we will soon show that the ^4He cannot begin forming until the temperature has dropped bellow $0.32MeV$.

Eq. (6.4) can be integrated, giving,

$$Y_\alpha \leq -\int_{T_0}^{T_d} \frac{n_M \langle \sigma v \rangle_{max}}{HT} X_N. \tag{6.5}$$

This integral can be done numerically however it requires we provide the temperature where helium starts being produced. The low temperature bound is T_d, below this temperature standard BBN converts virtually all the neutrons into ^4He. The upper bound on the temperature is more subtle. Naively the helium would be generated as soon as the photodisintegration rate drops below the Hubble rate. The photodisintegration rate of ^4He is on the order $1mb$ over the range $E_\gamma = 20 - 30MeV$ [21] and the energy required to break up ^4He is $19.8MeV$, this will allow the existence of stable

α particles as early as $T = 0.55MeV$.

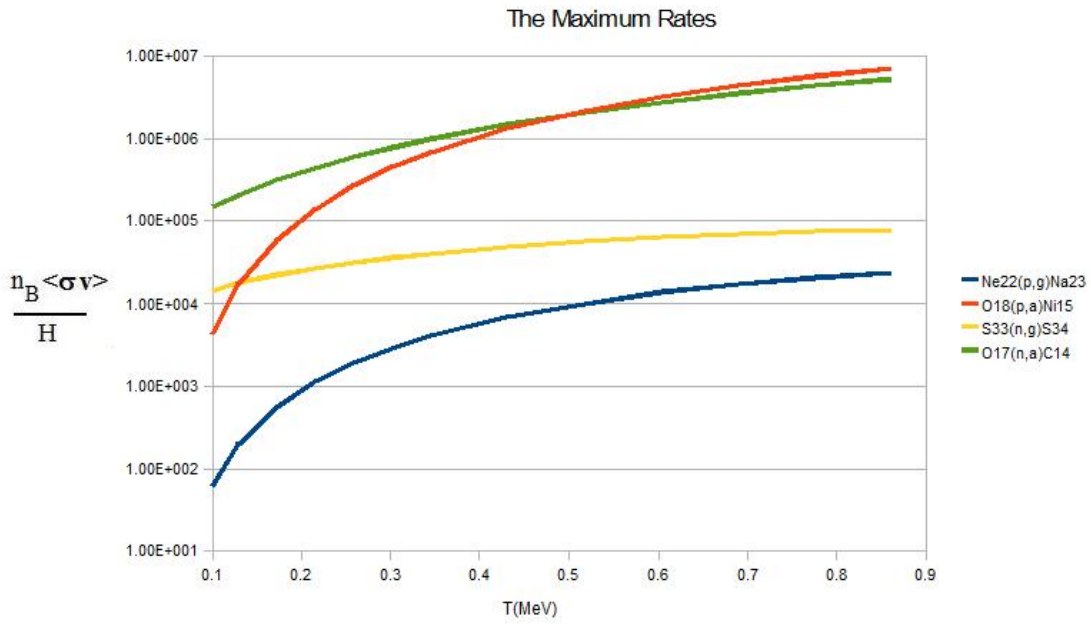

Figure 6.6: The maximum rates for the reactions of type (n, γ), (p, γ), (n, α), and (p, α). The proton capture rate is the weakest point in the process of α emission.

Despite the fact that ^4He is stable at $T < 0.55MeV$, this will not be the temperature at which the helium is synthesised. We cannot ignore the the fact that the reaction (N, α) must be exothermic for the cycle in figure 6.4 to function. This imposes a bottleneck on at least one of the nucleon capture rates in the catalysing process. Consider the reactions:

$$\begin{aligned} MN^{A-3} + N &\rightarrow MN^{A-2} + \gamma \quad Q_1 \\ MN^{A-2} + N &\rightarrow MN^{A-1} + \gamma \quad Q_2 \\ MN^{A-1} + N &\rightarrow MN^{A} + \gamma \quad Q_3 \end{aligned} \cdot \tag{6.6}$$

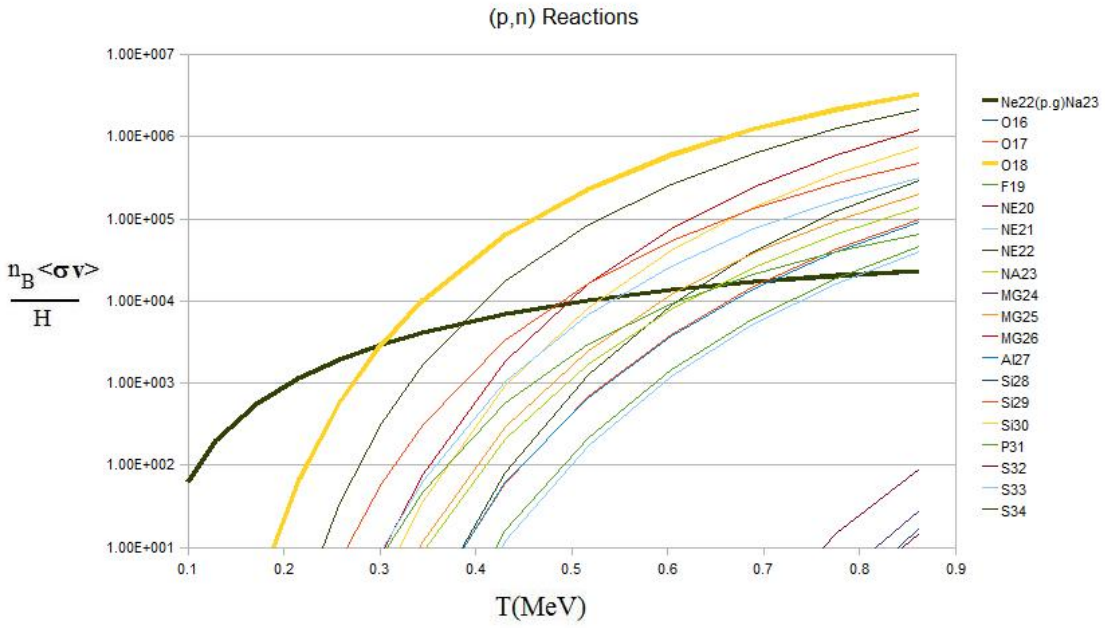

Figure 6.7: Plotted are the rates of a proton replacing a neutron in a nucleus. The thick green curve is the maximum proton capture rate and is plotted for easy comparison.

The largest possible value for $min\left[Q_1, Q_2, Q_3\right]$ is one third the binding energy of the α particle or $9.5MeV$. Otherwise the (N, α) reaction would not be exothermic.

As with the deuterium bottleneck, each step in 6.6 must overcome photodisintegration before helium catalysis can actually begin. The fact that the reactions are in equilibrium means we can use the results for T_{MDS} calculated in chapter 5 to estimate the temperatures where intermediate mule elements form. For a binding energy of $10MeV$, the fraction $X_{MN^{A+1}}/X_{MN^A} > 0.1$ when $T < 0.32MeV$. This is a realistic upper bound on the starting temperature of the Helium cycle. The integral in Eq.

(6.5) is:

$$Y_\alpha \leq \int_{T_d}^{0.32MeV} \frac{n_M \langle \sigma v \rangle_{max}}{HT} X_p. \tag{6.7}$$

$$= \frac{n_M}{n_B} 2 \times 10^2 \tag{6.8}$$

$$= 3 \times 10^{-7} \tag{6.9}$$

A plot of the abundance pre-T_d is show in figure 6.8. We will investigate the maximum effect these α particles have on BBN in the next chapter.

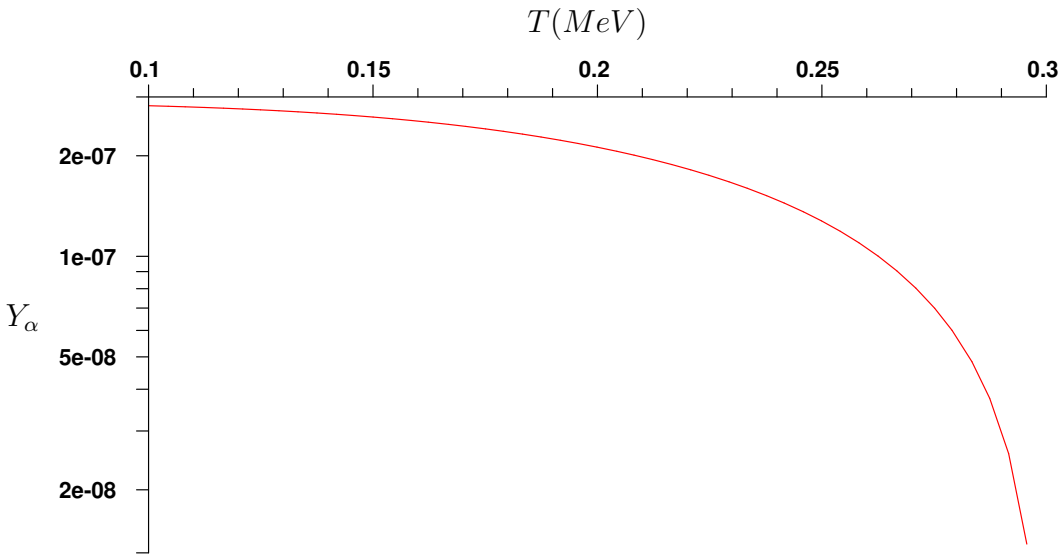

Figure 6.8: The plot shows the maximum size of Y_α generated by mesinos.

6.3 Maximum Growth

In the last scenario we dealt with the generation of large mule nuclei. If the mule nuclear binding energies are large enough to prevent the (N, α) processes from occuring, then the only thing controlling the number of nucleons a mesino can capture is the Coulomb barrier. The S-factor is a standard method of separating the nuclear and Coulomb physics in nuclear reactions. $S(E)$ is defined in terms of the cross section and the energy of the collision.

$$\sigma \equiv \frac{1}{E} S(E) e^{-2\pi Z_1 Z_2 \alpha \sqrt{\frac{m_n}{2E}}}, \tag{6.10}$$

E is the centre of mass energy and Z_1 and Z_2 are the charges of the two colliding particles [22].

For a given S-factor we will calculate how large the product $Z_1 Z_2$ has to be to force the reaction rate below the Hubble rate. This will give an estimate on the largest possible mule nucleus that can be formed during mule nucleosynthesis. If we treat the S-factor as a constant we get the following result for the velocity averaged cross section:

$$\langle \sigma v \rangle = \sqrt{\frac{8}{\pi}} \frac{1}{(m_N T)^{3/2}} S \int p dp e^{-\frac{2\pi Z \alpha m_N}{p} - \frac{1}{2}\frac{p^2}{m_N T}}. \tag{6.11}$$

The charges of the nuclei for which the (p, γ) rate drops below the Hubble rate is plotted in figure 6.9. We calculate this for the following S-factors, $10eV \cdot b$, $1keV \cdot b$, and $100keV \cdot b$.

The S-factor for proton capture fluctuates drastically over a wide range of magnitudes. The S factor in the range $0.1MeV$ to $1MeV$ for standard elements between ^6Li and ^{17}F vary from $O\left(10eV \cdot b\right)$ to $O\left(10^5 eV \cdot b\right)$. These values are taken from [22].

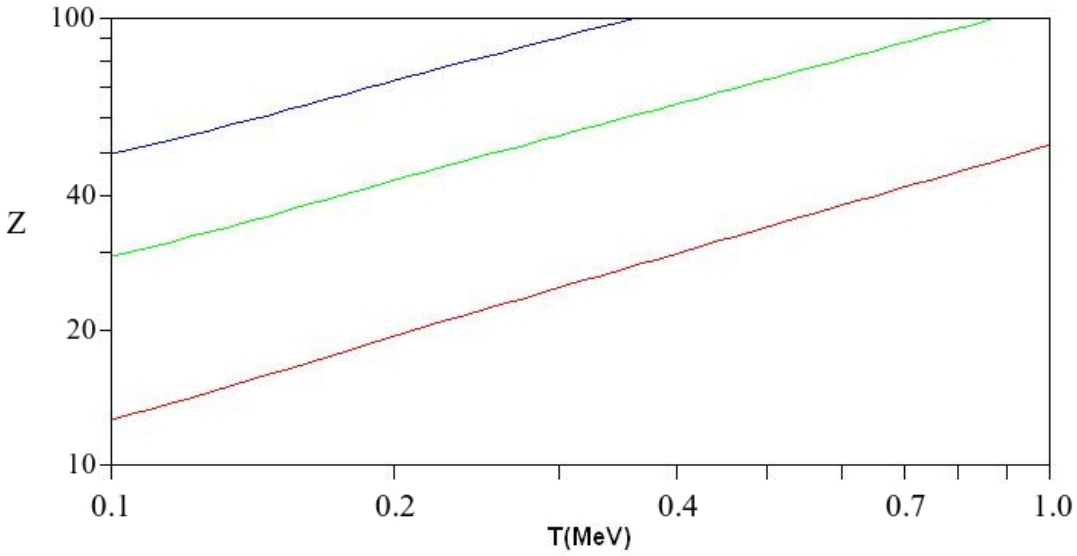

Figure 6.9: These curves show how large the charge of a mule nucleus, Z, must be for the coulomb interaction to force the proton capture rate to freeze out. The red curve is for a constant S-factor of $10eV \cdot b$, the green curve for $S = 1keV \cdot b$, and the blue for $S = 100keV \cdot b$.

The result of this calculation is that under certain conditions the mule nuclei can grow quite large. If the binding energies of the mule nuclei are large enough to prevent the (N, α) reactions, then the mule nuclei may be able to grow until the Coulomb

barrier causes the rate to freeze-out. Figure 6.9 shows us that even when the S-factor is as small as $10eV \cdot b$, it is still possible for the mule nuclei to grow to the charge $Z = 12$ pre-T_d. We will see in the next section why we expect α emission to prevent this. For this reason we do not look at possible ways around the Coulomb bottleneck such as the conversion of neutrons to protons through (p, n) or β decay reactions.

6.4 Mule Nuclear Binding Energies

The previous sections demonstrated the importance of the spectrum of binding energies of the mule nuclei in mule nucleosynthesis. In this section we will explain why it is not possible to calculate this spectrum, though it is possible to make certain general predictions about the spectrum.

6.4.1 Difficulties in Calculating Binding Energies

Even if someone invested a massive amount of time in an attempt to calculate the properties of these systems using effective field theory, the results would be virtually impossible to trust in mule nuclei more complicated than the mule deuteron. The uncertainties in the mesino-nucleon potential would be compounded as each nucleon was added to the system. In addition to the uncertainties that arise from the short distance behaviour of the nucleon-mesino potential, there are further complications

due to three-body forces.

In standard nuclei, only including the nucleon-nucleon potential in models of nuclei larger that deuterium leads to an underestimation of their binding energies [23]. For example, the predicted ^4He binding energy is approximately $5MeV$ too small. This error is only compounded in more complicated nucleons.

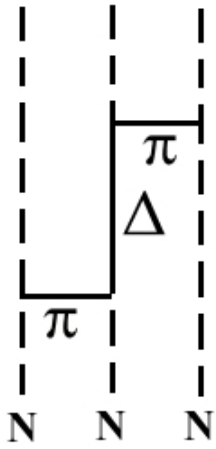

Figure 6.10: A three nucleon interaction that involves the Δ resonance.

Dealing with three nucleon forces in mule nuclei is non-trivial. An important contribution to three body interactions is due to the Δ resonance, an example of this effect is shown in figure 6.10. Even though mesinos have the same spin and isospin as nucleons, these similarities do not hold for the resonances. For example the mass difference between the Δ resonance and a nucleon is on the order of $300MeV$. Whereas the mass splitting between the lightest B mesons and their first resonance

B^* is on the order $45MeV$. If the spectrum of mesino resonances is similar to the B mesons', then the smaller mass difference implies the three-body effects may be more important in mule nuclei than in standard nuclei.

Another complication in this problem is that the shell structure of the mule nuclei will be different than that of standard nuclei. This is due to the fact that the Pauli exclusion principle will not affect the mesino as it does the other nucleons. These uncertainties make it virtually impossible to calculate accurate predictions for the spectrum of binding energies.

6.4.2 General Features

In the limit of large A we expect the mule nuclei to behave similarly to nuclei with sizes of approximately A nucleons. In particular, the binding energy gained by the capture of a nucleon should fluctuate around the average for such processes in standard nuclei of a similar size. This is because in a large mule nucleus the captured nucleon does not interact directly with the mesino. When a nucleon is outside the range of the mesino's potential the two particles cannot interact directly with one another, the nucleon's binding energy will arise from interactions with other nucleons. In this case the excess mass of the mesino does not help increase the binding energy of the system.

We estimate the range of the 1PE potential to be the inverse pion mass, or $\approx 1.4fm$. If we compare it to the proton charge radius, $\approx 0.88fm$ [2] we see that the

largest number of nucleons that can interact directly with the mesino is a shell one layer thick. Using classical geometry, the largest number of spheres that can be fit into this shell is 12, as shown in figure 6.11.

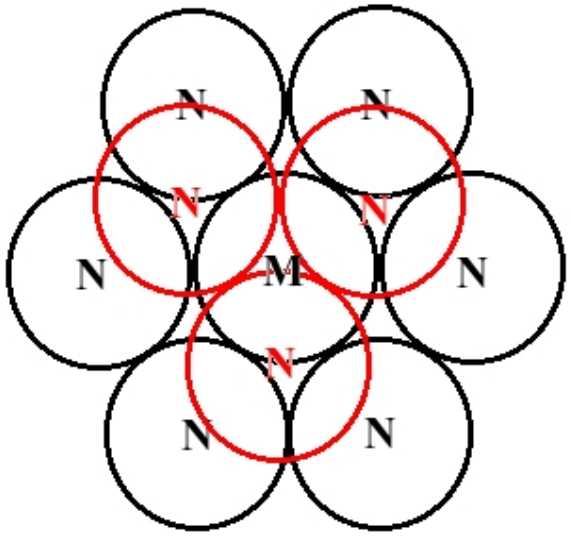

Figure 6.11: This is a cartoon picture of how nuclei could bind to the mesino to maximise binding energy. Captured nucleons in a mule nucleus could only interact directly with the mesino when there are no more than 12 nuclei there already.

This means the binding energy spectrum of mule nuclei larger than MN^{12} is expected to oscillate around a similar average as those of similar size in figure 6.3. The natural fluctuations in the binding energy makes it very likely an (N, α) rate will become dominant before the coulomb barrier is able to halt the (p, γ) reactions.

The issue remains of how to deal with the binding energies of the mule nuclei smaller than MN^{12}. As we have previously mentioned we expect some or all of these binding energies to be larger than those of standard nuclei. In the next chapter we will examine the various ways different binding energy spectra can affect BBN predictions.

6.5 Catalysed BBN after the deuterium bottleneck

There are very few ways for the mule nuclei to grow after the deuterium bottleneck has been overcome. The lack of neutral particles means the only proton and α reactions can allow the mule nuclei to grow. These protons could undergo reverse β decay, however this rate is slow. This slow rate and the coulomb barrier will eventually put a stop to mule nuclear growth.

The last step in mule nucleosynthesis is the decay of the squark. The fact that we do not observe the mesinos bound in nuclei today means that they must decay at some point.

The decay can affect BBN abundances in two ways. The first is by introducing energetic hadrons into the early universe. The second is the left-over nucleons that had been bound into mule nuclei. If the collection of nucleons decay to the ground state of a rare element then it is possible to generate an observable signature. These

scenarios will be discussed in the next chapter.

Chapter 7

Observable Signature Generated by Relics

There are now five mechanisms that may allow the mesinos to impact primordial abundances. They are:

- The weak interaction between mesinos and neutrinos affecting X_n.
- The catalysed production of α particles pre-T_d.
- The possible isospin flipping of standard nucleons by a mule nucleus.
- The decay of the squark generating a source of energetic ^3He and T.
- Large nuclear remnants can be ejected from the mule nucleus after the decay of the squark.

In this chapter we discuss the current experimental bounds on highly constrained light elements. We then show that only the last mechanism listed is able to affect these constraints or abundances.

7.1 Constraints On Primordial Abundances

The elements that are most sensitive to the mesino's influence are those for which there are stringent constraints on their primordial abundances.

For ^6Li, with its unexplained abundance, we look to the mesinos for a possible explanation. The strict constraints on the abundances of ^9Be and B may in turn provide a constraint on the mesino abundance. The abundances of these elements are summarised in table 7.1. The ^7Li fraction is a well known result summarised in [24]. The ^6Li fraction has been summarised in [25]. Due to uncertainties in how stars burn the isotope we are left with a range of abundances. A conservative upper bound on the fraction $^6Li/^7Li$ is 0.66. The observed abundance in population II stars is on the order $0.03 \leq^6 Li/^7Li \leq 0.07$, as discussed in [26]. A constraint on the primordial abundance of ^9Be is discussed in [27], where they find a 3σ upper limit of $^9Be/H \leq 2.1 \times 10^{-13}$.

The upper bound on boron is discussed in [28]. Observations of boron in metal poor stars shows no evidence of a primordial abundance. If boron were only produced through standard BBN channels then this negative result is expected. Ignoring stellar

processes that may destroy or dilute primordial boron, [28] produces a constraint on the primordial abundance of $\frac{B}{H} < 10^{-12}$.

Nuclei		Fraction	Source
$^6Li/^7Li$	$\leq$	0.66	[25]
	$\geq$	0.03	[26]
$^7Li/H$	$=$	1.7×10^{-10}	[24]
$^9Be/H$	$\leq$	2.1×10^{-13}	[27]
B/H	$\leq$	10^{-12}	[28]

Table 7.1: The constraints on the primordial abundances of rare elements.

7.2 A Direct Impact On X_n

Before dealing with complicated nuclear processes we examine a mechanism that may impact the neutron fraction. In the case where, $0 < m_{M\downarrow} - m_{M\uparrow} < m_n - m_p$, it is possible for the mesinos to alter the neutron abundance after the nucleon-weak isospin mixing rate has frozen out. This mechanism works if the mesino-weak reactions stay in chemical equilibrium longer than the nucleon-weak rates. The reaction network of interest is:

$$n + M_\uparrow \rightarrow p + M_\downarrow \tag{7.1}$$

$$M_\downarrow \rightarrow M_\uparrow \tag{7.2}$$

$$n + M_\uparrow \rightarrow p + M_\downarrow. \tag{7.3}$$

The step in Eq. (7.2) is mediated by the weak reactions like in Eq. (5.9). To test the feasibility of this mechanism we plot the relative size of the weak rates for mesinos and nucleons. If the mesino-weak rate is significantly greater than the nucleon-weak rate before the mesinos are bound into mule deuterons, then it is possible for this to alter the neutron fraction X_n.

In section 5.1.1 we calculated the relative size of the weak rates to the Hubble rate. Figure (5.1) showed that for mass splittings in the range of interest, the mesino weak rate is invariably smaller than the nucleon weak rate. A larger axial vector coupling to the mesino could push the mesino rate above the nucleon rate, however this will not impact the fraction X_n nearly enough to be observable.

We will estimate the minimum size the weak mesino rate, λ_W, must have for this mechanism to generate an observable impact on the neutron abundance. Approximating the uncertainty in X_n as 1%, implies the weak process must convert at least $0.01X_n$ neutrins to protons by T_d. The same process used to calculate the amount of Helium produced pre-T_d in Eq. (6.5) can be used to estimate how large the fraction λ_W/H must be to generate an observable signature. Assuming the nucleon-mesino interactions are infinitely fast, the relationship between the neutrons converted to protons and the weak rate is:

$$0.01X_n \;\leq\; -\int_{T_f}^{T_d} \frac{n_M \lambda_W}{n_B H T} dT, \tag{7.4}$$

T_f is the tempereature at which the nucleon weak rates freeze out. Remember that the density fraction for the mesinos is a very small parameter, $\frac{n_M}{n_B} = 4 \times 10^{-10}$. Lastly, if we approximate the ratio λ_W / H to be constant, we can solve for it easily,

$$\frac{\lambda_W}{H} \geq 2.5 \times 10^6 \ln \left(\frac{T_f}{T_d} \right)^{-1}. \tag{7.5}$$

This shows that the weak mesino rate must be roughly six orders of magnitude larger than the Hubble rate, something that is simply not possible. We conclude that there is no observable impact on the n-p freeze out ratio.

7.3 Catalysed α Production

In section 6.2 we calculated how much ^4He could form before the deuterium bottleneck. We calculated an upper bound of $Y_\alpha \leq 3 \times 10^{-7}$.

Despite the early source of α particles it is actually somewhat difficult for complex elements to form. The strong binding of ^4He and the absence of stable $A = 5$ and $A = 8$ nuclei make generating large elements difficult. The only way for the catalysed helium to leave an observable impact on primordial abundances is for it to generate elements that are extremely rare. The first step in this process is the generation of the elements between $A = 5$ and $A = 8$. That is ^6Li, ^7Li, and ^7Be.

First we will look at ^7Li generation. The reactions that can generate this element

are:

$$\alpha\,(\alpha,p)^{7}\,Li \quad , \quad Q = -17.3MeV \tag{7.6}$$

$$\alpha\,(T,\gamma)^{7}\,Li \quad , \quad Q = 2.47MeV. \tag{7.7}$$

The large amount of energy required to fuse two α particles is so large that the mechanism in Eq. (7.6) only provides a channel for destroying ^{7}Li, not creating it. The Boltzmann equation for lithium generation is:

$$\frac{dY_{7Li}}{dT} = n_B\Sigma_{7,1}\left[\kappa_{7,1}Y_\alpha^2 - Y_{7Li}\right] + \Sigma_{7,2}\left[n_B Y_\alpha Y_T - \kappa_{7,2}Y_{7Li}\right] \tag{7.8}$$

$$\Sigma_{7,1} = \left\langle \sigma_{^7Li(p,\alpha)\alpha} v \right\rangle \tag{7.9}$$

$$\kappa_{7,1} = \frac{n_{^7Li}^{(0)} n_p^{(0)}}{n_\alpha^{(0)2}} \tag{7.10}$$

$$\Sigma_{7,2} = \left\langle \sigma_{T(\alpha,\gamma)^7Li} v \right\rangle \tag{7.11}$$

$$\kappa_{7,2} = \frac{n_\alpha^{(0)} n_T^{(0)}}{n_{^7Li}^{(0)}} \tag{7.12}$$

The rate of destruction $n_B\Sigma_{7,1}$ is far greater than the Hubble rate meaning the Boltzmann equation is in chemical equilibrium. This implies an upper bound on ^{7}Li of:

$$Y_{^7Li} \leq X_p^{-1}\left(Y_\alpha^2 \exp\left(-\frac{17.6MeV}{T}\right) + \frac{\Sigma_{7,2}}{\Sigma_{7,1}} Y_\alpha Y_T\right). \tag{7.13}$$

The Tritium abundance pre-T_d is less than 10^{-10}. The rates are taken from [22]

and [29]. This mechanism generates a maximal amount of:

$$Y_{^7Li} \leq 10^{-20}. \tag{7.14}$$

Similar calculations for ^6Li and ^7Be place upper bounds on their abundances fractions of $Y < 10^{-20}$. These bounds not only prevent the generation of observable amounts of ^6Li, ^7Li, and ^7Be, but also on the creation of the heavier elements ^9Be, ^{10}B, and ^{11}B. This means the catalysed α production can not impact observed BBN abundances.

7.4 Nuclear-Mule Nuclear Scattering post-T_d

When a mule nucleus scatters off a standard nucleus there is a small probability that they exchange a pion. As with the α producing cycle, the only way for the mesinos effect the abundance of a nucleus with a larger number density than it is for there to be some mechanism that restores the mesino to its previous isospin state. An example of this type of mechanism is shown in figure 7.1.

The first step in calculating the rate at which the cycle in figure 7.1 converts a given element is to estimate the rate of each step in the cycle. An upper bound on

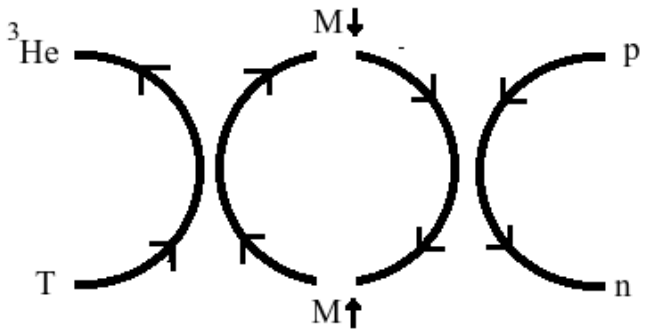

Figure 7.1: This cycle allow the generation of neutrons from protons. Note that due to the distribution of nuclear binding energies, the process is not exothermic.

the flipping reaction will be:

$$\frac{dY_i}{dT} \approx \frac{n_M \langle \sigma v \rangle}{HT} Y_i X_M. \tag{7.15}$$

Ignoring the coulomb repulsion between the mesino and nucleus, we approximate cross section for the interaction to be $\approx \frac{\pi}{(140MeV)^2}$. The velocity of the mule nucleon is on the order $\frac{2T}{m_i}$. The velocity averaged cross section for an exothermic reaction is on the order $\langle \sigma v \rangle \approx \frac{\pi}{(140MeV)^2}\sqrt{\frac{2T}{m_i}}$. The factor in Eq. (7.15) can be expressed as:

$$\frac{n_M \langle \sigma v \rangle}{H} \approx \left(\frac{T}{MeV}\right)^{3/2} 6.7 \times 10^{-5}. \tag{7.16}$$

This immediately rules out the mule nuclei being able to affect the fraction of $T/^3He$, or $^7Li/^7Be$ with this mechanism since their abundances are much closer than this. However the neutron's abundance could still be affected, as the temperature drops

below $40keV$, the fraction of protons to neutrons becomes, $n/p \leq 10^{-6}$. There are two factors that will prevent the cycle from actually affecting the neutron abundance. The first of these is that the cycle cannot be exothermic. The net energy required by the cycle is:

$$\begin{aligned} Q_c &= (m_{M\downarrow} + m_p) - (m_{M\uparrow} + m_n) + (m_{M\uparrow} + m_T) - (m_{M\downarrow} + m_{^3He}) \\ &= (m_p - m_n) + (m_T - m_{^3He}) \\ &= -1.29MeV + 0.53MeV = -0.76MeV. \end{aligned} \tag{7.17}$$

The overall rate of the cycle in figure 7.1 depends on the slowest step. This means that if the cross sections of the reactions are of the same size and $Y_T \approx Y_p$, then the cycle is fastest when the energy required for each step is $Q_1 = Q_2 = \frac{|Q|}{2}$. Q_i is the energy required at each step. An additional suppression occurs due to the fact that $Y_T \ll Y_p$, causing Q_1 and Q_2 to no longer be equal, however the overall upper bound on the rate will be:

$$\frac{n_M \langle \sigma v \rangle}{H} \approx \left(\frac{T}{MeV}\right)^{3/2} 6.7 \times 10^{-5} \exp\left(-\frac{|Q_c|}{2T}\right). \tag{7.18}$$

For $T < 0.1MeV$, this is far smaller than the fraction of neutrons to protons as shown in figure 7.2.

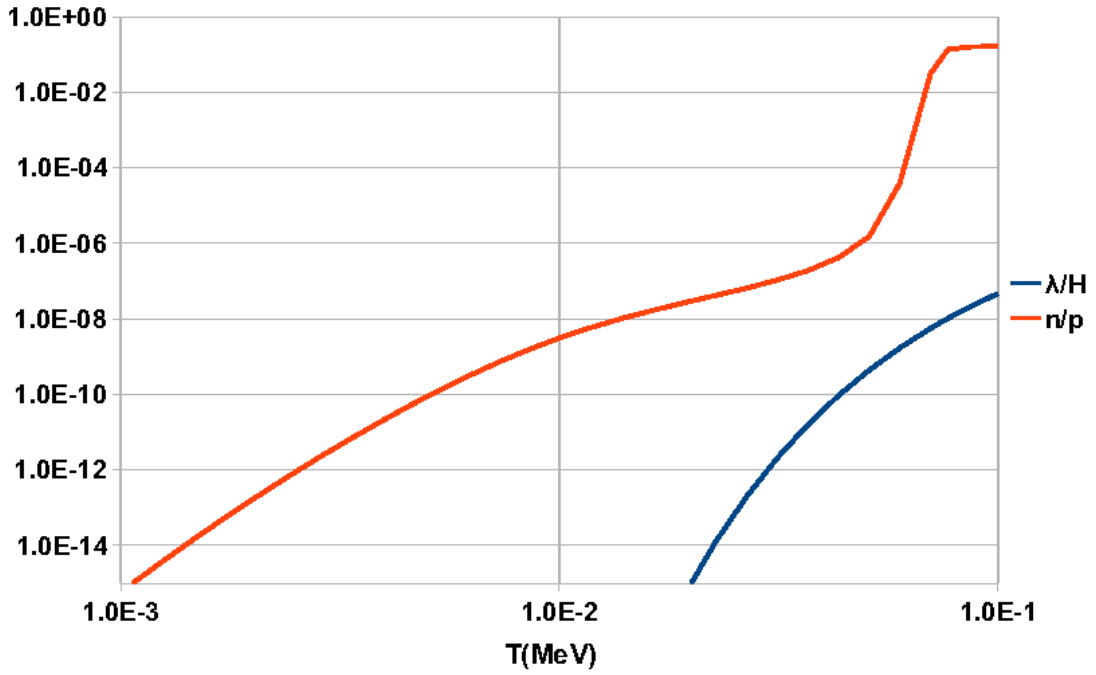

Figure 7.2: The plot shows the maximum rate of neutron creation. At all temperatures the rate is at least three orders of magnitude below the n/p ratio.

7.5 Energetic ^3He and T

When the squark decays it can generate high-energy ^3He and T (N^3). These nuclei can collide with the abundant α particles and form ^6Li. We will show that the mesino abundance is not large enough to generate enough ^6Li to explain the observed abundance.

There are two ways of generating the N^3 particles. The first is by ejecting an N^3 from the mule nucleon directly. This occurs if the majority of the nuclei are in the form MN^3 or MN^4. In this scenario the kinetic energy of the N^3 particle

comes from the kinetic energy it possessed when bound to the mesino. The binding energy of the nucleons is the difference of their kinetic and potential energy. When the mesino decays it eliminates the potential energy while leaving their kinetic energy undisturbed. We examine the impact of N^3 on BBN for a range of energies on the order of $20MeV$.

The second method of generating N^3 nuclei is through energetic hadrons emitted by the decay of the squark, or nucleons knocked free of the mule nucleus by this decay. These high energy particles can break apart the abundant ^4He nuclei, producing an energetic N^3.

While both scenarios could potentially generate ^7Li and ^7Be, ^6Li is the element that would most easily be observable. This is because the reactions that generate it do not involve the emission of a photon, and there is no source of ^6Li in standard BBN. This means that more ^6Li will be created and what is created is easier to observe. The reactions that generate the various elements are:

$$T +^4 He \rightarrow {}^6Li + n \tag{7.19}$$

$$^3He +^4 He \rightarrow {}^6Li + p \tag{7.20}$$

$$T +^4 He \rightarrow {}^7Li + \gamma \tag{7.21}$$

$$^3He +^4 He \rightarrow {}^7Be + \gamma. \tag{7.22}$$

The high energy N^3 will be slowed down quickly by the ambient electrons. The rate at which the N^3 loses energy with displacement is calculated in [30] to be:

$$\frac{dE}{dx} = \frac{Z^2\alpha}{\beta^2}\omega_p^2 \ln\left(\frac{\Lambda m_e \beta^2}{\omega_p}\right). \tag{7.23}$$

Z is the charge of the N^3, β is its velocity, m_e is the electron mass, Λ is an order 1 constant, and $\omega_p^2 = 4\pi n_e \alpha / m_e$ is the plasma frequency. n_e is the number density of the electrons.

In the case where N^3 are emitted directly from the mule nuclei we can calculate the amount of ^6Li produced to be:

$$Y_{Li6} = \frac{n_M}{n_B}\int_Q^{E_{max}} \sigma_{N^3(\alpha,N)^6Li} n_\alpha \left(\frac{dE}{dx}\right)^{-1} dE \tag{7.24}$$

This is a simplified version of the calculation where we assume one N^3 is ejected by each mule nucleus, and that the decay occurs instantaneously at a fixed energy. A more detailed calculation is not necessary due to the fact that too little ^6Li is generated to produce an observable effect. Q is the minimum energy required for the reaction $N^3\,(\alpha, N)^6\,Li$ to proceed, and E_{max} is the energy of the N^3 when it is emitted. The cross section for both of these reactions is taken to be $35mb$ in the range of energies of interest [31]. We can plot the fraction of ^6Li generated by high energy ^3He and T in figure 7.3. The energetic N^3 are unable to generate even the minimum

amount of ^6Li observed in the universe today, mostly due to the small n_M/n_B ratio.

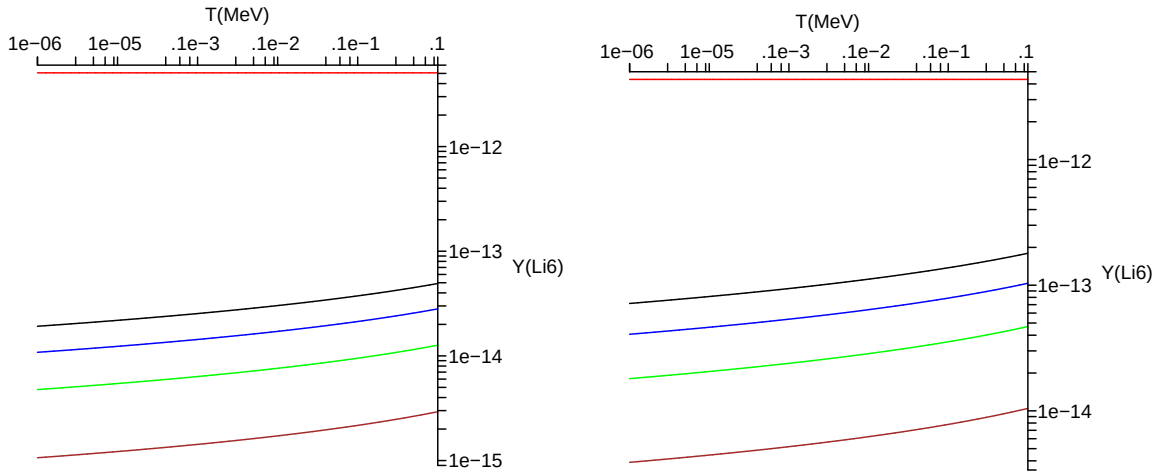

Figure 7.3: Plotted is the maximum fraction of ^6Li that can be produced through reactions $^3He\,(\alpha,p)^6\,Li$ (left) and $T\,(\alpha,n)^6\,Li$ (right). The red line is the minimum amount of ^6Li observed. The brown, green, blue, and black curves represent the ^6Li produced by an N^3 with energies $10MeV$, $20MeV$, $30MeV$, and $40MeV$.

In the case of high energy hadrons, a single high energy nucleon can disperse its energy among many others, possibly generating multiple energetic N^3 nuclei for each decaying relic. [25] reviews the impact on primordial nuclear abundances of a hadronically decaying relic. If the hadron branching rate of a decaying relic is of order 1 and the relic has a mass of $1TeV$, then the minimum abundance needed to generate the observed ^6Li is:

$$\Omega_X h^2 \;>\; 10^{-6}, \tag{7.25}$$

Comparing this to the expected abundance for a TeV mass relic predicted by [1],

$$\Omega_X h^2 = \frac{n_x}{n_\gamma} m_x \frac{1}{2.578 \times 10^{-8} GeV} \tag{7.26}$$

$$\approx 9.3 \times 10^{-9}, \tag{7.27}$$

We see that this mechanism is not able to explain the ^6Li abundance.

7.6 Remnant Of The Mule Nucleon

The final mechanism that can be used to generate an observable signature in the early universe is the nuclear remnant of the mule nucleon. Depending on the final state of the mule nuclei and the kinetic energy of the remnant, it is possible for the remnant to end up in the ground state of elements not normally produced during BBN.

This mechanism is only able to affect nuclear fractions smaller than the mesino baryon fraction. This means the remnants could affect the observed abundances of ^6Li, ^7Li, ^9Be, and B.

Unfortunately deriving the mule nuclear abundances and their decay remnants depends on an understanding of nuclear physics we do not have. This means the farthest we can go with this method is to estimate the maximal branching ratio of the decaying mule nucleon allowed by observations. These rates can be found by comparing the mesino abundance with the abundances in table 7.1.

For the mule nuclei to generate more ^6Li than observed the branching rate into ^6Li must be of order one. To generate enough ^6Li to explain the observed abundance, the branching rate must be at least 0.013. For the mule nuclei to generate more ^7Li, ^9Be, and B than observed, the branching rate must be at least order 1, 10^{-3} and 10^{-2} respectively.

Chapter 8

Summary

After a brief review of BBN and the cosmology behind it we discussed the benefits supersymmetry has on the renormalisation of the Standard Model. This background is used to motivate our study of the scalar quark and its potential impact on the primordial abundances of elements. The process of incorporating these particles into the BBN framework occurs in six steps.

The first step in this process is the formation of meson and baryon like objects from squarks and standard quarks. These object start forming during the QCD phase transition, however their large size allows them to annihilate through an enhanced cross section [1]. This drastically reduces the possible number density of these particles during BBN.

Next we study the formation of bound states between standard nuclei and mesinos.

The resulting deuteron-like bound states or mule deuterons are mixtures of the proton and down mesino state with a neutron and up mesino state. Due to uncertainties in the nuclear physics at short distances, the expected binding energy of this state is between $10MeV$ and $30MeV$. These binding energies correspond to a synthesis temperature for the mule deuteron between $0.34MeV$ and $1.0MeV$.

Once the abundance fraction of mule deuterons becomes $O(1)$ complex mule nuclei can form through nucleon capture. This is the third step in mule nucleosynthesis. The final size of the mule nuclei depends predominantly on their spectrum of binding energies. This spectrum is virtually impossible to calculate. Rather than spending large amounts of time attempting to do so, we focus on the various mechanisms that could affect primordial element abundances. We look at the largest possible effect that any binding energy spectrum can have on the abundances. If the small number of squarks that survive until BBN cannot generate an observable signature in this way then it is not possible for them to generate one at all.

One mechanism that can generate a significant affect is the creation of α particles pre-T_d. As with the size mule nuclei can achieve, the rate of α generation depends heavily on the mule nuclear binding energies as well at the rate of proton capture in mule nuclei. We showed that even under maximal rates, the ^4He produced in this way is unable to affect BBN predictions.

Once the deuterium bottleneck has been overcome, mule nuclei have limited in-

teractions with standard nuclei. No mechanism exists that can affect the primordial abundances before the squark decays.

The eventual decay of the squark could cause the mule nucleus to eject a nucleus not normally produced in BBN. Unfortunately calculating the amount of beryllium, boron, or lithium ejected is simply not possible with our current understanding of nuclear physics.

Chapter 9

Conclusions

We have studied the effects of a strongly interacting relic of spin 0 on BBN. We calculated an estimate on the binding energy of the mesino-nucleon bound state (mule deuteron). This binding energy most likely lies in the range $BE \in [10MeV, 30MeV]$. The large uncertainty is due to the strong dependence of the binding energy on the short distance behaviour of the mesino nucleon potential, as well as uncertainties in the size of the axial vector coupling constant $\tilde{g}_A$.

For any of these binding energies, nucleosynthesis is able to begin long before the deuterium bottleneck of standard BBN is overcome. The exact path of nucleosynthesis at this point depends implicitly on the binding energies of the most deeply bound mule nuclei. We showed that, due the effects of three body resonances, the error on binding energies of multi-nucleon mule nuclei are extremely difficult to calculate.

We believe that the large binding energy of the mule deuteron will be a general feature of small mule nuclei. This effect should become negligible by the time 12 nucleons are bound to a single mesino. At this point α emission is able to dominate the nucleosynthesis channels.

Given the low relic abundance of the mesinos, the only mechanism that may be able to generate an observable effect on primordial abundances is the nuclear remnant ejected when the mesino decays. If the yield of ^6Li, ^9Be, and B were in excess of $O(1)$, $O(10^{-3})$, and $O(10^{-2})$ respectively, then the existence of the relics would leave a trace in the primordial values of these elements. This scenario remains highly speculative due to nuclear uncertainties in formation and decay rates of the mule nuclei.

Bibliography

[1] Junhai Kang, Markus A. Luty, and Salah Nasri. The Relic Abundance of Long-lived Heavy Colored Particles. *JHEP*, 09:086, 2008.

[2] WM Yao et al. Review of particle physics. *Journal of Physics G: Nuclear and Particle Physics*, 33:1–1232, 2006.

[3] S. Dodelson. *Modern cosmology*. Academic Pr, 2003.

[4] E. Komatsu, J. Dunkley, MR Nolta, CL Bennett, B. Gold, G. Hinshaw, N. Jarosik, D. Larson, M. Limon, L. Page, et al. Five-Year Wilkinson Microwave Anisotropy Probe Observations: osmological Interpretation. *Astrophys. J. Suppl*, 180:330–376, 2009.

[5] Richard H. Cyburt et al. Nucleosynthesis Constraints on a Massive Gravitino in Neutralino Dark Matter Scenarios. *JCAP*, 0910:021, 2009.

[6] E.W. Kolb and M.S. Turner. *The early universe*. Westview Press, 1994.

[7] S. Weinberg. Gravitation and cosmology: principles and applications of the general theory of relativity. *American Journal of Physics*, 41:598–599, 1973.

[8] V. Mukhanov. Nucleosynthesis Without Computer. *International Journal of Theoretical Physics*, 43(3):669–693, 2004.

[9] Lawrence Kawano. Let's go: Early universe. 2. Primordial nucleosynthesis: The Computer way. FERMILAB-PUB-92-004-A.

[10] Martin Asplund, David L. Lambert, Poul Erik Nissen, Francesca Primas, and Verne V. Smith. Lithium isotopic abundances in metal-poor halo stars. *Astrophys. J.*, 644:229–259, 2006.

[11] Roger Cayrel et al. Line shift, line asymmetry, and the 6Li/7Li isotopic ratio determination. 2007.

[12] Maxim Pospelov. Particle physics catalysis of thermal big bang nucleosynthesis. *Phys. Rev. Lett.*, 98:231301, 2007.

[13] Chris Bird, Kristen Koopmans, and Maxim Pospelov. Primordial Lithium Abundance in Catalyzed Big Bang Nucleosynthesis. *Phys. Rev.*, D78:083010, 2008.

[14] Lev Davidovich Landau, Vladimir B Berestetskii, Evgenii Mikhailovich Lifshitz, and Lev Petrovich Pitaevskii. *Relativistic quantum theory*. Course Theor. Phys. Pergamon, Oxford, 1974. Trans. from the Russian.

[15] M.E. Peskin and D.V. Schroeder. *An introduction to quantum field theory*. Westview press, 1995.

[16] Silas R. Beane, Paulo F. Bedaque, Wick C. Haxton, Daniel R. Phillips, and Martin J. Savage. From hadrons to nuclei: Crossing the border. 2000.

[17] JL Friar, BF Gibson, and GL Payne. One-pion-exchange potential deuteron. *Physical Review C*, 30(3):1084–1086, 1984.

[18] J.J. Sakurai. *Modern quantum mechanics*. Addison-Wesley, 1985.

[19] JA Weideman and SC Reddy. A MATLAB differentiation matrix suite. *ACM Transactions on Mathematical Software (TOMS)*, 26(4):465–519, 2000.

[20] Talys prediction of astrophysical reaction rates for nuclei with z=8-102. http://www-astro.ulb.ac.be/html/talys.html. 2009.

[21] G. Sigl, K. Jedamzik, D. N. Schramm, and V. S. Berezinsky. Helium photodisintegration and nucleosynthesis: Implications for topological defects, high energy cosmic rays, and massive black holes. *Phys. Rev. D*, 52(12):6682–6693, Dec 1995.

[22] C. Angulo, M. Arnould, M. Rayet, P. Descouvemont, D. Baye, C. Leclercq-Willain, A. Coc, S. Barhoumi, P. Aguer, C. Rolfs, R. Kunz, J. W. Hammer, A. Mayer, T. Paradellis, S. Kossionides, C. Chronidou, K. Spyrou, S. Degl'Innocenti, G. Fiorentini, B. Ricci, S. Zavatarelli, C. Providencia, H. Wolters, J. Soares, C. Grama, J. Rahighi, A. Shotter, and M. Lamehi Rachti. A compilation of charged-particle induced thermonuclear reaction rates. *Nuclear Physics A*, 656(1):3 – 183, 1999.

[23] Steven C. Pieper, V. R. Pandharipande, Robert B. Wiringa, and J. Carlson. Realistic models of pion-exchange three-nucleon interactions. *Phys. Rev.*, C64:014001, 2001.

[24] David Thomas, David N. Schramm, Keith A. Olive, and Brian D. Fields. Primordial nucleosynthesis and the abundance of beryllium and boron. *Astrophys. J.*, 406:569–579, 1993.

[25] Karsten Jedamzik. Big bang nucleosynthesis constraints on hadronically and electromagnetically decaying relic neutral particles. *Phys. Rev.*, D74:103509, 2006.

[26] Martin Asplund, David L. Lambert, Poul Erik Nissen, Francesca Primas, and Verne V. Smith. Lithium isotopic abundances in metal-poor halo stars. *Astrophys. J.*, 644:229–259, 2006.

[27] Maxim Pospelov, Josef Pradler, and Frank Daniel Steffen. Constraints on Supersymmetric Models from Catalytic Primordial Nucleosynthesis of Beryllium. *JCAP*, 0811:020, 2008.

[28] Ramon J. Garcia Lopez et al. Boron in Very Metal-Poor Stars. *Astrophys. J.*, 500:241, 1998.

[29] Georgeanne R. Caughlan and William A. Fowler. Thermonuclear reaction rates v. *Atomic Data and Nuclear Data Tables*, 40(2):283 – 334, 1988.

[30] John David Jackson. Classical Electrodynamics, 3rd ed. 1999.

[31] Masahiro Kawasaki, Kazunori Kohri, and Takeo Moroi. Hadronic decay of late-decaying particles and big-bang nucleosynthesis. *Phys. Lett.*, B625:7–12, 2005.

[32] L. Hulthén and M. Sugawara. *The two-nucleon problem.* Berlin.

[33] T. E. Simos and P. S. Williams. New insights in the development of numerov-type methods with minimal phase-lag for the numerical solution of the schrdinger equation. *Computers & Chemistry*, 25(1):77 – 82, 2001.

Appendix A

The Boltzmann Equation

As mentioned earlier, the Boltzmann is used to calculate the quantitative abundance of the light elements in the early universe.

The equation is a coupled set of ordinary differential equations that allow us to numerically, and in certain cases analytically, calculate the nuclear abundances of the light elements as a function of time or temperature.

Here we review a general set-up of the Boltzmann's equations equations when applied to the calculation of cosmological nuclear and relic abundances.

For reactions of the form, $1 + 2 \rightarrow 3 + 4$, the Boltzmann equation is of the form:

$$a^{-3}\frac{d(n_1 a^3)}{dt} = \prod_{i=1}^{4}\int \frac{d^3p_i}{(2\pi)^3 2E_i}(2\pi)^4\delta^4(p_1+p_2-p_3-p_4)|M|^2 \quad (A.1)$$

$$\{f_3 f_4(1 \pm f_1)(1 \pm f_2) - f_1 f_2(1 \pm f_3)(1 \pm f_4)\}. \quad (A.2)$$

f_i is the Bose-Einstein or Fermi-Dirac distributions of species i:

$$f_i \equiv \frac{1}{e^{\frac{(E-\mu)}{T}} \mp 1}, \quad (A.3)$$

the sign is $-$ for bosons, and $+$ for fermions. E and μ are the energy and chemical potential respectively. At BBN temperatures, $E - \mu \gg T$, meaning:

$$f_i \approx e^{\frac{\mu}{T}} e^{\frac{-E}{T}}. \quad (A.4)$$

The chemical potential and number density of a particle i are related by the

formula:

$$n_i = g_i e^{\mu_i/T} \int \frac{d^3p}{(2\pi)^3} e^{-E_i/T} \quad (A.5)$$

$$\equiv e^{\mu_i/T} n_i^{(0)}. \quad (A.6)$$

The definition of $n_i^{(0)}$ is:

$$n_i^{(0)} \equiv g_i \int \frac{d^3p}{(2\pi)^3} e^{-E_i/T} = \begin{cases} g_i \left(\frac{m_i T}{2\pi^2}\right)^{3/2} e^{-m_i/T} & m_i \gg T \\ g_i \frac{T^3}{\pi^2} & m_i \ll T \end{cases} \quad (A.7)$$

This means the distribution term in the Boltzmann equation becomes:

$$\{f_3 f_4 (1 \pm f_1)(1 \pm f_2) - f_1 f_2 (1 \pm f_3)(1 \pm f_4)\} \approx e^{-(E_1+E_2)/T} \left(\frac{n_3 n_4}{n_3^{(0)} n_4^{(0)}} - \frac{n_1 n_2}{n_1^{(0)} n_2^{(0)}} \right). \quad (A.8)$$

With the definition:

$$\langle \sigma v \rangle = \frac{1}{n_1^{(0)} n_2^{(0)}} \prod_{i=1}^{4} \left(\int \frac{d^3 p_i}{(2\pi) 2E_i} \right) e^{-(E_1+E_2)/T} (2\pi)^4 \delta^4 (p_1 + p_2 - p_3 - p_4) |M|^2, \quad (A.9)$$

the Boltzmann equation simplifies to the form:

$$a^{-3} \frac{d\,(n_1 a^3)}{dt} = n_1^{(0)} n_2^{(0)} \langle \sigma v \rangle \left(\frac{n_3 n_4}{n_3^{(0)} n_4^{(0)}} - \frac{n_1 n_2}{n_1^{(0)} n_2^{(0)}} \right) \quad (A.10)$$

When dealing with nuclei of mass number A we can simplify this equation further by converting the number densities to abundance fractions, $Y_i \equiv \frac{n_i}{n_B}$. The derivative term in Eq. (A.10) is simplified considerably. Since the number of Baryons in the universe is constant, $d(a^3 n_B)/dt = 0$.

There are three cases that will be used in the nuclear reaction rates of interest. The first case is of two nuclei in the initial state and two in the final state.

$$\frac{dY_1}{dt} = n_1^{(0)} n_2^{(0)} \langle \sigma v \rangle \left(\frac{Y_3 Y_4}{n_3^{(0)} n_4^{(0)}} - \frac{Y_1 Y_2}{n_1^{(0)} n_2^{(0)}} \right) n_B. \quad (A.11)$$

The second is a single nuclei being broken into two smaller nuclei by a photon:

$$\frac{dY_1}{dt} = n_1^{(0)} n_2^{(0)} \langle \sigma v \rangle \left(\frac{Y_3 Y_4}{n_3^{(0)} n_4^{(0)}} n_B - \frac{Y_1}{n_1^{(0)}} \right). \tag{A.12}$$

The third is the Boltzmann equation for a relativistic particle scattering off a single nuclei:

$$\frac{dY_1}{dt} = n_1^{(0)} n_2^{(0)} \langle \sigma v \rangle \left(\frac{Y_3}{n_3^{(0)}} - \frac{Y_1}{n_1^{(0)}} \right). \tag{A.13}$$

It is easier to get an intuitive feel for these equations when everything is a function of temperature rather than time. It is straitforward to write the ODE as a function of temperature by using the substitution:

$$\frac{1}{T}\frac{dT}{dt} = -H, \tag{A.14}$$

where H is the Hubble rate. The change of basis can now be given by:

$$\frac{dY}{dt} = \frac{dT}{dt}\frac{dY}{dT} = -HT\frac{dY}{dT}. \tag{A.15}$$

Eq. (A.13) now simplifies to:

$$\frac{dY_1}{dT} = -\frac{n_2^{(0)} \langle \sigma v \rangle}{H(T)T} \left(\frac{n_1^{(0)}}{n_3^{(0)}} Y_3 - Y_1 \right). \tag{A.16}$$

When the rate of reaction is far greater than the Hubble rate, the only way for equality of the previous equation to hold is if the quantity inside the brackets is approximately zero. In this case the Boltzmann equation is said to be in dynamical equilibrium and can be solved analytically.

Appendix B

Purturbative Relic Abundance Calculation

In this appendix we solve the Boltzmann equation of Eq. (3.14) to find the mass density of the relic using perturbation theory.

The equilibrium abundance for a non relativistic species like the squarks is given by:

$$Y_{eq} = \frac{45}{2\pi^4}\left(\frac{\pi}{8}\right)^{\frac{1}{2}}\frac{g}{g_{*s}}x^{\frac{3}{2}}e^{-x} \tag{B.1}$$

$$= 0.145\frac{g}{g_{*s}}x^{\frac{3}{2}}e^{-x}. \tag{B.2}$$

Here g_{*s} is similar to the total number of effectively massless degrees of freedom. It is defined slightly differently:

$$g_{*s} = \sum_{i=bosons} g_i\left(\frac{T_i}{T}\right)^3 + \frac{7}{8}\sum_{i=fermions} g_i\left(\frac{T_i}{T}\right)^3. \tag{B.3}$$

For the temperatures we are interested in, $g_{*s} = g_*$.

When looking at the perturbation approach it is possible to approximate the velocity averaged cross section as follows:

$$\langle\sigma|v|\rangle = \sigma_0 x^{-n}. \tag{B.4}$$

The Boltzmann equation now becomes:

$$\frac{dY}{dx} = -\lambda x^{-n-2}\left(Y^2 - Y_{EQ}^2\right) \tag{B.5}$$

$$\lambda \equiv \left[\frac{\sigma_0 s}{H_m}\right]_{x=1}, \tag{B.6}$$

rewriting the Boltzmann equation in terms of $\Delta \equiv Y - Y_{eq}$ results in the equation:

$$\Delta' = Y'_{eq} - \lambda x^{-n-2}\Delta\left(2Y_{eq} + \Delta\right). \tag{B.7}$$

To solve this system quasi analytically we look at the two limits. The early time limit $1 < x \ll x_f$, and the late time limit $x \gg x_f$. Where x_f is the freeze out value of x. At the early times Y follows Y_{eq} very closely, and Eq. (B.7) is solved to give:

$$\Delta \approx \frac{x^{n+2}}{2\lambda}. \tag{B.8}$$

At late times Y no longer tracks the equilibrium abundance, giving the late time abundance:

$$Y_\infty = \Delta_\infty = \frac{n+1}{\lambda} x_f^{n+1}. \tag{B.9}$$

This abundance can be expressed in terms of the mass density of the relic:

$$\Omega_Q h^2 = \frac{1.07 \times 10^9 x_f GeV^{-1}}{m_{pl}\sigma_0} \tag{B.10}$$

We can now calculate the fraction of the number densities of squarks to the number density of baryons A.

$$A = \frac{\Omega_Q}{\Omega_B}\frac{m_B}{m_Q}. \tag{B.11}$$

The fraction depends explicitly on the freeze out temperature, or equivalently x_f. To determine this temperature we find the temperature at which $\Delta(x_f) = cY_{EQ}(x_f)$. Where c is a constant of order one. The solution to the Boltzmann equation during this time is $\Delta(x_f) \approx x_f^{n+2}/(\lambda(2+c))$. This allows us to solve for the approximate value of x_f:

$$x_f \approx \ln[(2+c)\lambda ac] - \left(n + \frac{1}{2}\right)\ln\{\ln[(2+c)\lambda ac]\}. \tag{B.12}$$

The constant $a \equiv 0.145\frac{g}{g_{*s}} \approx 0.0029$. Choosing $c(c+2) = n+1$ gives the best fit to the numerical results for the final abundance Y_∞.

Appendix C

Deriving The Schrödinger Equation For The Deuteron

The form of the Schrödinger equation for the deuteron is calculated in [32]. We will give a summary of this calculation here. The general wave function for a state with total angular momentum J and a z component J_z can be written as:

$$\psi = \frac{1}{r}\sum_{L} u_L(r)\Phi_{J,J_z,L}(\theta,\phi) \tag{C.1}$$

$$\Phi_{J,J_z,L}(\theta,\phi) = \sum_{L_z=J_z-1}^{J_z+1} c_{J,J_z,L,L_z} Y_{L,L_z}(\theta,\phi)\chi_{J_z-L_z}. \tag{C.2}$$

The coefficients are normalised such that $\sum_{L_z=J_z-1}^{J_z+1} |c_{J,J_z,L,L_z}|^2 = 1$. Finally χ_i is the spin one triplet described by:

$$\chi_1 = \alpha(1)\alpha(2) \tag{C.3}$$

$$\chi_0 = \frac{1}{\sqrt{2}}(\alpha(1)\beta(2) + \beta(1)\alpha(2)) \tag{C.4}$$

$$\chi_{-1} = \beta(1)\beta(2), \tag{C.5}$$

Where $\alpha(i)$ and $\beta(i)$ are the eigenfunctions of the Pauli matrix acting on i^{th} nucleon, whose eigenvalues are $+1$ and -1 respectively.

The normalisation condition of the eigenfunctions is:

$$\sum_{L}\int u_L(r)^2 dr = 1 \tag{C.6}$$

In the case of interest the angular functions can be written as:

$$\Phi_{1,J_z,0}(\theta,\phi) = \frac{1}{\sqrt{4\pi}}\chi_{J_z} \tag{C.7}$$

$$\Phi_{1,1,2}(\theta,\phi) = \sqrt{\frac{1}{10}}Y_{2,0}\chi_1 + \sqrt{\frac{3}{10}}Y_{2,1}\chi_0 + \sqrt{\frac{6}{10}}Y_{2,2}\chi_{-1} \tag{C.8}$$

$$\Phi_{1,0,2}(\theta,\phi) = -\sqrt{\frac{3}{10}}Y_{2,-1}\chi_1 - \sqrt{\frac{4}{10}}Y_{2,0}\chi_0 - \sqrt{\frac{3}{10}}Y_{2,1}\chi_{-1} \tag{C.9}$$

$$\Phi_{1,-1,2}(\theta,\phi) = \sqrt{\frac{6}{10}}Y_{2,-2}\chi_1 + \sqrt{\frac{3}{10}}Y_{2,-1}\chi_0 + \sqrt{\frac{1}{10}}Y_{2,0}\chi_{-1}. \tag{C.10}$$

While the angular distributions are not required for the calculation of the binding energy of the deuteron or mule deuteron; it is necessary to know the distribution when calculating the photodisintegration cross sections of these objects.

The Schrödinger equation can now be written as a sum over the orbital angular momentum of the state:

$$\sum_{L'}\left[-\frac{1}{2m}\frac{d^2}{dr^2} + \frac{L'(L'+1)}{2mr^2} - E + V_c(r)\sigma_1\cdot\sigma_2 + V_T(r)S_{12}\right]u_{L'}\Phi_{J,J_z,L'}(\theta,\phi) = 0. \tag{C.11}$$

The mass m is the reduced mass of the system. Multiplying Eq. (C.11) by $\Phi_{J,J_z,L}(\theta,\phi)$ then integrating over the solid angle $d\Omega$ gives the radial Schrödinger equations for the wave function:

$$\begin{aligned} 0 &= \left[-\frac{1}{2m}\frac{d^2}{dr^2} + \frac{L(L+1)}{2mr^2} - E + V_c(r)\right]u_L \\ &\quad + V_T(r)\sum_{L'}S_{J,L,L'}u_{L'}(r) \end{aligned} \tag{C.12}$$

$$S_{J,L,L'} = \int d\Omega\Phi_{J,J_z,L}S_{12}\Phi_{J,J_z,L'} \tag{C.13}$$

The value of $S_{J,L,L'}$ for the deuteron is given in [32] and summarised in Table C.2. Note that the total angular momentum of the deuteron is 1.

In simplified notation the ground state of the deuteron can be written as:

$$\psi = \frac{1}{r}u(r)\Phi_{1,J_x,0} + \frac{1}{r}w(r)\Phi_{1,J_x,2}, \tag{C.14}$$

where $u(r) \equiv u_0(r)$ and $w(r) \equiv u_2(r)$. In this form the deuteron Schrödinger equation

$S_{J,L,L'}$			
	$L' = J+1$	$L' = J$	$L' = J-1$
$L = J+1$	$-\frac{2(J+2)}{2J+1}$	0	$\frac{6\sqrt{J(J+1)}}{2J+1}$
$L = J$	0	2	0
$L = J-1$	$\frac{6\sqrt{J(J+1)}}{2J+1}$	0	$-\frac{2(J-1)}{2J+1}$

Table C.1: This table shows the values of $S_{J,L,L'}$ as a function of the total angular momentum of the system$J$

$S_{1,L,L'}$			
	$L' = 2$	$L' = 1$	$L' = 0$
$L = 2$	-2	0	$2\sqrt{2}$
$L = 1$	0	2	0
$L = 0$	$2\sqrt{2}$	0	0

Table C.2: This table shows the values of $S_{J,L,L'}$ from Table(C.1) for the case $J = 1$.

becomes:

$$\left(-\frac{1}{2m}\frac{d^2}{dr^2} - E + V_c(r)\right) u(r) + 2\sqrt{2}V_T(r)w(r) = 0 \quad \text{(C.15)}$$

$$\left(-\frac{1}{2m}\frac{d^2}{dr^2} + \frac{3}{mr^2} - E + V_c(r) - 2V_T(t)\right) w(r) + 2\sqrt{2}V_T(r)u(r) = 0.$$

This is the coupled ODE eigenvalue problem that must be solved in order to find the binding energy and ground state wave function of the deuteron.

[22]

Appendix D

The Mule Deuteron Photodisintigration Cross Section

We will estimate the cross section for mule deuteron photodisintegration discussed in section 5.3. The cross section for deuteron photodisintegration has been known for decades and can be calculated analytically with a few justified approximations. Unfortunately these approximation are not valid for the mule deuteron.

It is shown in section 5.3 that even if the cross section is are off by a factor of 100, the rate freeze out will still occur below T_{MDS}. That is, the mule deuterons will have formed before the synthesis rate freezes out.

The general cross section is calculated in [14] to be:

$$d\sigma = \frac{\alpha m|\overrightarrow{p}|}{2\pi\omega}|\overrightarrow{e}\cdot\overrightarrow{v_{fi}}|^2 d\Omega. \tag{D.1}$$

Here $\overrightarrow{p}$ is the momentum of the ejected proton, $\overrightarrow{e}$ is the unit vector of the incoming γ momentum, and m is the nuclear mass. The quantity $\overrightarrow{v}_{fi}$ is defined to be:

$$\overrightarrow{v}_{fi} = i\omega\int d^3r\psi'^*(r)\overrightarrow{r}\psi(r), \tag{D.2}$$

or

$$\overrightarrow{e}\cdot\overrightarrow{v}_{fi} = i\omega\int d^3r\psi'^*(r)r\,(\overrightarrow{e}\cdot\overrightarrow{n_1})\,\psi(r). \tag{D.3}$$

Where ψ and ψ' are the initial and final states of the nucleon, ω is the energy of the photon, and $\overrightarrow{n}_1 \equiv \frac{\overrightarrow{r}}{r}$. Up till this point no approximations have been made.

In the derivation of the deuteron's photodisintegration cross section it is assumed

that the outgoing wave function can be approximated by the plane wave:

$$\psi'(r) \;=\; e^{i\overrightarrow{p}\cdot\overrightarrow{r}}. \tag{D.4}$$

This assumes that the size of the deuteron $\left(\frac{1}{\sqrt{2\mu BE}}\right)$ is large compared to the effective interaction radius $a = 1.5fm$, where BE is the absolute value of the binding energy of the system. While valid for the deuteron, $\left(\sqrt{2\mu BE}\right)^{-\frac{1}{2}} = (m_n 2.225MeV)^{-\frac{1}{2}} = 4.31fm$, it is not so for the mule deuteron. When the binding energy of the mule deuteron is taken to be $BE = X10MeV$, X being a constant between 1 and 3, the size is $\approx \left(\sqrt{2\mu BE}\right)^{-\frac{1}{2}} = (2m_n X10MeV)^{-\frac{1}{2}} = 1.43X^{-\frac{1}{2}}fm$.

This is an unfortunate situation, in order to accurately measure the cross section we need to know what the free nucleons wave function is on scales where the potential is not negligible. To do this accurately one would need to tackle the problem numerically. [33] develops a useful strategy for this type of problem. However we will show that the lower bound for the cross section that we calculate predicts a freeze out temperature bellow T_{MDS} and is therefore sufficient for our purposes.

Since the outgoing nucleon's momentum is small compared to the length scale of the mule deuteron we can expand the exponential and keep only linear order terms.

$$\psi'(r) \;\approx\; 1 + i\overrightarrow{p}\cdot\overrightarrow{r} \tag{D.5}$$

The initial state of the wave function is given by the mule deuteron bound state function:

$$\psi(r) \;=\; R_S\frac{1}{\sqrt{4\pi}} + R_D\Phi_{1J_z2}, \tag{D.6}$$

Where Φ is defined in Eq. (C.2). The integral in Eq. (D.3) is now given by:

$$\begin{aligned}\overrightarrow{e}\cdot\overrightarrow{v}_{fi} \;=\; & i\omega\int d^3r\,(1 + i\overrightarrow{p}\cdot\overrightarrow{r})\,r\left(R_S\frac{1}{\sqrt{4\pi}} + R_D\chi_f\Phi_{1J_z2}\right) \\ & (\overrightarrow{e}\cdot\overrightarrow{n}_1)\,.\end{aligned} \tag{D.7}$$

Here, χ_f is the final spin state.

The S and D components of the ground state wave function have parity such that the leading order term in the final state wave function, 1, does not contribute to the integral. To correctly calculate the cross section we must average over the initial angular momentum J_z and sum over the out going spin states. The algebra is not particularly enlightening so we will not reproduce it here, however the cross section

becomes:

$$\sigma = \frac{8\pi}{27}\alpha m p^3 \omega (I_S^2 + \frac{2}{5} I_D^2) \quad (D.8)$$

$$I_S = \int dr r^2 R_S \quad (D.9)$$

$$I_D = \int dr r^2 R_D. \quad (D.10)$$

For the sake of this approximation we can write:

$$R_S \approx \cos(\Theta)\sqrt{\kappa}\frac{e^{-\kappa r}}{r} \quad (D.11)$$

$$R_D \approx \sin(\Theta)\sqrt{\kappa}\frac{e^{-\kappa r}}{r}, \quad (D.12)$$

where $\kappa = \sqrt{2mBE}$. The constant Θ allows us to deal with the relative contributions of the two wave functions to the total ground state. This is consistent with the normalisation condition:

$$\int \left(R_S^2(r) + R_S^2(r)\right) r^2 dr = 1 \quad (D.13)$$

These functions have the correct long distance behaviour of the wave functions, that is they seem to be valid on scales greater than $\frac{1}{\kappa} = 1.44fm$. This rough approximation allows us to carry out the rest of the approximation analytically rather than numerically. The cross section is now:

$$\sigma \approx \frac{8\pi}{27}\alpha m p^3 \omega \left(\sin^2(\Theta) + \frac{2}{5}\cos^2(\Theta)\right) \kappa \left(\int r^3 e^{-\kappa r} dr\right)^2 \quad (D.14)$$

$$> \frac{8\pi}{27}\alpha m p^3 \omega \frac{2}{5}\kappa \left(\int r^3 e^{-\kappa r} dr\right)^2 \quad (D.15)$$

$$= \frac{8\pi}{27}\alpha \frac{m\left(2m(\omega - BE)\right)^{\frac{3}{2}}\omega}{\kappa^7}\frac{2}{5}\left(\int u^3 e^{-u} du\right)^2. \quad (D.16)$$

Conservation of energy in the reaction gives $p = \sqrt{2m(\omega - BE)}$. To get a strict upper bound on the cross section we can make sure that we only integrate over the region where the wave function is valid, the interval $r = [1.44fm, \infty]$, or $u = [1.73, \infty]$. The greater the binding energy, the smaller the range giving a lower bound on σ at

$BE = 30MeV$. Evaluating the integral for these bounds gives:

$$\sigma \quad > \quad \frac{8\pi}{27}\alpha\frac{m\left(2m(\omega - BE)\right)^{\frac{3}{2}}\omega}{\kappa^7}\frac{2}{5}\left(5.4\right)^2. \tag{D.17}$$

This is an upper bound on the photodisintegration cross section.